DIPLOMARBEIT

Trends of Atmospheric Water Vapor from VLBI and GPS

Ausgeführt an der Forschungsgruppe Höhere Geodäsie
zum Zwecke der Erlangung des akademischen Grades eines Diplom-Ingenieurs

unter der Leitung von
Univ.Prof. Dipl.-Ing. Dr.techn. Johannes Böhm

und der Betreuung durch
Dipl.-Ing. Daniel Landskron

eingereicht an der Technischen Universität Wien
Fakultät für Mathematik und Geoinformation
von

Patrick Greimeister

Matrikelnummer 1027423
Schumanngasse 52/3
1180 Wien

Wien, am 11. Dezember 2016   . . . .

Danksagung

Abstract

Variability in water vapor plays an important role in determining how much a signal gets delayed during the propagation through the atmosphere. This delay through the neutral atmosphere can be split up into a hydrostatic and a wet part. The latter can also be converted into precipitable water and its variation is an indicator for climate change. In this thesis, a long time series of tropospheric wet delays in zenith direction is computed from three different sources and compared to each other. The time frame chosen for the analysis is from 1985 - 2014, including data from a number of stations with different measuring activity and therefore varying data availability. Eighteen Very Long Baseline Interferometry (VLBI) stations and eight Global Positioning System (GPS) stations, co-located with the VLBI stations, are used for the analysis. Data from ray-tracing through numerical weather models (NWM) with operational data, available with the Vienna Mapping Function 1 (VMF1), are used for comparison as well.

The data processed with the Vienna VLBI Software (VieVS) show a satisfying correlation with different pressure inputs, whereas the results obtained from VMF1 and GPS are contradicting. The data obtained from VMF1, using operational NWM data, shows that this kind of data is not ideal for determining a trend over many years. For a trend analysis, reanalysis data would be better suitable but is not always available. The GPS data have their limit in the small observation time span of only twelve years. The VLBI data using pressure values from in-situ pressure records, show quite uncertain results, especially at the station Zelenchukskaya. Outliers and missing values have been corrected for, but could still influence the quality of the results, as well as random errors.

The results with all methods show a worldwide increase in the zenith wet delay (ZWD) of 0.1 mm/year (single solutions ranging from -0.5 to 0.4 mm/year) averaged over all stations or a decrease of -0.02 mm/year (single solutions ranging from -0.5 to 0.2 mm/year) when excluding the station Zelenchukskaya. The ZWD trends for single stations (averaged over all methods) range from -0.9 to 1.7 mm/year or -0.9 to 0.3 when excluding the station Zelenchukskaya, yielding mostly realistic results with a few exceptions.

In general, there is a common pattern visible, even with all the possible errors in the data, but more research is needed to get conclusive and congruent results across all methods. Also the detection of potential remaining offsets is important to avoid a negative influence on the result. For future studies, the usage of longer time series should be considered in order to further improve the reliability of the trends.

Kurzfassung

Die Variabilität des Wasserdampfgehalts spielt eine wichtige Rolle bei der Bestimmung der Verzögerung eines Signals während seiner Ausbreitung durch die Atmosphäre. Die Verzögerung durch die neutrale Atmosphäre kann in einen hydrostatischen und feuchten Anteil aufgeteilt werden. Letzterer kann in ausfällbares Wasser umgewandelt werden und dessen Änderung gilt als Indikator für den Klimawandel. In dieser Arbeit werden lange Zeitreihen des Feuchtanteils troposphärischer Verzögerungen in Zenitrichtung aus drei verschiedenen Quellen berechnet und miteinander verglichen. Der für die Analyse gewählte Zeitrahmen ist von 1985 - 2014, einschließlich Daten von mehreren Stationen mit unterschiedlicher Messaktivität und damit variierender Datenverfügbarkeit. Für die Analyse werden 18 Very Long Baseline Interferometry (VLBI) Stationen und acht Global Positioning System (GPS) Stationen verwendet, die sich in der Nähe von den VLBI-Stationen befinden. Als Vergleich werden auch Daten aus Raytracing durch numerische Wettermodelle, die mit der Vienna Mapping Function 1 (VMF1) zur Verfügung gestellt werden, verwendet.

Die mit der Vienna VLBI Software (VieVS) verarbeiteten Daten zeigen eine zufrieden-stellende Korrelation zueinander mit den verschiedenen Druck Inputs, wohingegen die Ergebnisse von VMF1 und GPS einander widersprechen. Die Daten, die von VMF1 unter Verwendung von operationellen Numerischen Wettermodellen (NWM) erhalten wurden, zeigen, dass diese Art von Daten nicht ideal ist, um einen Trend über viele Jahre zu bestimmen. Für eine Trendanalyse wären Re-Analysedaten besser geeignet, aber diese sind nicht immer verfügbar. Die GPS-Daten sind begrenzt durch ihre kurze Beobachtungszeit von nur zwölf Jahren. Auch die VLBI-Daten, mit Druckwerten aus in-situ-Drucksätzen zeigen unsichere Ergebnisse, vor allem bei der Station Zelenchukskaya. Ausreißer und fehlende Werte wurden korrigiert, aber weitere undetektierte Offsets könnten die Qualität der Ergebnisse noch weiter beeinflussen.

Die Ergebnisse zeigen einen weltweiten Anstieg des Zenith Wet Delay (ZWD) von 0.1 mm/Jahr (einzelne Ergebnisse im Bereich von -0.5 bis 0.4 mm/Jahr) mit allen Stationen oder einen Rückgang von -0.02 mm/Jahr (einzelne Ergebnisse im Bereich von -0.5 bis

0.2 mm/Jahr) ohne Einbeziehung der Station Zelenchukskaya. Die Trends für einzelne Stationen liegen im Bereich von -0.9 bis 1.7 mm/Jahr oder -0.9 bis 0.3 mm/Jahr ohne Einbeziehung der Station Zelenchukskaya und ergeben mit wenigen Ausnahmen weitgehend realistische Ergebnisse.

Im Allgemeinen sind Trends des ZWD, trotz aller möglichen Fehler in den Daten, sichtbar. Trotzdem ist noch mehr Forschung notwendig um zufriedenstellende und übereinstimmende Ergebnisse aller Methoden zu erhalten. Auch der Nachweis möglicher unentdeckter Offsets ist wichtig, um einen negativen Einfluss auf das Ergebnis zu vermeiden. Für zukünftige Studien sollte die Verwendung längerer Zeitreihen berücksichtigt werden, um die Ergebnisse weiter zu verbessern.

Contents

List of Acronyms

AZEL	Azimuth and Elevation
EOP	Earth Orientation Parameters
ECMWF	European Centre for Medium Range Weather Forecasts
GMF	Global Mapping Function
GNSS	Global Navigation Satellite Systems
GPS	Global Positioning System
GPT	Global Pressure and Temperature Model
ICRF	International Celestial Reference Frame
IGS	International GNSS Service
ITRF	International Terrestrial Reference Frame
IVS	International VLBI Service for Geodesy and Astrometry
IMF	Isobaric Mapping Function
IWV	Integrated Water Vapor
JD	Julian Date
MF	Mapping Function
MJD	Modified Julian Date
NGS	National Geodetic Survey
NASA	National Aeronautics and Space Administration
NMF	Niell Mapping Function
NWM	Numerical Weather Model
PW	Precipitable Water
PWLF	Piecewise Linear Function
SD	Standard Deviation
TRF	Terrestial Reference Frame
UT1	Universal Time 1

UTC	Universal Time Coordinated
VLBI	Very Long Baseline Interferometry
VMF1	Vienna Mapping Function 1
ZHD	Zenith Hydrostatic Delay
ZWD	Zenith Wet Delay
ZTD	Zenith Total Delay

List of Figures

List of Tables

Chapter 1

Introduction

Climate Research has become very important in the last few decades, not least because of ecological calamities like tornados and floodings. The climate is affected by many different factors and one of them is the atmospheric water vapor which still is very insufficiently researched and understood. Work on this topic has been done by Heinkelmann (2008), who computed long time series of atmospheric water vapor using VLBI measurements. This thesis shall be a continuation of his work, using longer time series, different calculation software and different ways to calculate the Integrated Water Vapor content.

This thesis uses data from Very Long Baseline Interferometry, Global Positioning System and Vienna Mapping Function 1 from the European Centre for Medium Range Weather Forecasts to calculate the zenith wet delay with long time series and compares those methods using linear trends and seasonal fits. The goal is the creation of a climate study with space geodetic methods to answer questions for example concerning postglacial rebound, global warming or sea level rise, being widely discussed topics at the moment.

The tropospheric wet delay can be converted into precipitable water (which is the water content above the station) to study the variation of water vapor content (diurnal and seasonal variations) over a certain time period. The water vapor content is one of the most important climate feedback processes (according to Watson (2009) it accounts for about 60% to 70% of the natural greenhouse gas effect) and therefore very important to monitor.

Faulty pressure sensors or wrong handling of the station keeper can cause offsets and missing values in the in-situ pressure records, indirectly leading to wrong values used for determining the ZWD. The range of the offset has to be determined and corrected before the analysis.

Chapter 2 starts with covering the fundamentals and explaining several basic concepts necessary for understanding the topic.

In chapter 3, previous work in this field will be described. Chapter 4 provides the full workflow of the analysis of the different datasets, from a description of the raw data to the estimation of the trends and an explanation of the reasons why this method was used.

In chapter 5 the results will be analyzed per method, but between the methods as well. A validation with results of past studies is carried out.

Finally, chapter 7 finishes with the conclusion and outlook for possible future projects and modifications at this topic.

Chapter 2

Fundamentals

In this chapter some basic concepts will be explained to get a better understanding about the several subjects. Most of this chapter is based on Böhm and Schuh (2013) unless otherwise specified.

2.1 Very Long Baseline Interferometry (VLBI)

Very Long Baseline Interferometry (VLBI) uses radio telescopes to observe extragalactic radio sources (quasars) and exists already since the 70's. With this method it is possible to determine the position of the earth in an inertial system or to determine physical parameters of the earth very precisely.

VLBI is needed for the realization of the International Celestial Reference Frame (ICRF) and also provides an important contribution to the realization of the International Terrestrial Reference Frame (ITRF). Both of these reference frames are connected with the Earth Orientation Parameters (EOP) which can only be determined all at once with VLBI from all space geodetic methods available. VLBI is used to measure the nutation parameters as well and is the only method to determine the earth rotation angle (dUT1=UT1-UTC). Currently it is also used for earth rotation studies or to map movements of tectonic plates very precisely see e.g. Böhm (2012).

Over several years new ITRF solutions have been provided over time (starting from ITRF2000, ITRF2005, ITRF2008 to the newly ITRF2014) due to increasing accuracy, tectonic movements and new stations. In this thesis the effects of using the ITRF2014 to calculate the Integrated Water Vapor (IWV) with the program VieVS [Böhm et al., 2012] will be explored in comparison to the VieVS-TRF, which is used for all other VLBI analysis calculations.

ITRF2014 is the newest realization of the ITRS, and uses input data time series of station positions and EOP provided by several geodetic Technique Centers (VLBI, SLR, GNSS and DORIS). Advantages to the previous realizations are improved solutions in station position at a given epoch, station velocities and Earth Orientation Parameters [Altamimi et al., 2016].

2.1.1 Basic Principle

The basic principle of geodetic Very Long Baseline Interferometry (VLBI) consists of a minimum of two radio telescopes, which measure the distance to extragalactic radio sources (quasars) on the far end of the observable universe. Because of the long range (the signals reach the earth after several billion years), the wave front can be assumed as plane instead of spherical [Böhm, 2004].

Because of the different positions of the observing telescopes, the measured signal arrives at the stations with a certain time offset. This difference between arrival time t_1 and t_2 is called the time delay L_g and is the primary measuring unit of VLBI. It can be geometrically calculated with the baseline B (distance from station one to station two), the unit vector to the radio source k and the light speed c (see Figure 2.1)

$$L_g = -\frac{\overrightarrow{B} * \overrightarrow{K}}{c} = t_2 - t_1 \tag{2.1}$$

The total delay is made up of this geometrical delay and several correction terms [Schuh and Behrend, 2012]:

$$L_t = L_g + L_{ab} + L_{clk} + L_{inst} + L_{trop} + L_{ion} + L_{rel} \tag{2.2}$$

L_t ... total delay
L_g ... geometrical delay
L_{ab} ... correction term for daily aberration
L_{clk} ... correction term for errors in the synchronisation of atom clocks
L_{inst} ... correction term for delay caused by the technical hardware
L_{trop} ... correction term for the neutral atmosphere (troposphere)
L_{ion} ... correction term for the ionosphere
L_{rel} ... correction term for effects caused by the special and general relativity
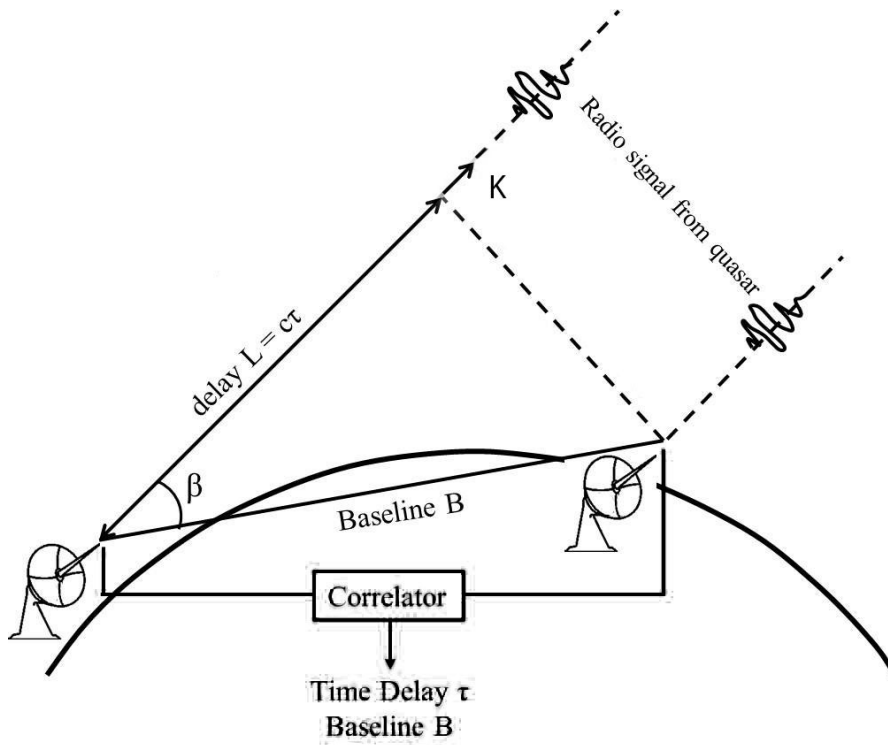
Figure 2.1: *Principle of Very Long Baseline Interferometry (modified from Computational Physics, Inc. (CPI) (2014))*

Furthermore, corrections like temperature dependent deformation of the antenna, cable calibration, and correct antenna axial distance can be applied.

The received signals are sent from both telescopes to a VLBI correlator where the delay is calculated (with the time stamps from the station clocks). This is done using a cross correlation function, which finds the maximum for the correlation function. This shift then corresponds to the difference in arrival times.

2.1.1.1 Modeling of the troposphere delay

The modeling of the troposphere portion (actually it is the neutral atmosphere, but the troposphere accounts for the biggest portion of the effect so it is called like that in the literature) is one of the major error sources for VLBI. It is usually modelled using the following equation:

$$L_{trop} = ZHD * mf_h(el) + ZWD * mf_w(el) + mf_g(el) * [G_n * cos(az) + G_e * sin(az)] \quad (2.3)$$

L_{trop} ... troposheric delay
ZHD ... zenith hydrostatic delay
mf_h ... hydrostatic mapping function
ZWD ... zenith wet delay
mf_w ... wet mapping function
mf_g ... gradient mapping function
G_n ... north gradient
G_e ... east gradient

As seen in equation 2.3, the model of the zenith delay is split into a hydrostatic and wet part (first and second term, respectively). The hydrostatic zenith delay (ZHD) can be calculated from models and meteorological data recorded at the stations, but the wet zenith delay (ZWD) has to be estimated in the VLBI analysis as the data from the ground is not meaningful enough to make a statement about the distribution of water vapor above the station. It is approximately 10-15% of the total delay. Another reason for the high variability of the ZWD is that the troposphere contains about 75-80 % of the mass of the atmosphere and is the layer where most clouds are found and almost all weather occurs. This is the reason why several models have been developed over several decades for the wet delay which are not as precise as the estimation during the data analysis but nevertheless useful for applications not requiring high accuracy.

Saastamoinen (1972) calculates the ZWD based on ideal gas law:

$$ZWD = 0.0022768(1255 + 0.05T_0)\frac{p_{w0}}{T_0} \quad (2.4)$$

p_{w0} ... water vapor pressure at the surface
T_0 ... temperature at the surface

Another expression is that the ZWD in cm equals to the water vapor pressure in hPa at the earth's surface:

$$ZWD[cm] \approx p_{w0}[hPa] \tag{2.5}$$

In both of those cases the water vapor pressure and the temperature at the surface has to be known. There is the simple model of the standard atmosphere with the relative humidity to calculate p_w:

$$p_w = \frac{f}{100} exp(-37.2465 + 0.213166T - 0.000256908T^2) \tag{2.6}$$

The ZWD is proportional to the integrated water vapor (IWV) above the station, which is highly variable but can be easily obtained from numerical weather models or measured by other techniques. For this the mean temperature T_m, which on the other hand needs the vertical profiles of the water vapor and temperature, is needed. Water vapor is mainly located near the earth surface and therefore the mean temperature T_m is highly correlated with temperature at the earth surface T_0.

Bevis et al. (1992) formulate the following equation using 8718 profiles of radiosonde over Northern America:

$$T_m \approx 70.2 + 0.72T_0 \tag{2.7}$$

They state that if ZWD and the surface temperature are known without errors, the IWV can be calculated with an average error of less than 4 %. Therefore the IWV is calculated with the following equation:

$$IWV = \Pi * ZWD \tag{2.8}$$

$$\Pi = \frac{10^6}{R_{H_2O}[(k_3/T_m) + k_2']} \tag{2.9}$$

R_{H_2O} ... specific gas constant of water vapor

T_m ... Weighted averaged temperature of the atmosphere

k_3, k_2' ... Empirical refraction constants

The IWV in zenith direction can be converted into precipitable water (PW), being the height of the water column above the station, using the density of water:

$$PW = \frac{IWV}{\rho_{H_2O}} \tag{2.10}$$

ρ_{H_2O} ... Density of liquid water $[1000 \; \frac{kg}{m^3}]$

The PW is approximately 0.16 ZWD and highly variable. It is recommended to use real weather data to derive the mean temperature as in equation 2.7 as it is only an empirical approach and not always valid.

Both the hydrostatic as well as the wet mapping functions (used to map the zenith delays to the elevation of the observation) are needed and taken directly from VMF1. Theoretically, the ZWD can be taken from VMF1 but the estimated one from the analysis is more accurate.

Mapping functions play a very important role in VLBI as well as in GNSS analysis and describe the dependence of the tropospheric influence on the elevation angle. For the dry component, they can be modeled with the highest precision at the equator because there are less pressure and temperature changes. For the wet component, it can be modeled with the highest precision at the poles because of less humidity (does not apply for mapping functions in general, but as the mapping function gets multiplied with the ZWD, it is valid).

It is possible to summarize them into a so-called total mapping function as well, with the advantage that the results are not affected by bad a priori hydrostatic zenith delays. The disadvantage is that the result is close in value to the hydrostatic mapping function and that fast changes from the wet component cannot be considered. It is recommended to separate both components as long as the time resolution of the underlying NWM is not better than three hours or even more (at the moment the ECMWF provides data every six hours).

Several mapping functions have been developed over the years starting from Saastamoinen [Saastamoinen, 1972], to the Niell Mapping Function (NMF) [Niell, 1996], Global Mapping Function (GMF) [Böhm et al., 2006], GPT2 [Lagler et al., 2013] and the updates GPT2w [Böhm et al., 2015] and Site-augmented GPT2w [Landskron et al., 2015]. All of those mentioned are empirical mapping functions, which only need Day of year (DOY) and station coordinates (latitude, longitude and station height) for the calculation (except Site-augmented GPT2w which use data from NWM, see below)

Then there are the Isobaric Mapping Function (IMF) [Niell, 2000], Vienna Mapping Function (VMF) [Böhm and Schuh, 2004] and VMF1 (update of VMF with new coefficients) [Böhm et al., 2006], which all use data from Numerical Weather Data (NWM) from the European Centre for Medium Range Weather Forecast (ECMWF) developed. The advantage of using NWM are getting a priori zenith hydrostatic delays for GNSS stations in which local pressure measurements usually are not available and the greater accuracy in comparison to empirical models due to discrete data [Böhm, 2004].

The European Centre for Medium Range Weather Forecasts (ECMWF) is an organization of 21 countries, aiming to provide reliable medium range weather forecasts. An important aspect of their work is the reanalysis which involves weather observations collected over several decades, what enables to get a clearer view of how much climate has changed. Such reanalysis products are e.g. ERA 15 (from 1979 - 1993), ERA 40 (from 1957 - 2002) and, the current one, ERA Interim (from 1979 - on).

VMF1 is not available at any location on the earth but only at discrete locations such as all stations of the International VLBI Service for Geodesy and Astrometry (IVS) and International GNSS Service (IGS) since 1984. IGS repro data have been available since 1995. Because of this, the aforementioned empirical mapping functions are used, which can be used at any date and station, independent of numerical weather models (e.g. in case no download of the newest NWM possible due to bad/no internet connection) but its spatial resolution is limited as it cannot model short term variations.

For more information and differences between some of those mapping functions, refer to Böhm (2004). More on the differences of empirical mapping functions can be found in Möller et al. (2014) and Böhm et al. (2015).

Another way to determine the delay is to use ray-tracing, which can determine the path delay directly without using models or an estimation in the data analysis together with mapping functions. From radiosonde or NWM data the refractivity field of the the atmosphere can be calculated. With it, the path delay can be obtained by integrating

the refractivity along the propagation path of the signal. As the propagation path is not known, the ray-tracing technique is used to obtain the ray path and optical length. Ray-tracing is relevant in many fields of science and used where the propagation of an electromagnetic wave through a stratified medium has to be quantified. The main advantages of ray-tracing is the increased accuracy of positioning estimates, as the standard approach of using mapping functions can not model such events accurately (e.g. for extreme weather situations like a tornado or typhoon) and it can be used if no pressure values are available from a station. Disadvantages are the time and computation power needed (done for every single observation and the latter is not so relevant in times of increasing computing power, but still, more precise numerical weather models are needed for the computation). Work on ray-tracing can be found in Landskron et al. (2015) and Hofmeister (2016) and further studies are imminent.

The third term of equation 2.3 accounts for the atmosphere, which is not equally "thick" due to Earth rotation (i.e. at the equator it is "thicker" due to the centrifugal force). This effect is called azimuthal asymmetry and causes path delays measured from stations at northern latitudes to stations at southern latitudes to be larger than towards the north. Another cause for this effect is due to different weather conditions for different azimuths (rain clouds for example). That means that the gradients can be divided into a systematic part (variable thickness) and random part (different weather conditions). The gradients are separated into a hydrostatic and a wet part as well.

All of the above methods and mapping functions are only valid for the assumption of azimuthal symmetry around the station as mentioned above. There are two concepts to model the gradients in the analysis. These are the models of MacMillan (1995) and Chen and Herring (1997). It is to note that the estimation of gradients is important for space geodesy techniques, especially for low elevation angles.

2.1.2 Vienna VLBI Software (VieVS)

Most of this subchapter is based on the VieVS manual, which can be found at Böhm et al. (2012). Here, only the modules and methods used for this thesis are briefly discussed. The VLBI analysis is done with the software VieVS, which has been developed at the Vienna University of Technology. It consists mainly of the three modules: INIT, MOD and LSM. In the INIT (initialising) module, the NGS files of the stations, which take part in the calculation, are read. The observations are stored in the NGS files and are the main input files for VieVS.
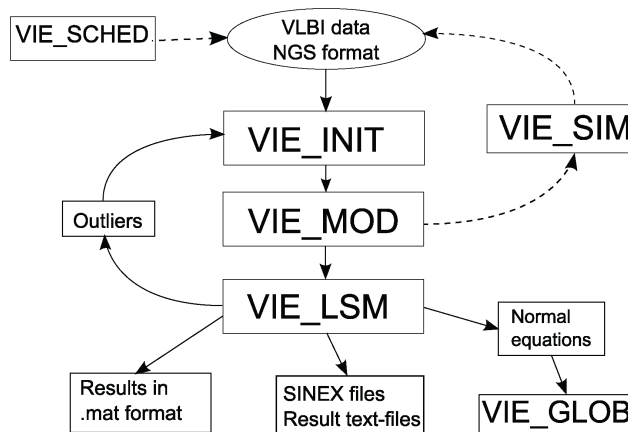
Figure 2.2: Principle of VieVS [Böhm et al., 2012]

The following information is stored:

- Header - including a description of the data set

- Stations - rough coordinates in [m]

- Radio Source - position in right ascension and declination

- Auxiliary parameters

- Data - other data parameters

More on the structure and content of NGS files can be found at IVS (1983). In the MOD (modeling) module, the calculation of the theoretical delays and their partial derivatives is carried out. Finally, in the LSM (least squares method) module, several variables are estimated including the ZWD (see Figure 2.2).

Of the many features and functionalities of VieVS, the command *Mk_list* was used to create a process list including every session in which a station took part in a given timeframe. So called ns codes are necessary, which are shortcuts of all VLBI stations provided by the International VLBI Services for Geodesy and Astrometry (IVS). The list can be found under IVS (2016b).

After a complete VieVS run, the estimated zenith delays are selected and displayed in the Submenu Plotting - Parameters. It is to note that those values are not exactly the "true" results but very close to them - they still represent an estimation. These datasets of every

single station can be exported and then be displayed with a plotting tool programmed in Matlab.

One important aspect of the VieVS processing is the usage of external tropospheric files, which provides an efficient way to choose e.g. which pressure acquisition method is used for calculating the ZWD. It is also the only way to apply the empirical troposphere model GPT2w at the moment as it is not possible yet in standard VieVS.

For the creation of the external tropospheric files, so-called AzEl files have to be available for all considered VLBI observations. AzEl-files are files available for every VLBI session and contain the exact time, azimuth and elevation (hence their name AzEl) of every observation and additionally involve in-situ measured meteorological data of all stations.

2.1.3 Internation VLBI Service for Geodesy and Astrometry (IVS)

The International VLBI Service for Geodesy and Astrometry (IVS) is a collaboration of organizations to provide geodetic products based on Very Long Baseline Interferometry (VLBI) and to promote research together with all participating organisations. It makes an important contribution in providing the Earth Orientation Parameters (EOP) and in establishing the International Celestial Reference Frame (ICRF). The respective organization for GNSS is the International GNSS Service (IGS) (see 2.2.4).

Figure 2.3: Map of the stations from the IVS Network [IVS, 2013]

One of the important products of the IVS are the CONT campaigns, which use continuous VLBI sessions to show what the highest accuracy achievable with VLBI currently is. It was performed irregularly over several years since 1994, but the last four CONT campaigns (CONT 05, CONT08, CON11, CONT14) were realized in the regular interval of three years and provide fast and high-resolution rotation rates and other important data such as reference frame stability and investigations of daily to sub-daily site motions [Schlüter and Behrend, 2007].

Figure 2.4: Map of the stations used in the CONT14 campaign [IVS, 2016a]

2.2 Global Positioning System (GPS)

The United States Global Positioning System (GPS) represents, together with the European Galileo, the Russian GLONASS and the Chinese BeiDou, the current Global Navigation Satellite System (GNSS) systems of the world. At the time of the writing of this thesis, GPS (since 1995) and GLONASS (since 2011) are fully operational. Galileo has 15 of 30 satellites in orbit [IGS, 2016b] and BeiDou became operational with 10 satellites in China by the end of 2012 for regional measurements and in mid 2015, China started the build-up of the 3rd generation BeiDou system with five in-orbit validation satellites launched already [IGS, 2016a]. Galileo and BeiDou are scheduled to be fully operational at 2020.

This chapter should only outline the basics of the comprehensive GPS system as it was the only system fully operational for the given time frame (1995-2007). For further studies please refer to Kaplan and Hegarty (2005) which this chapter is mostly based on, unless otherwise specified.

2.2.1 Basic Principle

The navigation principle of GPS is based on measuring pseudoranges between a receiver and at least four satellites (three satellites are used to determine the position and the fourth is needed to provide the difference between satellite and user clock).

GPS consists of the following three segments:

- Space Segment

- Control Segment

- User Segment

2.2.1.1 Space Segment

The GPS space segment is configured in six equally spaced (i.e. 60 degree from each other) orbital planes, each of them carrying four satellites and inclined 55 degree to the equator. This arrangement enables visibility of at least four satellites for almost every point on the Earth at all times and has a period of circulation of exactly 12 hours sidereal time (which equals to 11h 58min solar time). Therefore it consist of 32 active satellites, which rotate in nearly circular medium range orbits (MEO) at a height of approximately 20240 km around the earth [U.S.Naval Observatory, 2016].

Figure 2.5: *GPS Constellation [Kaplan and Hegarty, 2005]*

Every satellite sends out two carrier waves with a base frequency of 10.23 MHz, which is modulated onto two carrier frequencies called L1 (1575.42 MHz) and L2 (1227.60 MHz), after multiplication with the factors 154 and 120, respectively.

These two signals are the so called PRN-Code (Pseudo Range Noise), which consists of a random sequence of ± 1 which repeats itself after a certain length. The L1 signal consists of the C/A code (Coarse/Acquisition Code) and the P-code (Precise Code) and the L2 signal only transmits the P-code. The C/A code is open for civilians to use but the P-code is restricted only for military use. With the help of those codes, which have a special pattern for every single satellite, every single satellite can be distinguished from each other.

2.2.1.2 Control Segment

The control segment has the following tasks:

- Control the satellite system to determine the GPS system time

- Pre-estimate the satellite ephemeris and the satellite clock behavior

- Save the satellite navigation data into the memory of every satellite

It consists of a master station in Colorado Springs, USA, four ground antennas and 16 globally distributed monitoring stations. In the latter the satellite signals are received and sent to the master station together with meteorological data. Their future satellite ephemeris and future behavior of the satellite clocks are calculated, then sent back as message to the ground antennas and subsequently to the satellites.

2.2.1.3 User Segment

In order to receive the satellite signals, the user requires a suitable receiver, which can be any GPS receiver available on the market. Since those receivers usually have quartz clocks and no atomic clock (unlike the clock in the satellites, which makes them much more affordable) the user receives pseudo ranges instead of true distances.

2.2.2 Measuring Methods

For GPS observations a distinction is made between code measurement and phase measurement.

2.2.2.1 Code Measurement

The GPS receiver generates a reference signal, which gets phase shifted until the correlation between the reference signal and the received signal from the satellite reaches a maximum. At the point of maximal correlation in the receiver it is possible to determine the pseudo distance.

The observation equation for the code measurement is as follows:

$$L_c = p + c * \Delta t_u + c * \Delta t_a + c * \Delta t_T + c * \Delta t_I + \epsilon_R \tag{2.11}$$

p ... Geometrical distance
Δt_u ... Clock synchronization error of the receiver
Δt_a ... Error of the satellite clock to GPS Time
Δt_T ... Tropospheric propagation delay
Δt_I ... Ionospheric propagation delay
ϵ_R ... Measuring noise

2.2.2.2 Phase Measurement

In the phase measurement, the observable is the difference between the sent carrier phase from the satellite and the phase of the reference signal from the receiver. From this phase difference, a fraction of the distance can be derived from the wavelength. The problem lies in the determination of phase ambiguities, which is the unknown number of full wavelengths between the two signals. The determination of those ambiguities is one of the most demanding problems in the GPS evaluation.

The observation equation for the phase measurement is as follows (same as the code measurement but with an extra ambiguity term):

$$L_p = p + c * \Delta t_u + c * \Delta t_a + c * \Delta t_T - c * \Delta t_I - c * \frac{N}{f_{CR}} + \epsilon_R \qquad (2.12)$$

N ... Ambiguity

f_{CR} ... Frequency of the carrier

2.2.3 Accuracy Determination

In this section some factors limiting the accuracy of GPS measurements are presented.

2.2.3.1 Satellite Geometry

An important aspect for the accuracy of the GPS measurements is the geometric configuration of the used satellites. In satellite geodesy a scalar variable called DOP (Dilution of Precision) is introduced which is the standard deviation of a single pseudo distance measurement s_r and the associated standard deviation of of the geolocation s σ_r. There are many DOP notations like for example for the horizontal geolocation (HDOP) or for the vertical geolocation (VDOP).

2.2.3.2 Ionosphere

In the ionosphere the signal gets delayed due to the electron content along the signal path. The delay depends on the Total Electron Content (TEC) and the used frequency. Other parameters influencing the measurement are sun activity and the earth magnetic field. With measuring in two frequencies the effects from the ionosphere can be eliminated to a large part. Work on the ionosphere can be found in Hobiger (2006) who made comprehensive studies on the ionosphere itself.

2.2.3.3 Troposphere

The troposphere is the main subject of this thesis and the effect is explained in detail in the subchapter 2.1.1.1.

2.2.3.4 Multipath

Besides the direct signal received from the satellite also detour signals, which arrive from reflections near the receiver, are picked up. The direct and indirect waves overlay and create a signal with the same frequency but with a phase shift. Multipath effects can be recognized if a bad batch of received data occurs at the same time over and over again.

GPS is more prone to multipath effect than VLBI due to the smaller elevation angle. Common solutions to avoid multipath effects are to try not to use a GPS receiver near metal objects or to shield the antenna.
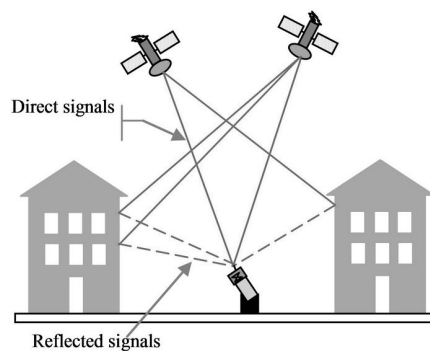
Figure 2.6: Principle of Multipath [Kumar et al., 2013]

2.2.3.5 Cycle Slips

This effect happens during carrier phase measurements if the GPS receiver loses track of the satellite and thus loses the current phase information (i.e., skips an integer number of cycles). Cycle slips can be caused by obstructions, low satellite elevation or weak signal-to-noise ratio.

Many of these systematic errors can be eliminated through the formation of differences of first order.

Two security policies have been put in place from the US government for civilian usage, which are Selective Availability (SA) and Anti Spoofing. If SA is turned on, the signals sent from the satellites get purposely distorted. Anti Spoofing causes an encryption of the P-code, which can only be decrypted with a special decoder that only the military own.

2.2.4 International GNSS Service (IGS)

The International GNSS Service (IGS) provides geodetic and geophysical research products for all GPS users and works tightly together with the International Earth Rotation Service (IERS), which on the other hand provides an important contribution for the calculation of the coordinates of points in the International Terrestrial Reference Frame (ITRF). The service started on January 1, 1994 and provides the following products and advantages:

- Orbit data from GPS satellites

- Satellite- and receiver clock information

- EOP, coordinates and velocity of IGS stations

- Tropospheric and ionospheric information

- Phase- and pseudo distances

For the calculation of those parameters the IGS uses measurement data from a wide range of stations available around the world (see Figure 2.7)
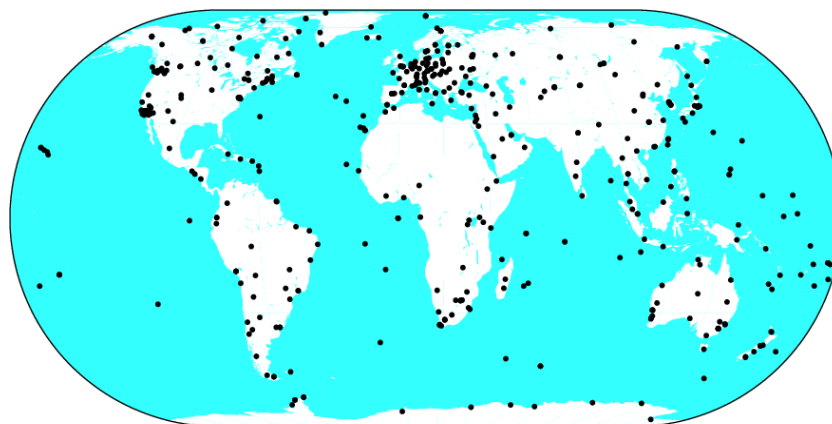
Figure 2.7: Map of the stations from the IGS Network [IGS, 2015]

Chapter 3

Previous Work on the Determination of Trends in ZWD

There have been several studies developed over the years in the research on the troposphere and its effects. One of the most important ones was the dissertation of Böhm (2004) on the subject of tropospheric delays with VLBI which laid the foundation for many of the following projects. In his thesis he used data from the ECMWF to derive the VMF which is, due to the data from the NWM, a more precise way to map the the hydrostatic and wet zenith delays down to lower elevations. He also showed that the VMF is superior over the mapping function of choice at that time, the Niel mapping function (NMF).

Gradinarsky et al. (2002) did a climate monitoring over Scandinavia from 1993 to 2000 using GPS measurements. The main subject was to study Precitable Water Vapor (PWV) trends over Scandinavia for this time series and to study the effects of antenna radome changes, which distort the result. The estimated trends showed an increase of 0.1 to 0.2 mm/year in PW especially in the south-west region. The trend was much larger in the winter periods than in the summer periods in the southern parts and vice versa for the northern regions of Scandinavia. It was concluded that the PWV trends can not always be used as reference for a temperature change, due to limited temporal and spatial resolution of the measurements.

Jin et al. (2007) determined the ZTD from 1994-2006 using GPS measurements with a time resolution of two hours. A goal was to determine the secular trend and seasonal variations of the ZTD. The mean secular trend was about 1.5 mm/year at all GPS sites. Lower mean ZTD values were located at higher altitudes and latitudes and higher mean ZTD values were located at middle-low latitudes. Also the mean ZTD decreased with increasing altitude. The trend (which showed the secular variation) showed that it was

positive for most of the northern hemisphere and negative for most parts of the southern hemisphere (except the Antarctic).

Steigenberger et al. (2007) used both GPS and VLBI to determine a long term trend for the ZWD over a time period of eleven years and compare those two to each other. Co-located sites were used as the homogeneity of the reprocessed GPS and VLBI time-series showed a very good agreement in the estimated troposphere parameters for both methods. Issues mentioned in their work were systematic offsets between the two techniques with different software packages, GPS tracking problems and other errors not considered (antenna phase center variations and equipment change). Also the trends estimated using the two techniques only agreed when the ZTD estimates from both techniques were available simultaneously, demonstrating that the estimated trend is very sensitive to the time period used. The bias between GPS and VLBI estimates for ZWD was generally smaller than 4 mm.

Heinkelmann (2008) wrote his PhD thesis on the determination of long term trend in zenith delays determined from VLBI observations in which he researched the possibilities of using long term time series of VLBI measurements for climate studies. He used data from IVS stations and compared those to IGS stations and data from the ECMWF in the time frame of 1984-2007. The IVS stations alone and the combination with the IGS stations showed in general overall good agreement, with a mean bias of the ZWD of 0.89 mm and RMS of 7.67 mm alone and a mean bias of 6.6 mm and RMS of 8.6 mm in combination. The combination with ECMWF data was not as consistent as the mean bias was 2.0 mm and RMS 20.4 mm. He concluded that this error could be due to outliers and artificial breaks in the pressure measurements and that further research is necessary to provide a trustworthy climate study.

Nilsson and Elgered (2008) determined long-term trends in the atmospheric water vapor over a time frame of 10 years, using 33 GPS measurement sites in Sweden and Finland. The data yielded a linear trend in the integrated water vapor (IWV) range from -0.2 to 1.0 $\frac{kg}{m^2 decade}$. Still the authors concluded that a ten year period is too short to obtain stable values for the estimated trends, but that the values measured are realistic.

Ning et al. (2012) determined the ZWD on the west coast of Sweden (Onsala Space Observatory and Landvetter Airport for RS observations) using different methods (GPS, VLBI, water vapor radiometer, radiosonde observations and data from ECMWF). Comparisons between three co-located techniques (GPS, VLBI, and WVR) resulted in mean values of the ZWD differences at a level of a few millimetres. The best agreement is

seen in the GPS-VLBI comparison with a mean difference of - 3.4 mm and a standard deviation of 5.1 mm over the ten year period.

This thesis will be primarily based on the dissertation of Heinkelmann (2008), but includes other stations, a somewhat longer time series (30 years) and a more modern software. It is hoped to get a better picture in what direction the climate is changing with the help of longer time series.

Chapter 4

Analysis

This chapter describes the analysis from the selection of the measuring stations to the determination of the trend.

4.1 Data Description

In this section the description of the datasets and analysis of the different methods will be explained.

For the understanding of the analysis, some basics of the VLBI analysis itself need to be explained beforehand. As mentioned in section 2.1.2 the usage of external tropospheric files is used to choose, which pressure acquisition method is selected to calculate the zenith hydrostatic delay (using Saastamoinen, equation 4.1). That means that the ZWD can be estimated with VLBI, either using pressure directly from the stations (NGS), from Numerical Weather Models or from an empirical model like GPT2w, if none of the options before are available. The ZWD is estimated with GPS and VMF1 measurements as well (See Chapter 5):

1. VLBI - Three different pressure acquisition methods

   a) Pressure at the site from NGS-file

   b) Pressure obtained from Numerical Weather Model (from the ECMWF)

   c) Pressure from Empirical model Global Pressure and Temperature2 (GPT2w)

2. GPS

3. VMF1 with data from Numerical Weather Model (NWM)

4.1.1 Selection of measuring sites

Observations of measurement sites are needed to determine the ZWD, therefore a selection of several sites was done based on VLBI station availability. As seen in Figure 4.3, not all stations measured constantly, either due to financial reasons or to little sensitivity of the antenna. Another criterium was the usage of stations which took part in the CONT14 campaign starting from May 6, 2014 00:00 UT and lasting through the May 10, 2014 24:00 UT. These eleven stations (not all stations of the campaign were chosen) provide the highest accuracy of which the current VLBI system is capable of (see more in 2.1.3). They also measure continuously and have good repeatability in measurements. It was also checked if there is a GNSS measuring site nearby. This was the case for eight stations which were used for subsequent analysis.

Seven other VLBI stations were chosen as well to provide a good global distribution which is important for a global capture of the atmospheric water vapor. This is quite challenging with VLBI as most of the stations are on the northern hemisphere (mostly USA, Europe and Japan) while the African continent and parts of Asia lack completely of VLBI stations (see Figure 4.1). Because of the globally inhomogeneous distribution of the stations, the small number in the southern hemisphere play a larger role in the analysis. In Figure 4.2 the VLBI and GPS measurements sites are displayed on a world map.
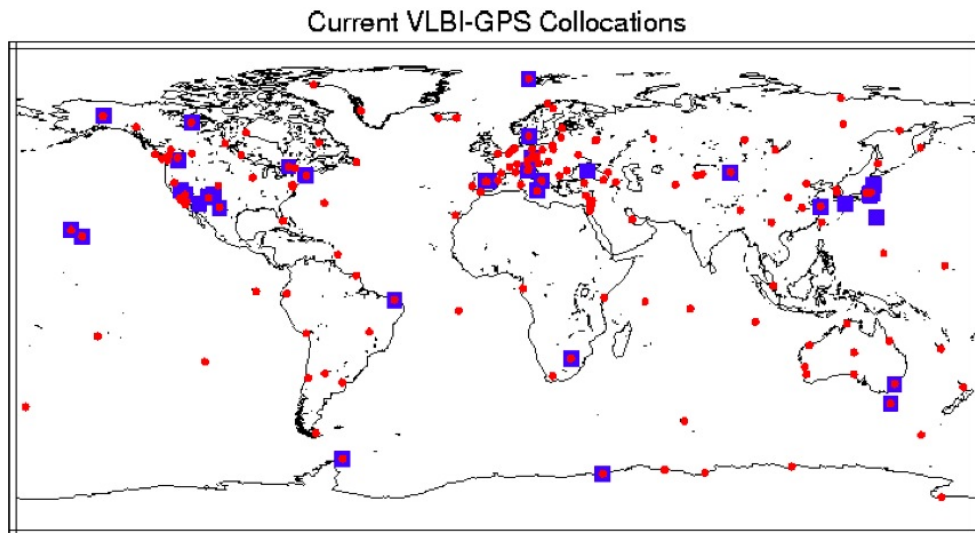
Figure 4.1: *VLBI - GPS Colocations (Red Dots - only GPS, Blue Squares - co-located Sites - VLBI + GPS measurement possible) [Altamimi and Rothacher, 2005]*

Table 4.1: VLBI stations (18 in total) used in the analysis

Station Name	Latitude[°]	Longitude[°]	Station Height [m]	Description
Algopark	45.9	281.9	224.0	Algonquin Park, Canada
Badary	51.8	102.2	821.6	Badary, Russia
Fortleza	-3.9	321.6	23.1	Fortaleza, Brazil
Gilcreek	64.9	212.5	332.1	Gilmore Creek, USA
Hartrao	-25.9	27.7	1415.7	Hartebesthoek, S. Africa
Hobart26	-42.8	147.4	65.1	Hobart, Australia
Kashim34	35.9	140.7	72.3	Kashima, Japan
Kokee	22.1	200.3	1176.6	Kokee Park, USA
Matera	40.6	16.7	543.4	Matera, Italy
Medicina	44.5	11.6	67.2	Medicina, Italy
Nyales20	78.9	11.9	87.3	Spitsbergen, Norway
Onsala60	57.4	11.9	59.3	Onsala, Sweden
Seshan25	31.1	121.1	29.4	Shanghai, China
Tigoconc	-36.8	286.9	171.0	Concepcion, Chile
Tsukub32	36.1	140.1	84.4	Tsukuba, Japan
Westford	42.6	288.5	86.8	Westford, USA
Wettzell	49.1	12.9	669.1	Wettzell, Germany
Zelenchk	43.8	41.6	1175.1	Zelenchukskaya, Russia

Table 4.2: GPS stations (8 in total) used in the analysis

Station Name	Latitude[°]	Longitude[°]	Station Height [m]	Description
Algo	45.9	281.9	202.0	Algonquin Park, Canada
Hob2	-42.8	147.4	41.1	Hobart, Australia
Ksmv	35.9	140.7	57.9	Kashima, Japan
Mate	40.6	16.7	535.6	Matera, Italy
Medi	44.5	11.6	50.0	Medicina, Italy
Onsa	57.4	11.9	45.5	Onsala, Sweden
Tskb	36.1	140.1	67.3	Tsukuba, Japan
Wes2	42.6	288.5	85.0	Westford, USA
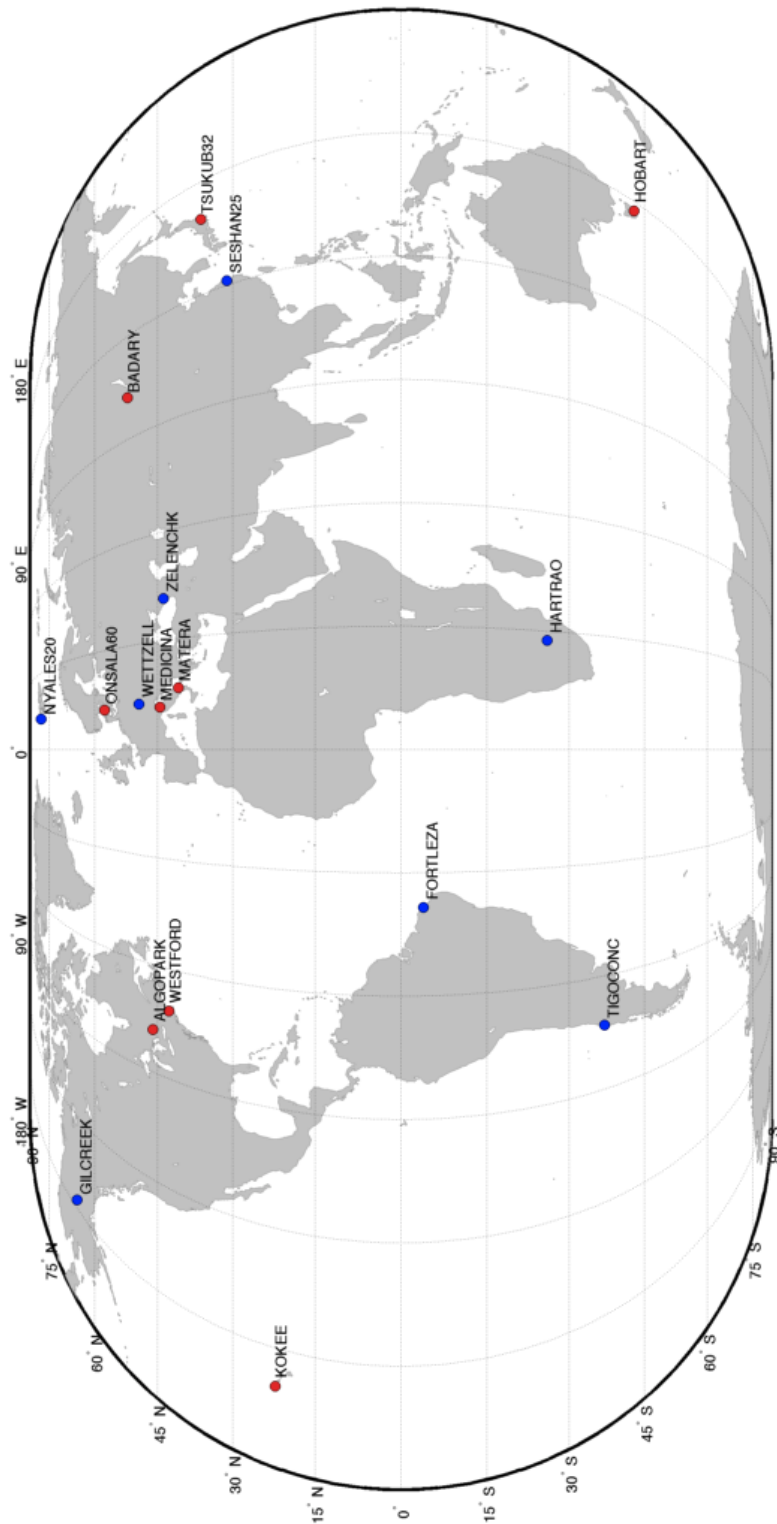
***Figure 4.2:** Used VLBI and GPS locations, Blue dots = only VLBI measurements, Red dots = co-located measuring stations (VLBI+GPS)*

Figure 4.3: *VLBI station availability [Bachmann et al., 2014]*

4.1.2 Determination of offsets in in-situ pressure records

Before starting with any processing, it was checked if there are offsets available in the datasets. They play a large role in the analysis as they can produce large errors and can occur at any station. The reasons for such offsets can be that the pressure sensor at the station is faulty and gets exchanged for a new one or that it is not placed properly. The installation of a new pressure sensor is often not noted from the station keeper. To find this offsets, pressure values from any station are plotted and a manual search for offsets is done. Another way often described in the literature is to use a standard homogeneity test.

The offset determination, which uses GPT2w as pressure reference value, is working on the assumption that the trend changes linearly over the time series. Because of this the smallest possible window should be chosen to determine the break. The mean is taken for only a few years before the break, called the faulty time series (FT) and a few years after the break (TS). Therefore the data is not smoothed too strongly. The corrected time series (CT) is then calculated by subtracting the offset from the FT.

$$Offset = mean(FT) - mean(TS) \qquad \text{and} \qquad CT = FT - Offset$$

Table 4.3: Offset correction at VLBI stations

Station Name	MJD-Start	MJD-End	Offset [hPa]
Hartrao	47965	49111	13.36
Hobart26	47795	48607	15.93
Zelenchk	53726	54391	9.90

Table 4.4: Pressure breaks and correction from Heinkelmann et al. (2007)

Station Name	MJD-Start	MJD-End	Offset [hPa]
Algopark	48068	52656	-2.8
Gilcreek	46501	49164	1.4
Kokee	49356	52807	1.6
Nyales20	49749	50995	2.8
Wettzell	46433	46649	1.9

An example of the correction of an offset is seen in Figure 4.4 for the station Hartrao. This correction is done for the time series with the values listed in Table 4.3. It is to note that the correction seen in 4.4 is only for vizualization purposes as the correction is done in VieVS with the external tropospheric files.
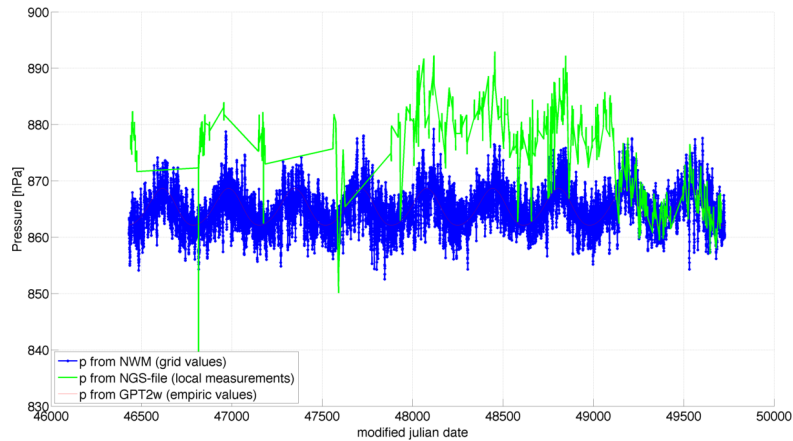
(a) Station Hartrao with Offset
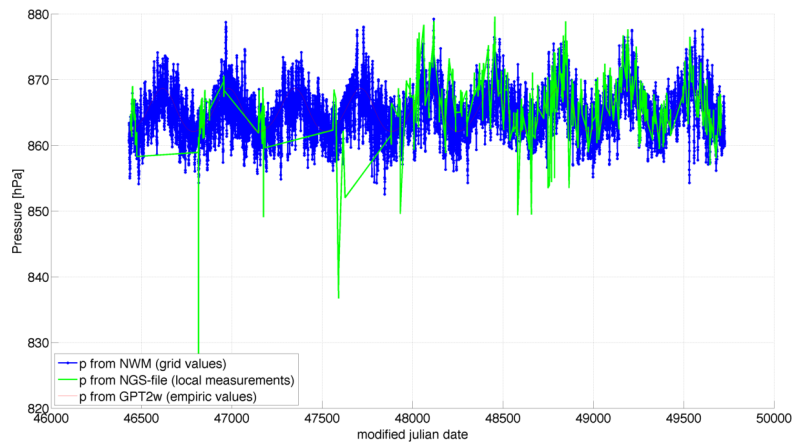
(b) Station Hartrao with corrected Offset

Figure 4.4: *Offset correction at station Hartrao (Correction of -13 hPa from 47965 to 49111 MJD), note that there are visible outliers for the local measurements (NGS) - green line*

The pressure breaks mentioned in Heinkelmann et al. (2007) for stations Algopark, Gilcreek, Kokee, Nyales20 and Wettzell were applied too (see Table 4.4). These breaks were determined by Heinkelmann using a standard normal homogeneity found in Alex-

andersson and Moberg (1997). These pressure values are considered when creating the external tropospheric files, for the NGS methods in the VieVS calculation. The figures for the correction of the offset (just visualization) at Hobart26 and Zelenchk can be found in the appendix.

```
if strcmpi(azel{8}(i_obs),'HOBART26')  &&  azel{2}(i_obs) > 47795  &&  azel{2}(i_obs) < 48607
    p_NGS = p_NGS-15.9316;
end
```

Figure 4.5: *Extract of the modification of the external tropospheric creation file at the station Hobart26*

4.1.3 Outlier Elimination

Also it was checked if the datasets contain any outliers in the in-situ pressure records as they can also produce large errors in the analysis later on. For this, so called statistical errors were removed, with a formal error exceeding the threefold mean formal error (3σ) for the whole time series.

There is an upper (UL) and lower limit (LL), which are calculated with the following equations:

$$UL = mean(p) + 3\sigma(p) \qquad \text{and} \qquad LL = mean(p) - 3\sigma(p)$$

This was unfortunately not possible to do before the VieVS analysis as single bad observations can not be excluded. Therefore the elimination of the outliers happened after the analysis for the ZWD time series itself. Before removing statistical outliers, so called physical outliers are eliminated as well. The limit for the physical outliers were defined as > 0.5 m and < -0.3 m. In Figure 4.6, a physical outlier at the station Kokee is shown on the September 11, 2011 with a pressure value of 313.81 hPa. This is only for visualization purposes and shows that large errors in the pressure can occur.

It should be noted that it would be possible to replace outliers in the pressure with data from Numerical Weather Model or if necessary GPT2w.

In Table 4.5 the number of physical and statistical outliers are displayed for the different pressure acquisition methods for the ZWD values.

Looking at Table 4.5 it seems that there are some systematical physical outliers occuring at most of the stations even though there are some stations where there are no outliers at all. For the statistical outliers there is no pattern visible but there is clearly a big number of statistical outliers at station Gilcreek and for the pressure input GPT2w at stations Hartrao and Tigoconc for the ZWD values.

Table 4.5: *Number of outliers to eliminate for the pressure acquisition methods NWM, NGS and GPT2w after the VieVS analysis for the ZWD data*

Station Name	Phy. Outliers (NWM/NGS/GPT2w)	Stat. Outliers (NWM/NGS/GPT2w)
Algopark	- /-/-	53/60/78
Badary	25/25/25	-/-/-
Fortleza	43/42/39	7/7/16
Gilcreek	-/-/5	165/183/261
Hartrao	-/-/6	32/43/289
Hobart26	25/25/25	11/13/15
Kashim34	-/-/-	2/2/2
Kokee	26/26/26	-/-/19
Matera	25/25/25	1/1/2
Medicina	-/-/-	6/6/12
Nyales20	25/25/25	2/1/26
Onsala60	25/25/25	-/-/32
Seshan25	-/-/1	-/-/18
Tigoconc	75/75/83	33/33/246
Tsukub32	25/25/25	-/-/-
Westford	25/26/25	1/-/14
Wettzell	26/26/26	4/14/215
Zelenchk	25/25/25	2/1/-
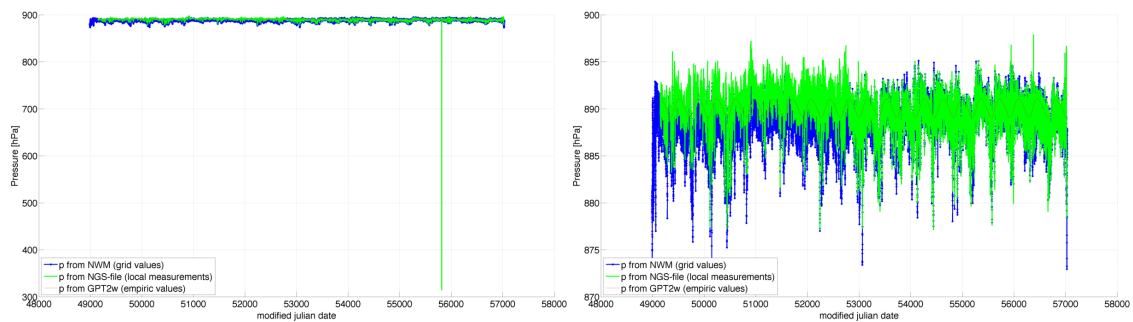
Figure 4.6: *Example of an outlier in the pressure data (correction not done in the thesis), Left: Physical outlier at station Kokee, Right: Result of the time series after elimination (visualization)*

4.2 Very Long Baseline Interferometry (VLBI)

The analysis of the VLBI data is done with VieVS for every station providing data in a one hour interval. For the VieVS analysis and for the determination of the hydrostatic zenith delay pressure values at the stations are needed, which can be obtained with the methods mentioned in Section 4.1.

All of these methods use the vievsTRF for the analysis but for the NWM calculation additionally the ITRF2014 was chosen as reference frame in order to compare the results to each other. The reason for this was to check if the usage of a different reference frame produces different values in the ZWD determination as different station heights might do.

The ZWD is estimated using a piecewise linear function (PWLF) with VMF every 60 minutes and a relative constraint of 1.5 cm after 60 minutes.

Table 4.6: Observation time VLBI data

Station Name	Time Span	# of years
Algopark	1984-2006	22
Badary	2007-2014	7
Fortleza	1993-2014	21
Gilcreek	1984-2005	21
Hartrao	1986-2014	18
Hobart26	1989-2014	25
Kashim34	1990-2014	24
Kokee	1993-2014	21
Matera	1990-2014	24
Medicina	1987-2014	27
Nyales20	1994-2014	20
Onsala60	1984-2014	30
Seshan25	1988-2014	26
Tigoconc	2002-2014	12
Tsukub32	1998-2014	16
Westford	1984-2014	30
Wettzell	1984-2014	30
Zelenchk	2005-2014	9

Heinkelmann (2008) mentioned that there is a correlation between the station height and the ZWD and that differences can occur when using different a priori TRF. He stated that this is only relevant for the determination of ZWD when the station coordinates are assumed to be fixed and are not estimated in the analysis. If the station coordinates are estimated in the the analysis, as it is the case with VieVS, then the a priori TRF does not play a significant role. This was confirmed when doing the analysis for both of the TRF as differences of the ZWD trends were in the range of 0.02 to 0.07 mm/year for both of the TRF.

After the calculation several parameters can be chosen but only the ZWD (in [cm]) was exported (as seen in Figure 4.7 for the station Fortleza).

```
# This file contains plotted data values from the Vienna VLBI Software (VieVS).
# File was created on 13.06.2016 (10:29:45.0)
#
# =========================================
# Folder 1 (subfolder: NGS)
# parameter: zwd (unit: cm), antenna: FORTLEZA
#  mjd (%16.7e)    value (%16.7e)     std (%16.7e)
    4.9099083e+04   3.2874387e+01    3.9762943e+00
    4.9099125e+04   3.2068859e+01    3.7492623e+00
```

Figure 4.7: *Extract of output after VieVS analysis at the station Fortleza*

The gradients were not calculated as our goal is to determine the ZWD. Therefore, the assumption was, that we only measure the ZWD above the station and the azimuth (and therefore the gradients, which take the curvature of the atmosphere into account) does not play a role in the calculation. This was unfortunately not correct, as the VLBI observations measure in different elevations and azimuths and the gradients have therefore an (although small) influence on the ZWD.

With a simple plotting script the output of VieVS can be displayed, with doing the aforementioned outlier test beforehand to eliminate physical and statistical outliers.

4.3 Global Positioning System (GPS)

Data from the Global Positioning System is provided by the IGS which computes the so-called IGS Final Troposphere Estimates for its GNSS receivers. They are generated with a GPS software using precise point positioning (PPP) and GMF, using IGS final satellite orbits/clocks and EOP as input. The troposphere parameters, which are called Repro 1, can be downloaded from IGS (2010). Currently another reprocessing is in the works, called Repro 2 [IGS, 2014].

In the following work we used data from Repro 1 which are available from 1995 to 2007. It provides output parameters such as daily GPS orbits & satellite clocks, daily satellite & tracking station clocks, daily Earth rotation parameters, weekly terrestrial coordinate frames with ERPs and other products which benefit from the usage of fully consistent models for the whole time span as well as constant temporal resolution. In this thesis only the tropospheric zenith path delays were used. An example of a file can be found in Figure 4.8 at the station Hobart.

When looking at the datasets it was noticed that at not all stations measure continuously and that the ZTD is only provided in the second half of the year respectively. This is not always ideal because in general the ZWD is higher in the summer months than in the winter. In this case, a trend is used to take this situation into account and to compare it to the other methods. The trend is explained in more detail in Section 4.5.

The data contains the following information:

- Epoch format year

- Day of year

- Seconds of day for every location site

- Zenith Total Delay

- Standard deviation of ZTD

- North gradient

- Standard deviation of north gradient

- East gradient

- Standard deviation of east gradient

```
+TROP/SOLUTION
*SITE EPOCH_____ TROTOT STDEV  TGNTOT STDEV  TGETOT STDEV
 HOB2 98:003:00600 2386.5   3.0  -1.598 0.441   1.741 0.461
 HOB2 98:003:00900 2386.4   2.9  -1.598 0.437   1.749 0.457
```

Figure 4.8: Example of the repro1 tropospheric data at station Hobart

Every 300s (5min) the zenith total delay and north/east gradients are estimated. The observations are stacked to epochs every five minutes (0:00) to 85500s (23:45) each day. For the analysis of the ZWD only the first 4 columns of the dataset are needed. It is

also mentioned that the data measurement does not always start at 0:00 but sometimes at 0:05 or 0:10.

The challenge concerning this dataset is that it is available every 5 minutes, leading to very large amounts of data. For performance reasons, this dataset has to be reduced. The time frame chosen for the reduction of data is the same as the temporal resolution of the numerical weather models provided by the ECMWF every 6 hours (0:00, 6:00, 12:00, 18:00) (see Table 4.7)

To make sure that unreliable data is not used for the processing, an interpolation is needed. First a check is done if epochs at the times of of the ECMWF are available. If so, then these values are saved in a new array. If not, a search for all the values from 6 hours before and after a certain epoch is carried out. If the condition of data being available five epochs before and after is fulfilled, a Spline interpolation is done

This makes sure that unreliable data is not used for the processing. Last of all, if the criteria is not fulfilled then no interpolation is done and the datapoint is neglected. As seen in Table 4.7 the reduction of the dataset of all the stations is enormous at minimum -97% of the original data and helps to reduce the processing time without losing valuable information.

Table 4.7: Number of GPS data points after interpolation

Station Name	Station Code	# of data points	# of data points after Interpolation	Data reduction in %
Algopark	algo	1150495	18989	-98.35
Hobart	hob2	976382	17657	-98.19
Kashima	ksmv	247300	8561	-96.54
Matera	mate	1139140	18953	-98.34
Medicina	medi	846983	15073	-98.22
Onsala	onsa	1108167	16157	-98.54
Tsukuba	tskb	1063646	17409	-98.36
Westford	wes2	656723	17529	-97.33

The ZTD can be converted indirectly into ZWD with the equation of Saastamoinen (1972). For this equation only the pressure at the station (in hPa), latitude and longitude (in radians) and the station height (in m) have to be known. The pressure is calculated with the empirical method GPT2w.

The equation is as follows:

$$ZHD = \frac{0.0022768 * p}{1 - 0.00266 * cos(2 * dlat) - 0.00000028 * hell} \tag{4.1}$$

Table 4.8: Observation time GPS data

Station Name	Station Code	Time Span	# of years
Algopark	algo	1995-2007	12
Hobart	hob2	1995-2007	12
Kashima	ksmv	2001-2007	6
Kokee	kokb	1995-2007	12
Matera	mate	1995-2007	12
Medicina	medi	1996-2007	11
Onsala	onsa	1996-2007	11
Tsukuba	tskb	1995-2007	12
Westford	wes2	1995-2007	12

The calculated ZHD can then be subtracted from the ZTD to get the ZWD.

4.4 Vienna Mapping Function 1 (VMF1)

The European Centre for Medium-Range Weather Forecasts (ECMWF) provides meteorological data since the year 1984 measured with radiosondes, which can be used to develop tropospheric delay models based on coefficients that hold for certain stations and time series. The total zenith delays contained in these data sets are derived by numerical integration through pressure values. The Vienna Mapping Functions (VMF1), created by Böhm and Schuh (in 2004) and revised by Böhm (in 2005), map the zenith delay from the vertical to the observation elevation angles. They are based on ray-tracing through numerical weather models and use ECMWF operational pressure level data for the mapping functions for the VLBI and GPS stations.

The parameters are provided station wise with a six-hourly interval for selected sites, which is the usual temporal resolution for NWM Data and also used for the GPS data as mentioned above.

VMF1 uses data from operational numerical weather models provided four times a day. As seen in Section 5.3 this data based on predictions is not ideal for determining a ZWD trend. For a trend study reanalysis data would be better suited but they are only

published a few times per year and as VMF1 has to be available at any time, this data is not usable for this study.

The VMF1 data is freely available for research purposes at the Research Group Advanced Geodesy (2016) for every year and consists of the following information (see example in Figure 4.9):

- Station Name

- Modified Julian date

- Hydrostatic mapping function coefficient

- Wet mapping function coefficient

- Hydrostatic zenith delay in [m]

- Wet zenith delay in [m]

- Mean temperature of the atmosphere above the site in [K]

- Pressure at the site in [hPa]

- Temperature at the site in [C]

- Water vapour pressure at the site in [hPa]

- Orthometric height of the station in [m]

```
YLOW7296  52271.25  0.00121077  0.00057164  2.2876  0.0233  260.5  1005.54  -20.08  0.96  205.9
AIRA      52271.50  0.00122965  0.00056981  2.2521  0.0692  267.1   987.57    6.06  6.43  290.9
ALGOPARK  52271.50  0.00119301  0.00052151  2.1952  0.0335  256.4   965.11   -7.08  3.04  260.7
```

***Figure 4.9:** Example of the VMF1 data for the year 2002*

The ZWD and the corresponding MJD are extracted from the datasets for each year, and displayed with a script to view the ZWD.

4.5 Trend of Zenith Wet Delay (ZWD)

To compare results from the different datasets to each other, a trend has to be implemented to get a statement how much the values have changed over a certain time.

First, the following methods were used:

- Linear regression $y = k * x + d$

- Polynomial curve fitting $y = a * x^2 + b * x + c$

However, both of these fitting methods did not prove to be very successfully because both of them cannot model the annual and semi-annual variations of the data properly. The variations are visible as a big peak for the annual variation and a smaller peak for the semi-annual variation. As no other significant peaks are seen, it is indicated that it is sufficient to use an annual and a semiannual term to describe the seasonal variations. For this the following trend, called seasonal fit, was implemented:

$$
\begin{aligned}
y = A_0 + A_1 \cdot cos(2 \cdot \pi \cdot doy/365.25) + B_1 \cdot sin(2 \cdot \pi \cdot doy/365.25) + \\
A_2 \cdot cos(4 \cdot \pi \cdot doy/365.25) + B_2 \cdot sin(4 \cdot \pi \cdot doy/365.25) + k \cdot doy
\end{aligned}
\tag{4.2}
$$

where the doy is the day of year, $A_{1,2}$ and $B_{1,2}$ are coefficients representing the annual and semi-annual variation and A_0 and k are the coefficients of the offset and the trend respectively. The coefficients A_0, A_1, B_1, A_2, B_2, and k are estimated in the least-squares calculation.

The seasonal terms can be used to determine the seasonal component amplitudes which describe how much the seasonal fit is swing off by that term:

$$
C_{1,2} = \sqrt{A_{1,2}^2 + B_{1,2}^2}
\tag{4.3}
$$

This seasonal fit is the most precise of all of these three solutions because it considers the above mentioned annual and semi-annual variations. It is to note that only linear variations can be modeled with it and no exponential increases of the ZWD (which is physically possible, but more probable only for even longer time series). The longer the time series, the sooner the slope approaches the same result for all three trend variation

methods. The change of ZWD per year is then calculated through multiplication of the slope k with 365,25 and displayed in Table 4.9 and in subsequent sections.

As already mentioned in Section 4.3, the GPS data is not always consistently provided so especially for uncertain data like this, the trend equation with annual and semi-annual terms is the most reliable one.

The trends from the VMF1 Data with the differences of the ZWD for every method is displayed in Table 4.9 with the related standard deviation respectively.

Table 4.9: Comparison of the different trend methods using VMF1 Data

Station Name	Seasonal Fit (mm/year)	Linear Fit (mm/year)	Polynomial Fit (mm/year)
Algopark	-0.37 ± 0.02	-0.33 ± 0.04	8.99 ± 1.28
Badary	-0.68 ± 0.07	-0.85 ± 0.18	-47.91 ± 19.9
Fortleza	-1.17 ± 0.03	-1.37 ± 0.05	-9.07 ± 2.42
Gilcreek	-0.26 ± 0.01	-0.24 ± 0.02	4.84 ± 0.81
Hartrao	-0.91 ± 0.02	-0.95 ± 0.03	11.59 ± 1.22
Hobart26	-0.29 ± 0.02	-0.32 ± 0.03	4.11 ± 1.07
Kashim34	-0.32 ± 0.04	-0.21 ± 0.07	20.13 ± 3.20
Kokee	-0.58 ± 0.02	-0.53 ± 0.03	16.79 ± 1.60
Matera	0.27 ± 0.02	0.32 ± 0.03	5.57 ± 1.27
Medicina	0.24 ± 0.02	0.29 ± 0.03	-2.03 ± 1.26
Nyales20	-0.05 ± 0.02	-0.02 ± 0.03	3.79 ± 1.44
Onsala60	0.03 ± 0.01	0.07 ± 0.02	5.62 ± 0.88
Seshan25	-0.86 ± 0.04	-0.81 ± 0.07	13.85 ± 2.88
Tigoconc	-1.43 ± 0.07	-1.53 ± 0.07	-53.08 ± 6.31
Tsukub32	-1.18 ± 0.06	-0.92 ± 0.13	-1.57 ± 8.82
Westford	-0.18 ± 0.03	-0.14 ± 0.04	8.96 ± 1.42
Wettzell	-0.13 ± 0.01	-0.10 ± 0.02	-2.57 ± 0.85
Zelenchk	-0.54 ± 0.08	-0.36 ± 0.14	-14.12 ± 15.9

As seen in Table 4.9 the trend using the polynomial fitting is not usable at all and yields unrealistic results. On the other hand, the linear trend and the seasonal fit produce very similar results. One could argue why the seasonal trend should be used as it is more complex and more complicated to calculate than the linear trend. But as the ZWD

increase or decrease is calculated with the slope and the given time series, even small differences can make a very big difference. The standard deviation is better at almost every station with a minimum of $\pm$ 0.01 mm/year as well for the seasonal fit.

For example the station Onsala, with a measuring time span of 30 years, produces an increase of the ZWD of 1.0 mm for the seasonal fit and 2.1 mm for the linear trend. This is more than 1 mm difference for this station and ranges to ± 4 mm for all stations.

Chapter 5

Results and Comparison

In the following sections the results of the analysis will be shown for the different methods separately and then further comparisons with each other will be made. Most of the results will be explained for station Onsala as this station has been used in many studies before and provides trustworthy data over a long time series.

5.1 Very Long Baseline Interferometry (VLBI)

The analysis of the VieVS data produces very different results between the different pressure acquisition methods for the trend. The values for the ZWD variation are calculated using the coefficient k multiplied with 365.25 and range from -1.4 to 4.0 mm/year.

When looking at the stations individually the station Zelenchk produces very high values for almost all pressure acquisition methods. For the NGS files the reason could still be more undetected offsets which falsify the determined ZWD even though known offsets have been already corrected before the analysis. But also with GPT2w and NWM as pressure input, Zelenchk shows very doubtful values in comparison with values from other stations which cannot be explained by the before mentioned challenges.

Table 5.1: *1a) Coefficients VLBI p=NGS - mean=A_0, annual and semi-annual amplitude=C_1 and C_2 and the seasonal fit trend=k,*

Station Name	$A_0(mm)$	C_1 (mm)	C_2 (mm)	k (mm/year)
Algopark	80	61.2	11.0	**-0.1 ± 0.08**
Badary	60	61.9	24.8	**-0.8 ± 0.13**
Fortleza	260	52.4	7.1	**0.2 ± 0.03**
Gilcreek	50	48.2	18.0	**0.5 ± 0.02**
Hartrao	90	62.9	6.5	**0.7 ± 0.04**
Hobart26	80	24.7	3.3	**1.0 ± 0.04**
Kashim34	150	109.6	33.1	**-0.1 ± 0.13**
Kokee	90	14.4	5.7	**0.1 ± 0.03**
Matera	100	42.1	3.2	**0.2 ± 0.03**
Medicina	120	56.4	2.4	**0.0 ± 0.05**
Nyales20	30	28.7	13.4	**0.6 ± 0.01**
Onsala60	80	41.7	9.5	**0.3 ± 0.03**
Seshan25	180	134.4	32.8	**-0.1 ± 0.12**
Tigoconc	90	12.0	4.0	**-0.3 ± 0.07**
Tsukub32	140	122.3	27.7	**-0.1 ± 0.10**
Westford	100	68.4	12.9	**0.4 ± 0.03**
Wettzell	80	44.7	6.6	**0.4 ± 0.01**
Zelenchk	60	52.3	7.8	**4.0 ± 0.12**

The result of the data processing is displayed for the VLBI data at Figure 5.1 for station Onsala60. It can be seen that there is an increase of 0.2 to 0.3 mm/year with NWM and NGS but a decrease of -0.1 mm/year when using the empirical model GPT2w. This shows how variable the ZWD is and that even small changes in the pressure values can lead to different ZWD values. This processing is done for every station and the plots for all VLBI stations can be found in the Appendix.

It seems that GPT2w produces the most realistic results but as it is an empirical model (assuming a constant pressure) determining a trend with data from GPT2w is not always reliable.

Table **5.2:** *1b) Coefficients VLBI p=NWM*

Station Name	$A_0(mm)$	$C_1(mm)$	$C_2(mm)$	k (mm/year)
Algopark	80	62.4	11.4	**0.3 ± 0.08**
Badary	60	60.8	25.5	**-1.0 ± 0.13**
Fortleza	260	52.3	6.9	**-0.1 ± 0.03**
Gilcreek	50	47.8	17.2	**0.3 ± 0.02**
Hartrao	110	63.3	6.4	**0.0 ± 0.04**
Hobart26	90	25.1	1.2	**0.3 ± 0.04**
Kashim34	150	109.5	33.4	**-0.2 ± 0.13**
Kokee	100	14.3	5.9	**-0.1 ± 0.03**
Matera	100	42.1	3.2	**0.3 ± 0.03**
Medicina	120	56.9	1.9	**0.2 ± 0.05**
Nyales20	40	28.1	12.7	**0.4 ± 0.02**
Onsala60	90	41.1	9.3	**0.2 ± 0.03**
Seshan25	180	134.0	33.4	**0.1 ± 0.12**
Tigoconc	90	12.0	4.1	**-0.2 ± 0.07**
Tsukub32	150	122.3	27.9	**-0.4 ± 0.10**
Westford	90	68.5	13.6	**0.7 ± 0.03**
Wettzell	80	44.7	6.9	**0.3 ± 0.01**
Zelenchk	70	53.8	7.0	**1.6 ± 0.11**

Table **5.3:** *1c) Coefficients VLBI p=GPT2w*

Station Name	$A_0(mm)$	$C_1(mm)$	$C_2(mm)$	k (mm/year)
Algopark	80	60.1	12.0	**0.5 ± 0.08**
Badary	60	64.3	23.2	**-1.0 ± 0.15**
Fortleza	260	51.0	6.9	**0.0 ± 0.03**
Gilcreek	60	49.1	18.6	**0.1 ± 0.03**
Hartrao	110	62.6	5.4	**-0.1 ± 0.04**
Hobart26	90	22.0	3.1	**0.4 ± 0.04**
Kashim34	150	107.7	30.8	**-0.2 ± 0.12**
Kokee	90	14.3	5.8	**-0.1 ± 0.03**
Matera	100	41.6	2.7	**0.0 ± 0.03**
Medicina	130	55.9	3.2	**-0.2 ± 0.05**
Nyales20	40	28.3	12.4	**0.3 ± 0.03**
Onsala60	90	41.2	5.4	**-0.1 ± 0.03**
Seshan25	180	134.5	30.8	**0.1 ± 0.11**
Tigoconc	90	11.1	3.8	**-0.3 ± 0.06**
Tsukub32	150	121.0	36.4	**-0.3 ± 0.10**
Westford	100	35.6	13.9	**0.3 ± 0.03**
Wettzell	90	43.8	7.6	**-0.1 ± 0.02**
Zelenchk	70	55.1	7.9	**1.8 ± 0.11**
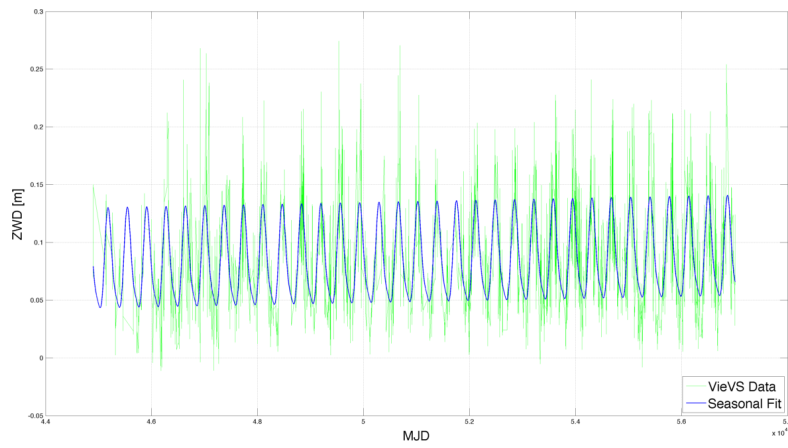
(a) Onsala60 VLBI p=NGS, Trend = 0.3 mm/year
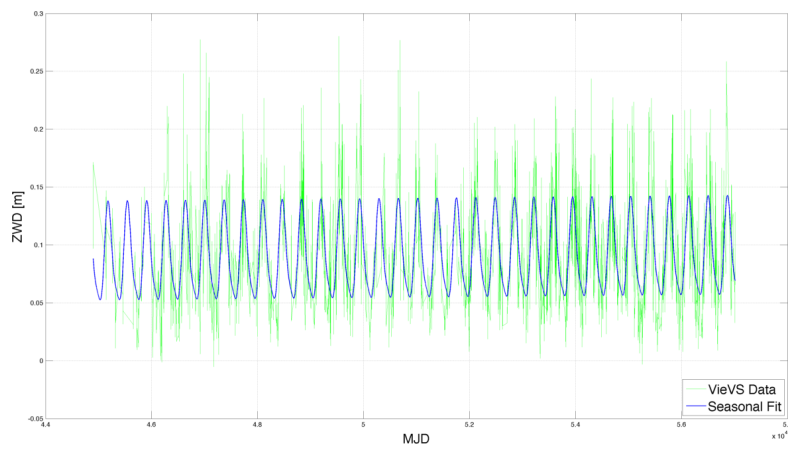
(b) Onsala60 VLBI p=NWM, Trend = 0.2 mm/year
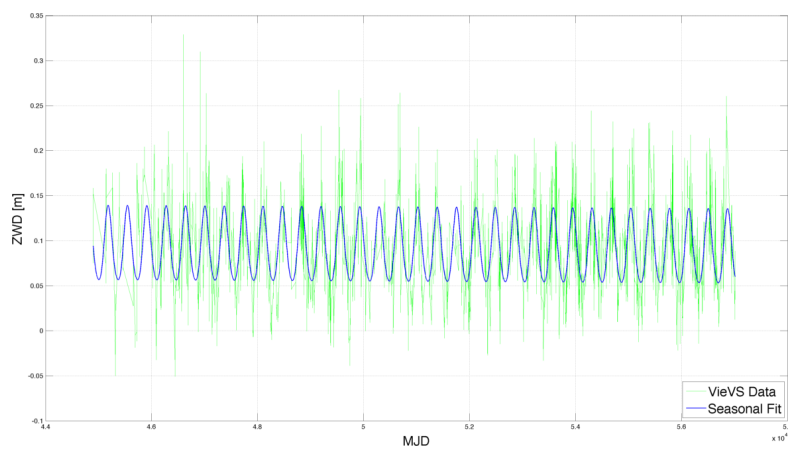
(c) Onsala60 VLBI p=GPT2, Trend = -0.1 mm/year

Figure 5.1: *Data processing of VLBI data at station Onsala60*

In Figure 5.2 the increase of the ZWD in mm/year is outlined on a world map. The big increase at Zelenchk is clearly visible for all methods. There is also a similar decrease at Badary, Tsukub32 and Tigoconc and a similar increase at Nyales20, Gilcreek, Westford and Hobart26.

Possible errors and causes for the different results of the different methods could be due to unprecisely known antenna heights, faulty pressure sensors, gravitational or thermal VLBI antenna deformation or systematic errors in the meteo data of the NGS file (which actually have been corrected beforehand). Another cause could be that the solution of the model for the ZWD is based on a piecewise linear function which is visible at stations where there is a high frequency of earthquakes like for example Gilcreek. When the trend is calculated and during the calculation a moving of the plates happens, the trend gets adjusted (piece-wise with a relaxation phase) until it slowly gets normal again.
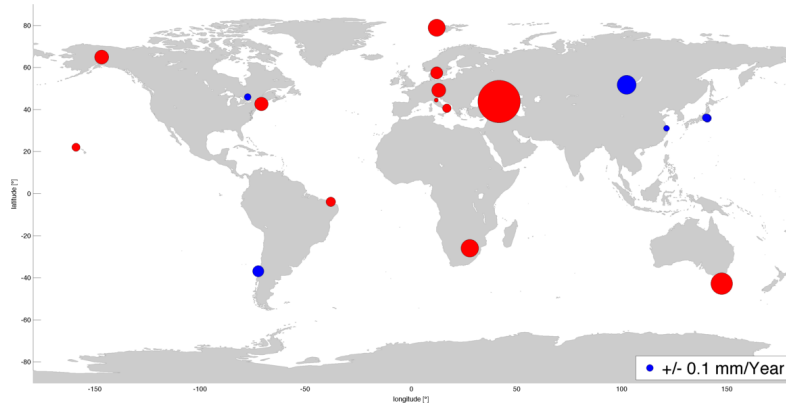
(a) *VLBI p=NGS, Trend = -0.8 to 4.0 mm/year*
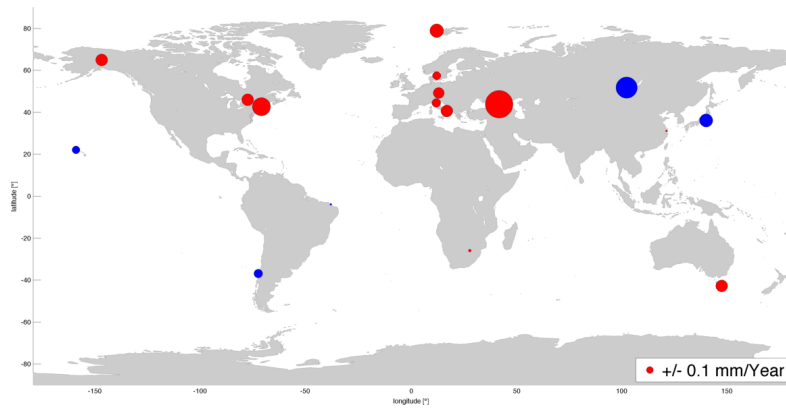
(b) *VLBI p=NWM, Trend = -1.0 to 1.6 mm/year*
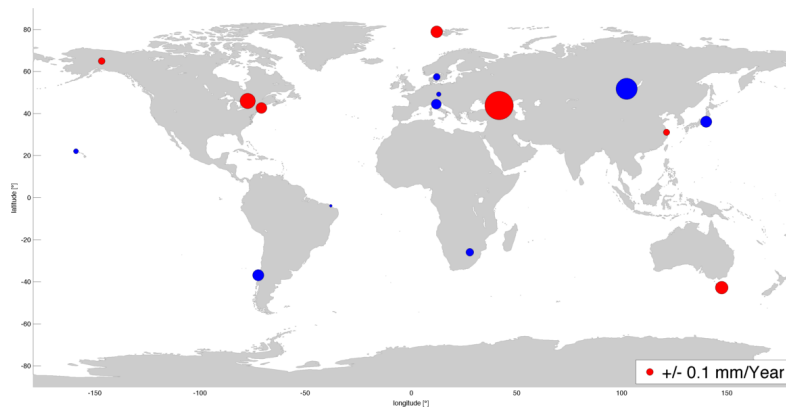
(c) *VLBI p=GPT2w, Trend = -1.0 to 1.8 mm/year*

***Figure* 5.2:** *ZWD trends of the Seasonal Fit for VLBI data, Red=Increase, Blue=Decrease*

5.2 Global Positioning System (GPS)

The results for the seasonal fit from the GPS data, range from -0.6 to 1.4 mm/year. Due to the short observation time of the GPS measurements (6 - 12 years), it is very hard to make a trustworthy statement about ZWD changes with just GPS alone. Again, when looking at the coefficients, it can be seen that the stations Kashim and Tsukuba have very large annual amplitudes compared to other stations.

Table 5.4: *2) Coefficients GPS - mean=A_0, annual and semi-annual amplitude=C_1 and C_2 and the seasonal fit trend=k*

Station Name	$A_0(mm)$	C_1(mm)	$C_2(mm)$	k(mm/year)
Algopark	90	61.5	12.9	**0.3 $\pm$ 0.08**
Hobart	100	23.7	4.8	**-0.3 $\pm$ 0.09**
Kashima	150	116.9	24.4	**1.4 $\pm$ 0.10**
Matera	100	38.5	1.4	**0.2 $\pm$ 0.07**
Medicina	120	56.8	6.3	**0.3 $\pm$ 0.11**
Onsala	90	45.1	9.5	**0.8 $\pm$ 0.09**
Tsukuba	150	123.9	25.1	**0.3 $\pm$ 0.12**
Westford	110	68.6	17.8	**0.3 $\pm$ 0.13**
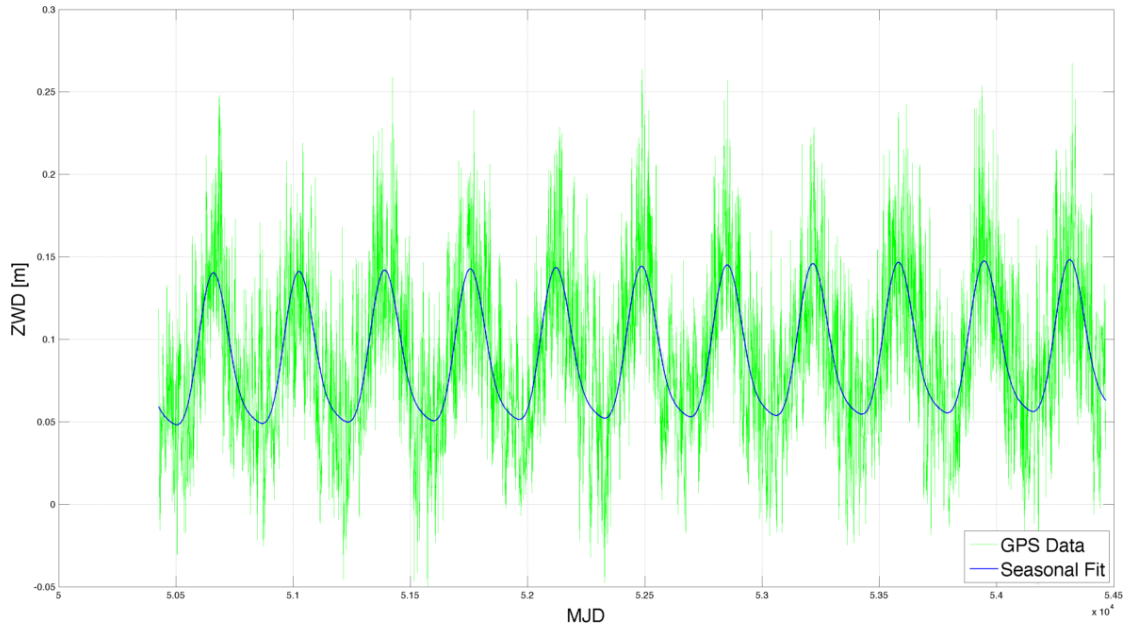
Figure 5.3: *Data processing of GPS data at station Onsala, Trend = 0.8 mm/year*

The ZWD increase of 1.4 mm/year at station Kashima seems to be very high in contrast to other stations. The reason for this can also be tectonic movements in this area (although there is no such increase or decrease at station Tsukuba, which is only 53.38 km away from Kashima).

Figure 5.4: *ZWD trends of the seasonal fit for GPS data, Red=Increase, Blue=Decrease, Trend = -0.3 to 0.8 mm/year*

Errors for the GPS measurements can be diverse. First, tectonic movements affect the stations itself. Then there are effects such as multipath that was discussed in the theory part of this thesis. It can be negated or weakened when using radomes shielding the station from reflected signals. Slow slip events can occur as well, altering the signals. Further there are many errors which can happen on the antenna itself. These are antenna changes, antenna deformations through heat or cold or other "human errors" like wrong antenna height or that the wrong or no specific antenna type is listed and therefore the position of the antenna center is unknown.

Another error is that that GPS uses minimum four satellites in different directions in contrast to VLBI which looks into one direction. Therefore it is possible that one of the GPS signals passes trough a local varying wet atmosphere layer [Kaplan and Hegarty, 2005].

The ZHD is determined with GPT2w so the trend is determined with constant pressure and therefore it is very hard to determine a trend using constant values.

5.3 Vienna Mapping Function 1 (VMF1)

The mean ZWD variation obtained from ECMWF data range from -1.2 to 0.3 mm/year. Looking at the seasonal fit in Table 5.5 it can be seen that most of the stations show a negative trend (all except Matera, Medicina and Onsala60). This is astonishing as the data from VieVS and GPS do not display that many negative trends. This could be due to the usage of operational forecast data and, as mentioned in the theory part, may not be reliable for long term climate studies as its predicted values vary strongly after one or two days.

The stations Kashim34, Seshan25 and Tsukub32 have very high annual amplitudes in comparison to other stations.

Table **5.5:** *3) Coefficients VMF1 - mean=A_0, annual and semi-annual amplitude=C_1 and C_2 and the seasonal fit trend=k*

Station Name	$A_0(mm)$	$C_1(mm)$	$C_2(mm)$	k (mm/year)
Algopark	100	66.1	10.6	**-0.4 ± 0.02**
Badary	70	62.7	21.9	**-0.7 ± 0.07**
Fortleza	270	56.0	6.6	**-1.2 ± 0.03**
Gilcreek	70	47.6	18.1	**-0.3 ± 0.01**
Hartrao	130	63.3	6.6	**-0.9 ± 0.02**
Hobart26	110	23.4	2.4	**-0.3 ± 0.02**
Kashim34	160	119.4	25.5	**-0.3 ± 0.04**
Kokee	100	15.8	3.8	**-0.6 ± 0.02**
Matera	100	39.3	0.9	**0.3 ± 0.02**
Medicina	120	58.2	4.9	**0.2 ± 0.02**
Nyales20	50	30.4	12.1	**-0.1 ± 0.02**
Onsala60	90	44.7	9.6	**0.0 ± 0.01**
Seshan25	190	124.7	31.7	**-0.9 ± 0.04**
Tigoconc	100	11.0	3.4	**-1.4 ± 0.07**
Tsukub32	160	124.0	27.1	**-1.2 ± 0.06**
Westford	120	71.9	13.7	**-0.2 ± 0.03**
Wettzell	90	45.4	6.9	**-0.1 ± 0.01**
Zelenchk	80	51.4	8.3	**-0.5 ± 0.08**

The high data density of VMF1 is seen in Figure 5.5 at the station Onsala60. This is characteristic for all the stations with ECMWF data. The almost global decrease in ZWD can be seen on a world map in Figure 5.6. Data from the ECMWF, used by VMF1, is actually one of the most reliable datasets. But as VMF1 - forecast data was used in

the analysis and not reanalysis data, it is challenging to determine a long term change of the ZWD.
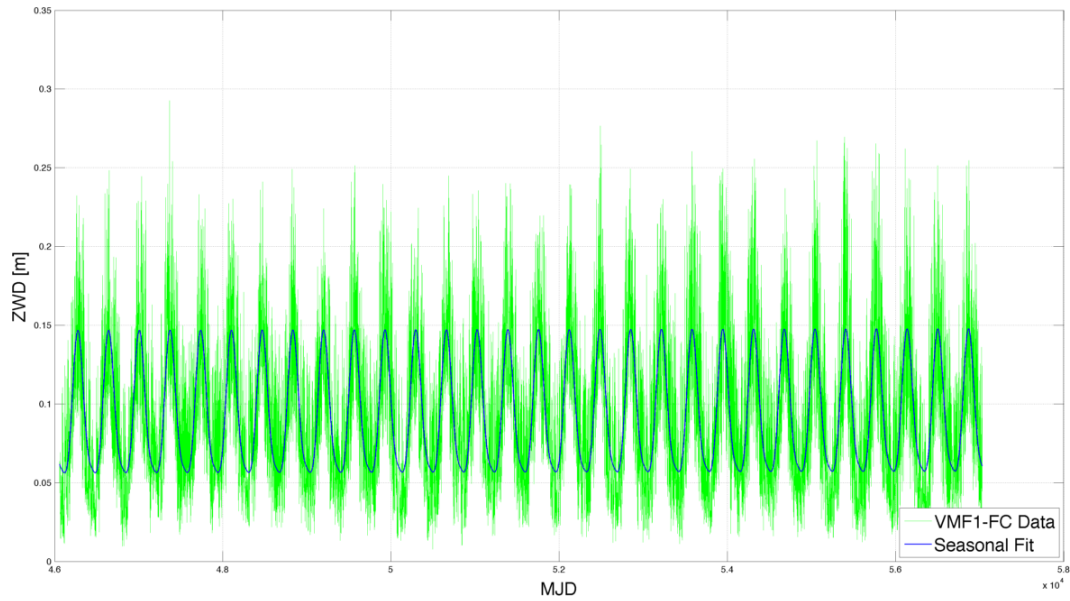
Figure **5.5:** *Data processing of VMF1 data at station Onsala60, Trend = 0.03 mm/year*
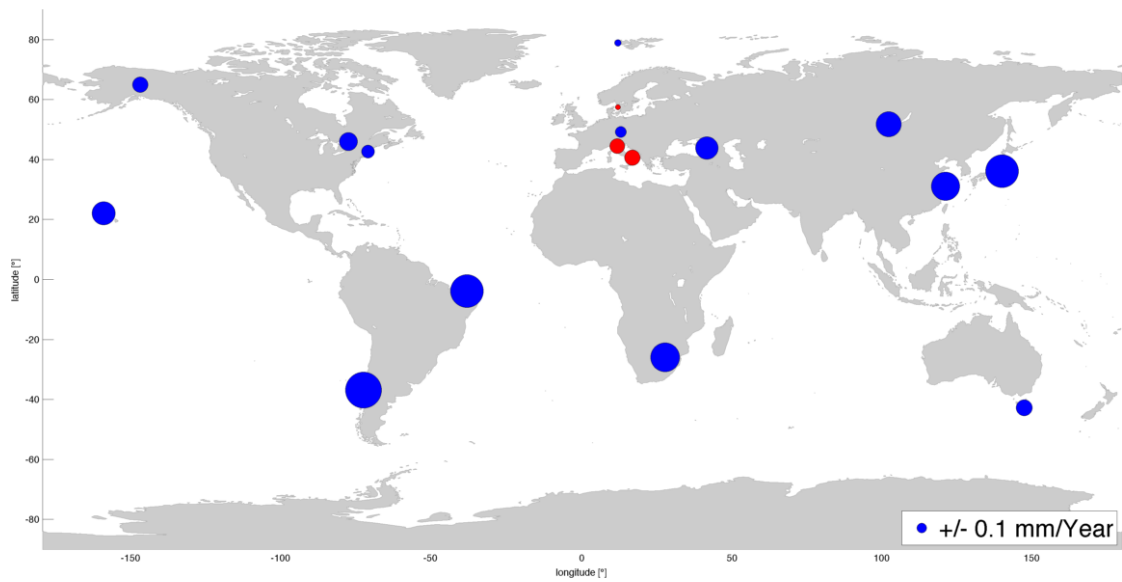
Figure **5.6:** *ZWD trends of the seasonal fit for VMF1 data, Red=Increase, Blue=Decrease, Trend = -1.4 to 0.3 mm/year*

5.4 Comparison

In this section the results will be compared to each other with the help of correlations, standard deviations and mean calculation. The solutions of the trends will only represent the seasonal fit from now on and the linear and polynomial fit will not be used anymore.
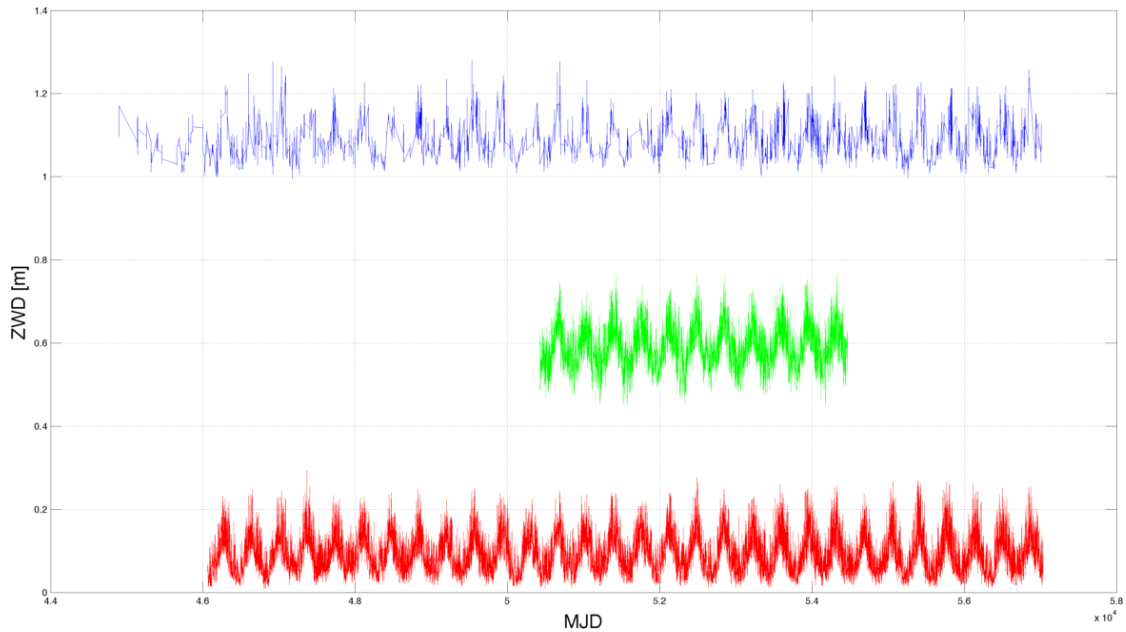
Figure 5.7: *Example of all methods combined at station Onsala, red=ECMWF, green=GPS + 0.5m, blue=VLBI(p=NWM) + 1m*

In Figure 5.7 the times series of the ZWD derived from the different techniques is displayed at the station Onsala. An offset of 0.5 m and 1 m has been added to the time series from GPS and VLBI respectively. In Figure 5.10 the determined ZWD trends for all methods (and all stations) are displayed in a bar graph for comparison purposes as well.

When comparing the coefficients of the different methods, there are high annual amplitudes at the stations Tsukub32, Seshan25 and Kashim34 over 100 mm in contrast to other stations. The mean of the ZWD from the different methods for all stations fit very well together. Noticeable is the slightly higher mean values of the the VMF1 data in comparison to the other methods.

While calculating the correlations of the ZWD trends over all methods it is noticed that the GPS data deviates very strongly from the other methods and even produces negative

correlations, as seen in Figure 5.8. Reasons for the deviation could be the low data basis of the stations and that the observation time is too short and therefore the climate signal is undersampled.

$$
\begin{array}{c}
\begin{array}{ccccc}
VMF1 & VieVS-NWM & VieVS-NGS & VieVS-GPT2w & GPS
\end{array} \\
\begin{array}{c}
VMF1 \\
VieVS-NWM \\
VieVS-NGS \\
VieVS-GPT2w \\
GPS
\end{array}
\left(
\begin{array}{ccccc}
1 & 0.36 & 0.11 & 0.16 & 0.19 \\
0.36 & 1 & 0.86 & 0.93 & -0.11 \\
0.11 & 0.86 & 1 & 0.89 & -0.42 \\
0.16 & 0.93 & 0.89 & 1 & -0.32 \\
0.19 & -0.11 & -0.42 & -0.32 & 1
\end{array}
\right)
\end{array}
$$

Figure 5.8: *Correlation of ZWD trends over all methods*

The VMF1 data produce a significant deviation to the other datasets. In Heinkelmann (2008) it was noted that the dataset of the IVS differed strongly from the data of the ECMWF. This is also the case in this thesis and very unfortunate as it was hoped that with the new ERA-interim data (including the new improved wet delay determination), new and useful information could be obtained. Also higher standard deviation for stations with a smaller observation time, are apparent for all methods.

5.4.1 Vienna VLBI Software (VieVS) Methods

Badary, Gilcreek, Nyales20 and Westford produce very similar results ranging from ±0.2 mm between the VieVS methods. When calculating the correlation just between the data of the VieVS datasets then a better correlation is acquired then using all methods. But the high correlation is to be expected as the data is the same and the only difference is the pressure acquisition method used (see correlation in Figure 5.9)

$$
\begin{array}{c}
\begin{array}{ccc}
VieVS-NWM & VieVS-NGS & VieVS-GPT2
\end{array} \\
\begin{array}{c}
VieVS-NWM \\
VieVS-NGS \\
VieVS-GPT2
\end{array}
\left(
\begin{array}{ccc}
1 & 0.86 & 0.93 \\
0.86 & 1 & 0.89 \\
0.93 & 0.89 & 1
\end{array}
\right)
\end{array}
$$

Figure 5.9: *Correlation of ZWD trends for VLBI methods*

Figure 5.10: *Comparison of ZWD trends for all stations and all datasets*

5.4.2 Standard Deviation of ZWD trends

As expected the standard deviation is much smaller when comparing just the VLBI data alone than all methods together. Over all stations the standard deviation is smaller than 0.4 mm except for the station Zelenchk with a standard deviation over 1 mm, regardless the method used. Also the standard deviation of GPS with VMF1 is listed, with lower standard deviations at Kokee, Matera, Medicina and Hobart26.

One assumption was that there should be a lower standard deviation for stations close to polar areas because there is less humidity than in equatorial regions. This could not be confirmed as there is no visible pattern in the standard deviation.

***Table* 5.6:** *Standard deviation of ZWD trends for all stations with seasonal fit, 1st row: using only VLBI, 2nd row: using all methods, 3rd row: using GPS and VMF1 data*

Station Name	σ-VLBI [mm/year]	σ-All methods [mm/year]	σ-GPS - VMF1 [mm/year]
Algopark	0.3	0.4	0.4
Badary	0.1	0.1	-
Fortleza	0.2	0.6	-
Gilcreek	0.2	0.3	-
Hartrao	0.4	0.7	-
Hobart26	0.4	0.6	0.01
Kashim34	0.01	0.7	1.2
Kokee	0.1	0.3	-
Matera	0.2	0.1	0.02
Medicina	0.2	0.2	0.1
Nyales20	0.2	0.3	-
Onsala60	0.2	0.4	0.5
Seshan25	0.1	0.4	-
Tigoconc	0.1	0.6	-
Tsukub32	0.1	0.5	1.0
Westford	0.2	0.3	0.4
Wettzell	0.2	0.3	-
Zelenchk	1.3	1.8	-

Comparing the standard deviation of ZWD trends over all methods (see Table 5.7), then the 1 mm standard deviation at the station Zelenchukskaya is eye catching. This is obvious when looking at the standard deviation and the trend itself producing unrealistic

results. It is to note that when Zelenchukskaya is excluded from the calculation then the NGS result has the lowest standard deviation.

.

Table 5.7: Standard deviation of ZWD trends for all methods

Method	σ [mm/year]
VieVS - NGS	1.0
VieVS - NGS (excl. ZELECNHK)	0.4
VieVS - NWM	0.5
VieVS - GPT2w	0.5
GPS	0.6
VMF1	0.5

5.4.3 Mean of ZWD trend

Compared to Heinkelmann (2008) who used eight analysis centers and compared the ZWD to each others, only the stations Gilcreek, Hobart26, Matera, Nyales20, Seshan25 and Westford agree within ± 0.2 mm/year with the results listed in Table 5.10, representing the mean of ZWD trends averaged over all methods. The trends range from -1.4 to 1.8 mm/year (or 0.8 mm/year excluding Zelenchukskaya) for all stations and are mostly positive (even with the VMF1 data, providing more negative trend values).

Table 5.8: Mean of ZWD trends averaged over all stations

Method	Mean [mm/year]
VieVS - NGS	0.4 (-0.8 to 4.0)
VieVS - NWM	0.2 (-1.0 to 1.6)
VieVS - GPT2w	0.1 (-1.0 to 1.8)
GPS	0.2 (-0.3 to 1.4)
VMF1	-0.5 (-1.0 to 1.6)
All methods	0.1 (-0.5 to 0.4)

Taking the average over all stations, an assumption can be made that there is a worldwide increase of the ZWD of 0.1 mm/year. This statement is very doubtful as the high increase at station Zelenchukskaya is also included in the calculation, distorting the results and also the different methods do not seem to correlate very well as seen before. When

excluding station Zelenchukskaya, there is a decrease of -0.02 mm/year over all stations (see Table 5.9). Reason for this are the mostly negative ZWD trends in the VMF1 data and also the exclusion of station Zelenchukskaya with its high ZWD values for the trend.

Table 5.9: Mean of ZWD trends averaged over all stations excluding Zelenchukskaya

Method	Mean [mm/year]
VieVS - NGS	0.2 (-0.8 to 1.0)
VieVS - NWM	0.1 (-1.0 to 1.6)
VieVS - GPT2w	-0.04 (-1.0 to 0.5)
GPS	0.2 (-0.3 to 1.4)
VMF1	-0.5 (-1.0 to 0.3)
All methods	-0.02 (-0.5 to 0.2)

Table 5.10: Mean of ZWD trends averaged over all methods

Station Name	Mean [mm/year]
Algopark	0.1 (-0.4 to 0.5)
Badary	-0.9 (-1.0 to -0.7)
Fortleza	-0.3 (-1.2 to -0.0)
Gilcreek	0.2 (-0.3 to 0.5)
Hartrao	-0.1 (-0.9 to 0.7)
Hobart26	0.2 (-0.3 to 1.0)
Kashim34	0.1 (-0.3 to 1.4)
Kokee	-0.2 (-0.3 to 0.1)
Matera	0.2 (0.0 to 0.3)
Medicina	0.1 (-0.2 to 0.3)
Nyales20	0.3 (-0.1 to 0.6)
Onsala60	0.2 (-0.1 to 0.8)
Seshan25	-0.2 (-0.9 to 0.1)
Tigoconc	-0.5 (-1.4 to -0.2)
Tsukub32	-0.3 (-1.2 to -0.1)
Westford	0.3 (-0.2 to 0.7)
Wettzell	0.1 (-0.1 to 0.4)
Zelenchk	1.7 (-0.5 to 1.8)

5.5 Conversion into precipitable water (PW)

As seen with equation 2.10 the ZWD can be converted into precipitable water with the factor $\Pi=0.16$ and the density of liquid water (ρ_{H_2O}). The declaration of the trend in PW is equal to a trend with the ZWD with the proportional factor and therefore it is actually not needed to convert it for the trend determination. Nevertheless it is written down here for researchers in other fields than geodesy, like e.g. meteorology.

The results of the conversion of ZWD to PW [in mm/year] are listed in Table 5.11 below.

Table 5.11: Conversion from ZWD to Precipitable Water [mm/year]

Station Name	VieVS - NGS	VieVS - NWM	VieVS - GPT2w	GPS	VMF1
Algopark	-0.02	0.05	0.08	0.04	-0.06
Badary	-0.13	-0.15	-0.16	-	-0.11
Fortleza	0.03	-0.01	0.00	-	-0.19
Gilcreek	0.07	0.05	0.02	-	-0.04
Hartrao	0.11	0.00	-0.02	-	-0.15
Hobart26	0.17	0.05	0.06	-0.04	-0.05
Kashim34	-0.02	-0.03	-0.03	0.22	-0.05
Kokee	0.02	-0.02	-0.01	-0.10	-0.09
Matera	0.03	0.05	0.00	0.04	0.04
Medicina	0.01	0.03	-0.03	0.05	0.04
Nyales20	0.10	0.07	0.05	-	-0.01
Onsala60	0.05	0.02	-0.02	0.13	0.01
Seshan23	-0.01	0.01	0.01	-	-0.14
Tigoconc	-0.04	-0.03	-0.05	-0.23	-0.23
Tsukub32	-0.02	-0.06	-0.04	0.05	-0.19
Westford	0.07	0.11	0.04	0.05	-0.03
Wettzell	0.07	0.04	-0.01	-	-0.02
Zelenchk	0.63	0.26	0.28	-	-0.09

5.6 Comparison with other studies

To validate the results of the analysis, they are also compared to results from other studies. This is complementary to the results listed in Chapter 3.

Gradinarsky et al. (2002) measured an increase of ZWD from 0.1 to 0.2 mm/year for stations in Sweden and Finland over a time span of seven years using GPS measurements. Only positive trends were determined in general. In comparison station Onsala yields a ZWD from -0.1 to 0.8 mm/year for all methods in this thesis. Noticeable is the increase of 0.8 mm/year for the GPS measurement but as it is only for a time span of eleven years it might not be very meaningful.

On the other hand when comparing it to Nilsson and Elgered (2008) who measured a trend range from -0.2 to 1 mm/year over a time span of 10 years using GPS measurements over Scandinavia then the results are very similar to each other.

Steigenberger et al. (2007) showed that the trend is very sensitive to the time frame used and that GPS and VLBI only agree when the ZTD from both techniques are available simultaneously. This can be confirmed for the trend results in this thesis which deviate strongly for the GPS data to the other datasets.

Heinkelmann (2008) listed the linear trend in mm/year and for some of those stations the trend agrees very well (Gilcreek, Hobart26, Matera, Nyales20, Westford, all in the range of ± 1 mm/year) but for other stations it deviates partly strongly.

Chapter 6

Conclusion and Outlook

In this thesis the determination of atmospheric water vapor on the basis of VLBI and GNSS was examined. Although previous work yielded promising results in the combination of GNSS and VLBI measurements to determine the ZWD and validating them with each other, the results in this thesis did not always agree very well between methods. This is mostly the case for the trend determination of the datasets, which was one of the main goals for this work. The standard deviation between all methods ranges from 0.1 to 1.8 mm and 0.1 to 1.3 mm for just using VLBI. The mean ZWD trends for all methods range from -0.9 to 0.3 mm/year excluding the station Zelenchukskaya.

The results of the trend determination are not easy to interpret because of non-optimal correlation between the methods and problems in the datasets themselves. In the following paragraphs, possible errors in the datasets and possible solutions for them are explained.

The analysis of the VMF1 data produces negative trends over almost all stations in the analysis. This might be due to the usage of NWM using operational forecast data. It was found that this forecast data is not suitable to determine the ZWD over a long time span. Instead, future projects should be evolved on using reanalysis data instead, applying real weather observations collected over several decades and recreating past atmospheric conditions. This kind of data might be usable to yield good usable results in determining long term trends of the ZWD.

The GPS data has an observation period of only twelve years at maximum, so a longer time series after a few years would probably increase the chance for more reliable data. The accuracy of the data will increase in the future as well due to the introduction of new GPS signals and combinations with other GNSS systems. For the ZWD acquired with in-situ pressure values, we still experienced unrealistic results which is probably due

to undetected offsets in the measurements. Therefore further projects should focus on the detection and elimination of these offsets and to note antenna changes. Also GPT2w is used for the GPS data and with its constant pressure it is not very easy to determine a trend with it.

The NGS data for the VLBI analysis is not measured by meteorologists but by station operators who apparently not always check if the pressure sensor is installed properly. Therefore huge errors can accumulate over time which are then represented in the datasets. A project could be to either manually or with a standard normal homogeneity test detect those offsets and correct for them. Realistically the detection and the elimination of offsets and the validation of the general increase of the ZWD can probably only be obtained with more accurate and advanced data sets. The data from GPT2w seems to be the most reliable one but difficult to determine a trustworthy trend with it.

For both GPS and VLBI another error source could be the usage of non-calibrated weather stations which can both occur for data from the IVS and IGS.

Another possibility could be that the global distribution is not sufficiently even enough to make a valid statement for the global atmospheric water vapor. Still the local determined long term atmospheric water vapor can be used for further regional studies in the hope that a correlated trustworthy global atmospheric water vapor can be determined.

When doing the VieVS analysis with the ITRF 2014 instead of the vievsTRF minimal to no differences were found which was to expect, as the usage of the terrestrial reference frame does not have much influence on the ZWD and rather more on station coordinates and EOP.

The results are not conclusive, as the different methods produce partly completely different results. It is hoped that with a more consistent and similar data comparison a clearer statement about water vapor changes can be made.

Bibliography

Alexandersson, H. and A. Moberg (1997). Homogenization of swedish temperature data. part i: Homogeneity test for linear trends. *International Journal of climatology 17*(1), 25–34.

Altamimi, Z., P. Rebischung, L. Métivier, and X. Collilieux (2016). ITRF2014: A new release of the international terrestrial reference frame modeling nonlinear station motions. *Journal of Geophysical Research: Solid Earth 121*(8), 6109–6131.

Altamimi, Z. and M. Rothacher (2005). ITRF and co-location sites. https://www.iers.org/SharedDocs/Publikationen/EN/IERS/Publications/ tn/TechnNote33/tn33_008.pdf?__blob=publicationFile&v=1/. Online; accessed 15 Oktober 2016.

Bachmann, S., L. Messerschmitt, and D. Thaller (2014). IVS contribution to ITRF2013. http://geophy.uni.lu/users/tonie.vandam/REFAG2014/SESS_II_ Techniques/Bachmann.pdf. Online; accessed 28 November 2016.

Bevis, M., S. Businger, T. A. Herring, C. Rocken, R. A. Anthes, and R. H. Ware (1992). GPS meteorology: Remote sensing of atmospheric water vapor using the global positioning system. *Journal of Geophysical Research: Atmospheres 97*(D14), 15787–15801.

Böhm, J. (2004). Troposphärische laufzeitverzögerungen in der VLBI. Geowissenschaftliche Mitteilungen, Heft 68, pp. 212. Wien: Geowissenschaftliche Mitteilungen.

Böhm, J., S. Böhm, T. Nilsson, A. Pany, L. Plank, H. Spicakova, K. Teke, and H. Schuh (2012). The new vienna VLBI software VieVS. pp. 1007–1011.

Böhm, J., G. Möller, M. Schindelegger, G. Pain, and R. Weber (2015). Development of an improved empirical model for slant delays in the troposphere (GPT2w). *GPS Solutions 19*(3), 433–441.

Böhm, J., A. Niell, P. Tregoning, and H. Schuh (2006). Global mapping function (GMF): A new empirical mapping function based on numerical weather model data. *Geophysical Research Letters 33*(7).

Böhm, J. and H. Schuh (2004). Vienna mapping functions in VLBI analyses. *Geophysical Research Letters 31*(1).

Böhm, J. and H. Schuh (2013). Atmospheric effects in space geodesy. pp. 231. Springer Verlag.

Böhm, J., B. Werl, and H. Schuh (2006). Troposphere mapping functions for GPS and very long baseline interferometry from european centre for medium-range weather forecasts operational analysis data. *Journal of Geophysical Research: Solid Earth 111*(B2).

Böhm, S. (2012). Tidal excitation of earth rotation observed by VLBI and GNSS. pp. 167. Department of Geodesy and Geoinformation of the Vienna University of Technology.

Chen, G. and T. Herring (1997). Effects of atmospheric azimuthal asymmetry on the analysis of space geodetic data. *Journal of Geophysical Research: Solid Earth 102*(B9), 20489–20502.

Computational Physics, Inc. (CPI) (2014). Very long baseline interferometry (VLBI). http://www.cpi.com/projects/vlbi.html. Online; accessed 15 Oktober 2016.

Gradinarsky, L., J. Johansson, H. Bouma, H.-G. Scherneck, and G. Elgered (2002). Climate monitoring using GPS. *Physics and Chemistry of the Earth, Parts A/B/C 27*(4), 335–340.

Heinkelmann, R. (2008). Bestimmung des atmosphärischen wasserdampfes mittels VLBI als beitrag zur klimaforschung. Geowissenschaftliche Mitteilungen, Heft 82, pp. 212. Wien: Geowissenschaftliche Mitteilungen.

Heinkelmann, R., J. Böhm, H. Schuh, S. Bolotin, G. Engelhardt, D. MacMillan, M. Negusini, E. Skurikhina, V. Tesmer, and O. Titov (2007). Combination of long time-series of troposphere zenith delays observed by VLBI. *Journal of Geodesy 81*(6-8), 483–501.

Hobiger, T. (2006). VLBI as a tool to probe the ionosphere. Geowissenschaftliche Mitteilungen, Heft 75, pp. 129. Wien: Geowissenschaftliche Mitteilungen.

Hofmeister, A. (2016). Determination of path delays in the atmosphere for geodetic VLBI by means of ray-tracing. Geowissenschaftliche Mitteilungen, Heft 98., pp. 318. Wien: Geowissenschaftliche Mitteilungen.

IGS (2010). Repro 1. `ftp://cddis.gsfc.nasa.gov/gps/products/troposphere/zpd/repro1`. Online; accessed 15 Oktober 2016.

IGS (2014). Repro 2. `http://acc.igs.org/reprocess2.html`. Online; accessed 28 November 2016.

IGS (2015). IGS tracking network. `http://kb.igs.org/hc/en-us/articles/202484696-IGS-tracking-network/`. Online; accessed 15 Oktober 2016.

IGS (2016a). Overview of Satellites in BeiDou Navigation Satellite System. `http://mgex.igs.org/IGS_MGEX_Status_BDS.html`. Online; accessed 15 Oktober 2016.

IGS (2016b). Overview of Satellites in Galileo Constellation. `http://mgex.igs.org/IGS_MGEX_Status_GAL.html`. Online; accessed 15 Oktober 2016.

IVS (1983). NGS Format for VLBI Data Transfer. `ftp://cddis.gsfc.nasa.gov/pub/reports/formats/ngs_card.format`. Online; accessed 15 Oktober 2016.

IVS (2013). Network stations. `http://ivscc.gsfc.nasa.gov/stations/ns-map.html`. Online; accessed 15 Oktober 2016.

IVS (2016a). Cont14. `http://ivs.nict.go.jp/mirror/program/cont14/`. Online; accessed 15 Oktober 2016.

IVS (2016b). IVS Network Station codes. `ftp://cddis.gsfc.nasa.gov/vlbi/ivscontrol/ns-codes.txt`. Online; accessed 15 Oktober 2016.

Jin, S., J.-U. Park, J.-H. Cho, and P.-H. Park (2007). Seasonal variability of GPS-derived zenith tropospheric delay (1994–2006) and climate implications. *Journal of Geophysical Research: Atmospheres 112*(D9).

Kaplan, E. and C. Hegarty (2005). Understanding GPS: principles and applications. pp. 703. Artech house.

Kumar, G. S., G. S. B. Rao, and M. Kumar (2013). GPS signal short-term propagation characteristics modeling in urban areas for precise navigation applications. *Positioning 4*(02), 192.

Lagler, K., M. Schindelegger, J. Böhm, H. Krásná, and T. Nilsson (2013). GPT2: Empirical slant delay model for radio space geodetic techniques. *Geophysical research letters 40*(6), 1069–1073.

Landskron, D., A. Hofmeister, and J. Böhm (2015). Refined and site-augmented tropospheric delay models for CONT11. In *EGU General Assembly Conference Abstracts*, Volume 17, pp. 325.

MacMillan, D. (1995). Atmospheric gradients from very long baseline interferometry observations. *Geophysical Research Letters 22*(9), 1041–1044.

Möller, G., R. Weber, and J. Böhm (2014). Improved troposphere blind models based on numerical weather data. Volume 61, pp. 203–211. Wiley Online Library.

Niell, A. (1996). Global mapping functions for the atmosphere delay at radio wavelengths. *Journal of Geophysical Research: Solid Earth 101*(B2), 3227–3246.

Niell, A. (2000). Improved atmospheric mapping functions for VLBI and GPS. *Earth, planets and space 52*(10), 699–702.

Nilsson, T. and G. Elgered (2008). Long-term trends in the atmospheric water vapor content estimated from ground-based GPS data. *Journal of Geophysical Research: Atmospheres 113*(D19).

Ning, T., R. Haas, G. Elgered, and U. Willén (2012). Multi-technique comparisons of 10 years of wet delay estimates on the west coast of sweden. *Journal of Geodesy 86*(7), 565–575.

Research Group Advanced Geodesy (2016). VMF1 Forecast Data. `http://ggosatm.hg.tuwien.ac.at/DELAY/SITE/VLBI`. Online; accessed 15 Oktober 2016.

Saastamoinen, J. (1972). Atmospheric correction for the troposphere and stratosphere in radio ranging satellites. *The use of artificial satellites for geodesy*, 247–251.

Schlüter, W. and D. Behrend (2007). The international VLBI service for geodesy and astrometry (IVS): current capabilities and future prospects. *Journal of Geodesy 81*(6-8), 379–387.

Schuh, H. and D. Behrend (2012). VLBI: a fascinating technique for geodesy and astrometry. *Journal of Geodynamics 61*, 68–80.

Steigenberger, P., V. Tesmer, M. Krügel, D. Thaller, R. Schmid, S. Vey, and M. Rothacher (2007). Comparisons of homogeneously reprocessed GPS and VLBI long time-series of troposphere zenith delays and gradients. *Journal of Geodesy 81* (6-8), 503–514.

U.S.Naval Observatory (2016). Current GPS Constellation. `http://tycho.usno.navy.mil/gpscurr.html`. Online; accessed 15 Oktober 2016.

Watson, T. (2009). Global warming - think green. `https://www.bmiestore.com/samples/BMIr/sdlsa3497is.pdf`. Online; accessed 16 Oktober 2016.

Appendix A

Additional Figures

Figure A.1 and Figure A.2 show images complementing Section 4.1.2.

Figure A.3 - Figure A.19 show images complementing Section 5.1.

Figure A.20 - Figure A.27 show images complementing Section 5.2.

Figure A.28 - Figure A.43 show images complementing Section 5.3.

A.1 Data Description
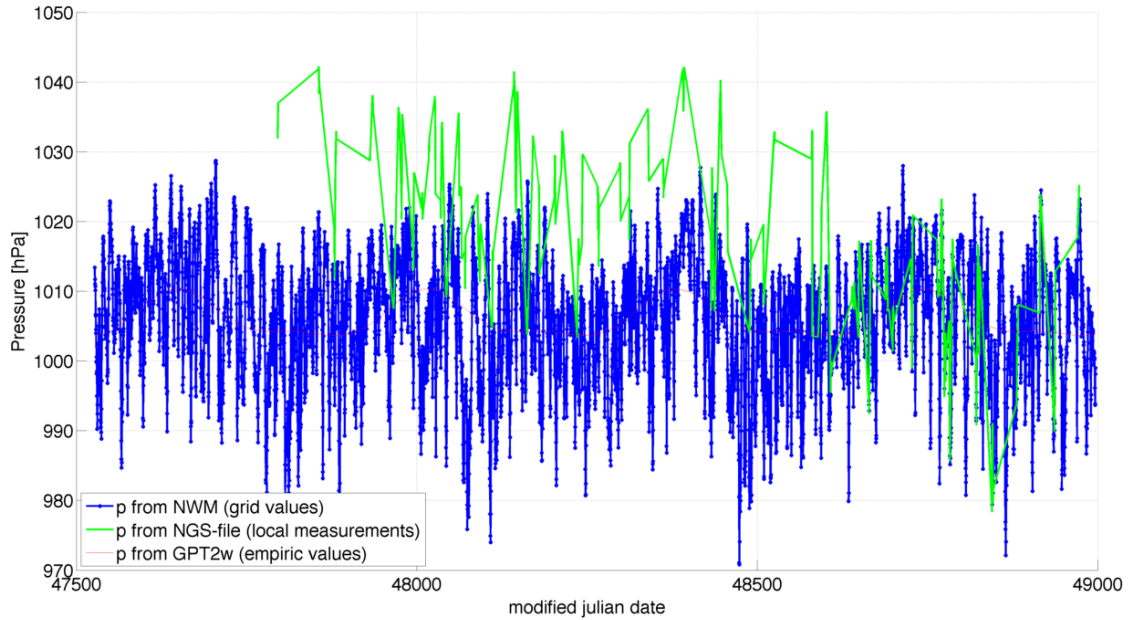
(a) Visualization of the offset at station Hobart26
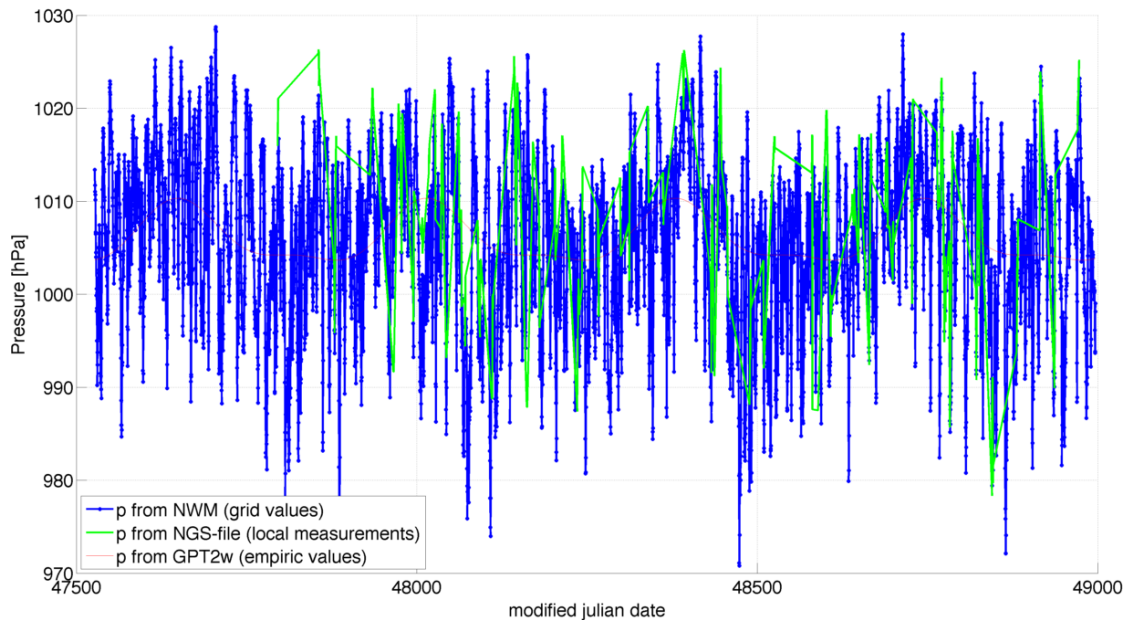
(b) Correction of the offset at station Hobart26

Figure A.1: *Visualization of the correction of an offset at station Hobart26*
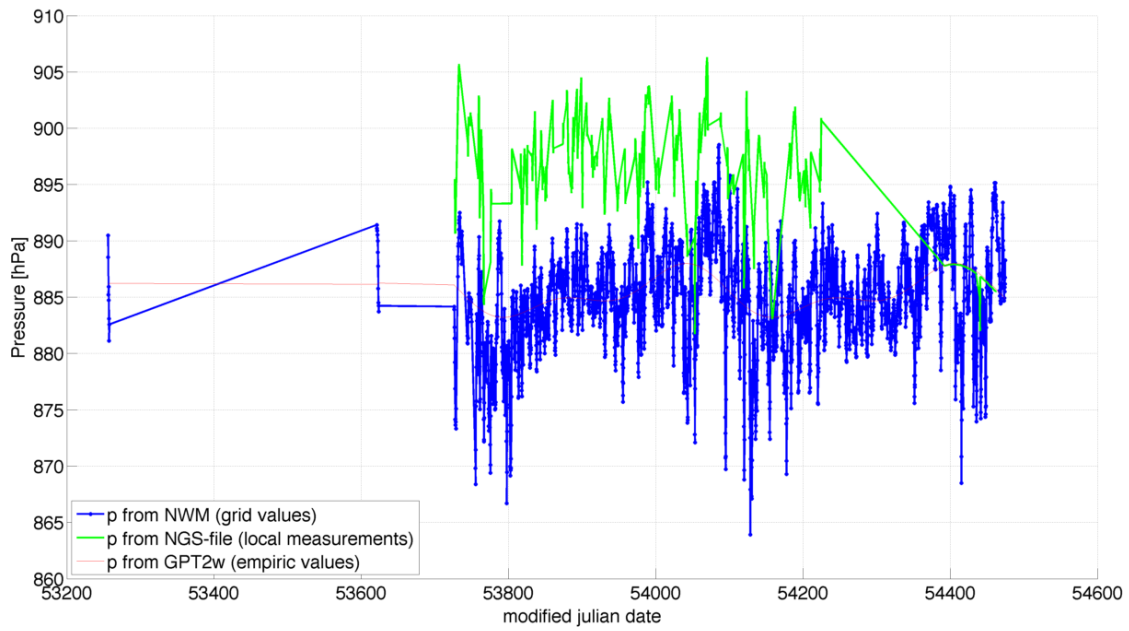
(a) *Visualization of the offset at station Zelenchk*
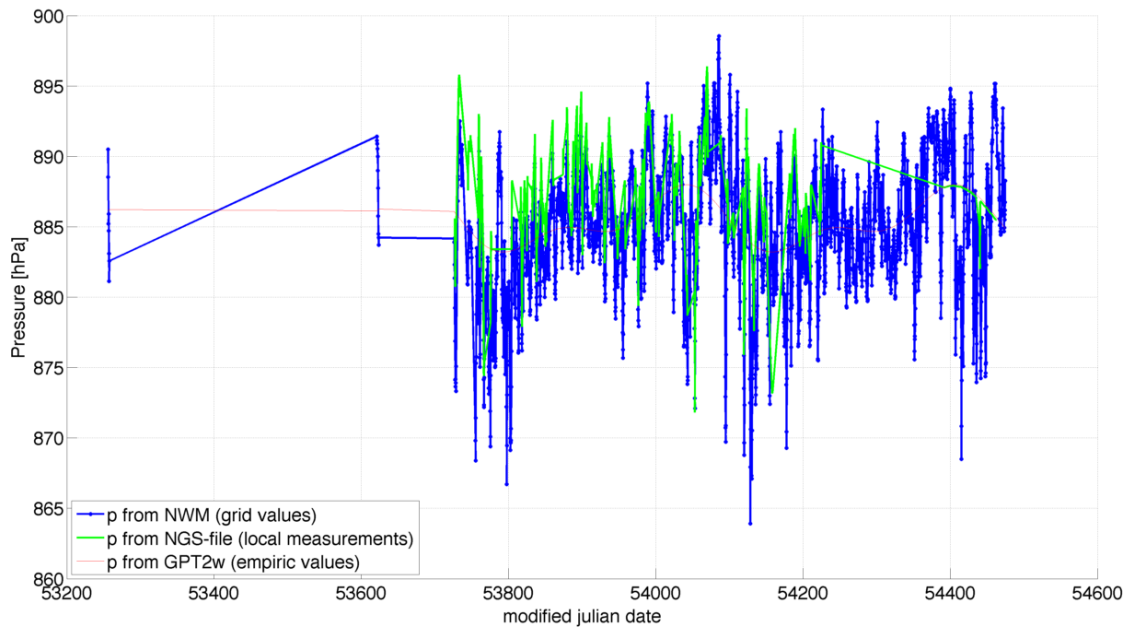
(b) *Correction of the offset at station Zelenchk*

Figure A.2: *Visualization of the correction of an offset at station Zelenchk*

A.2 Very Long Baseline Interferometry (VLBI)
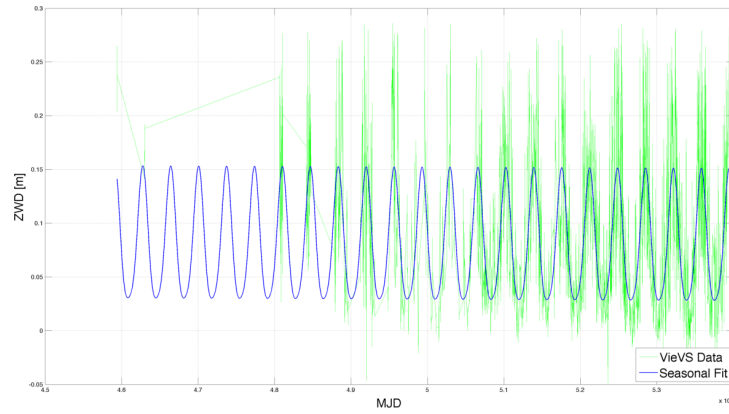

(a) Algopark NGS, Trend = -0.1 mm/year
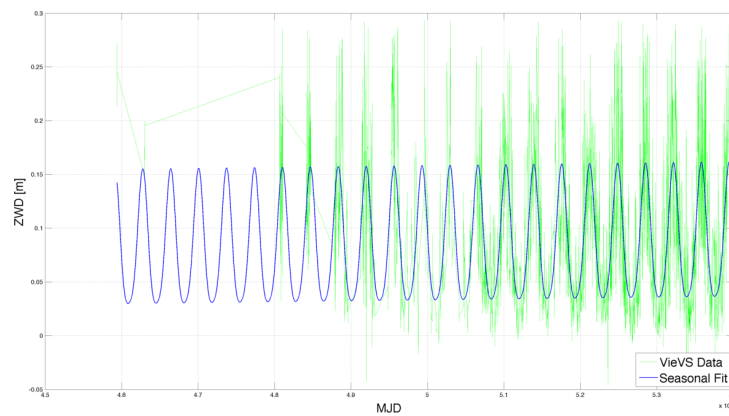
(b) Algopark NWM, Trend = 0.3 mm/year
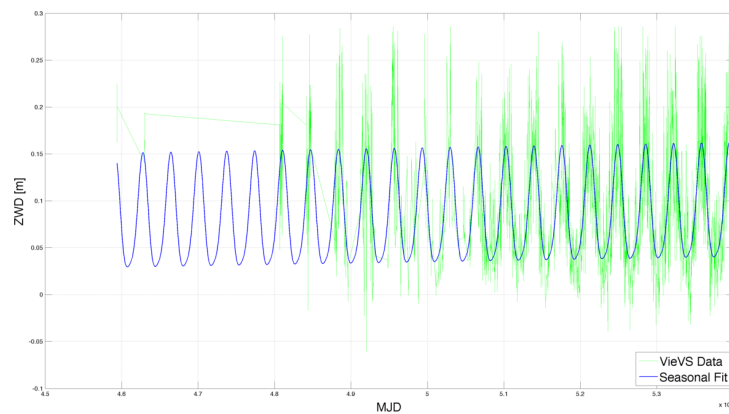
(c) Algopark GPT2, Trend = 0.5 mm/year

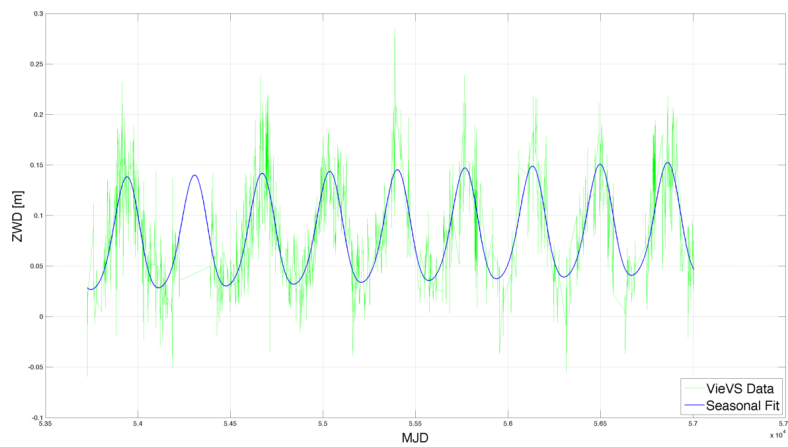***Figure A.3:*** *Example of a data processing for VLBI data at the station Algopark*
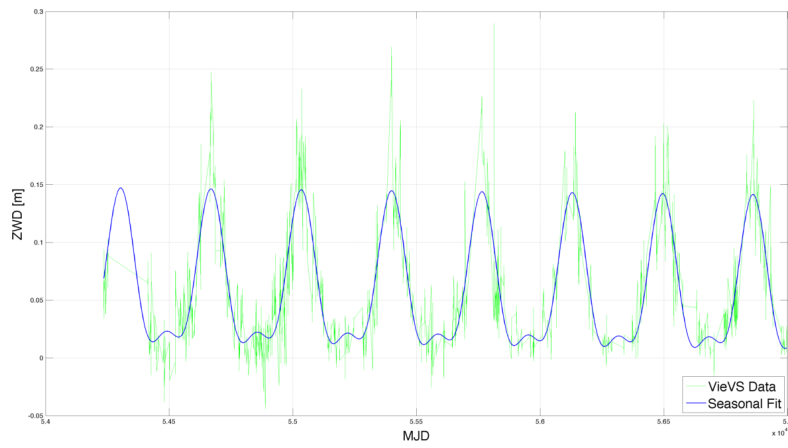
(a) Badary NGS, Trend = -0.8 mm/year
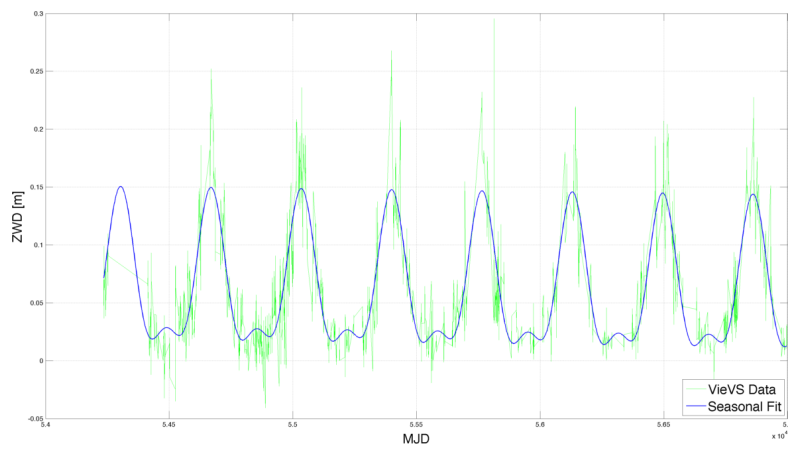
(b) Badary NWM, Trend = -1.0 mm/year
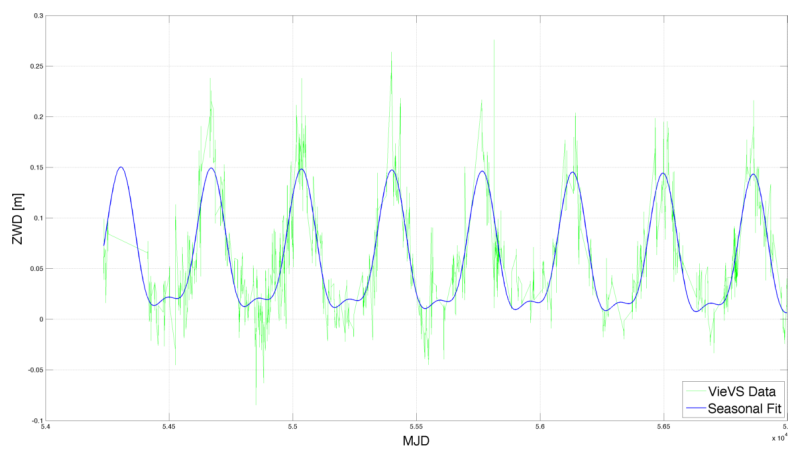
(c) Badary GPT2, Trend = -1.0 mm/year

Figure A.4: *Example of a data processing for VLBI data at the station Badary*
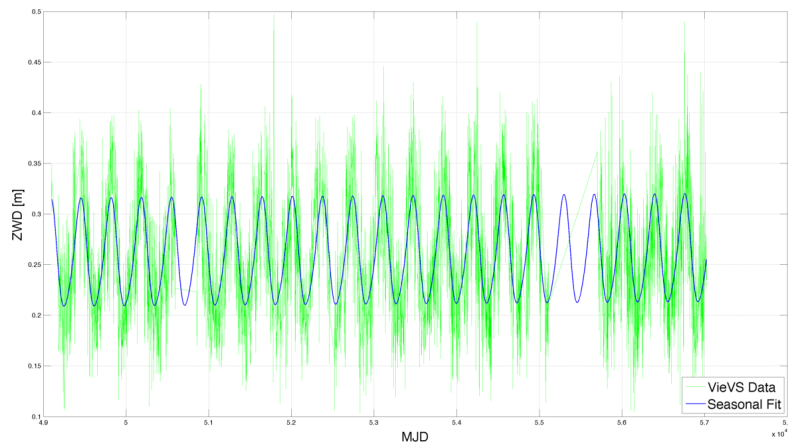
(a) Fortleza NGS, Trend = 0.2 mm/year
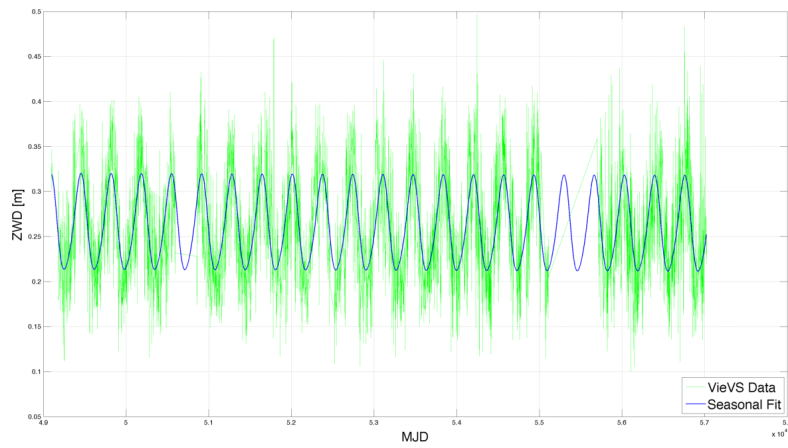
(b) Fortleza NWM, Trend = -0.1 mm/year
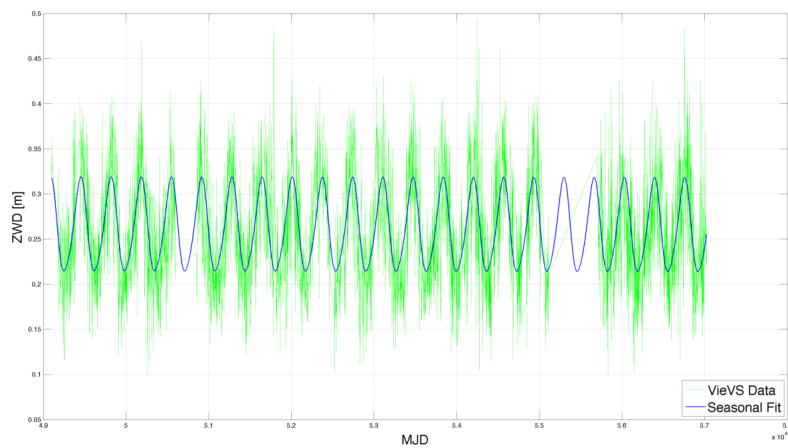
(c) Fortleza GPT2, Trend = -0.04 mm/year

Figure A.5: *Example of a data processing for VLBI data at the station Fortleza*
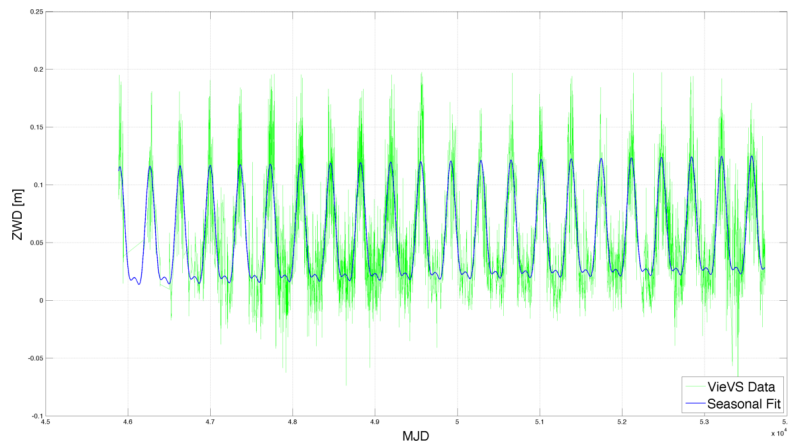
(a) Gilcreek NGS, Trend = 0.5 mm/year
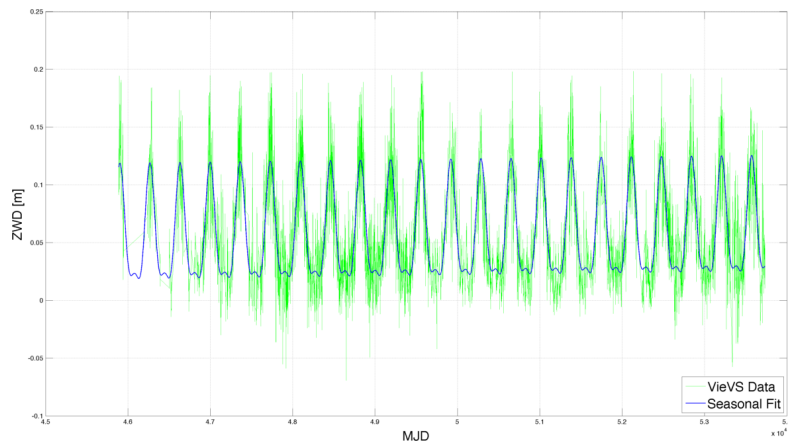
(b) Gilcreek NWM, Trend = 0.3 mm/year
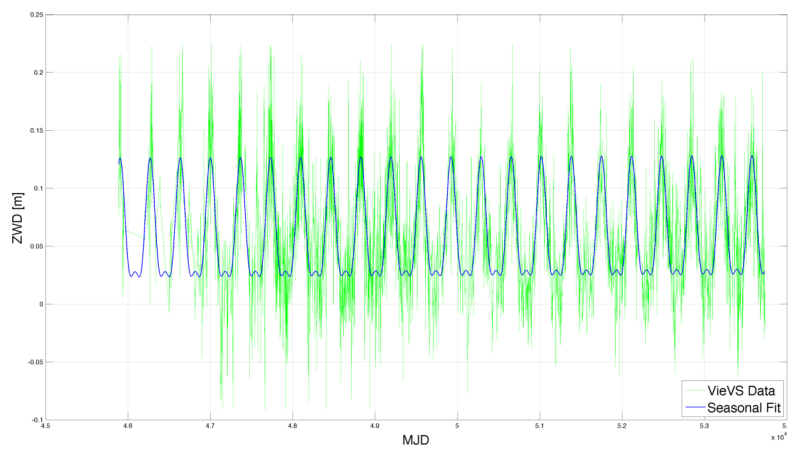
(c) Gilcreek GPT2, Trend = 0.1 mm/year

Figure A.6: *Example of a data processing for VLBI data at the station Gilcreek*
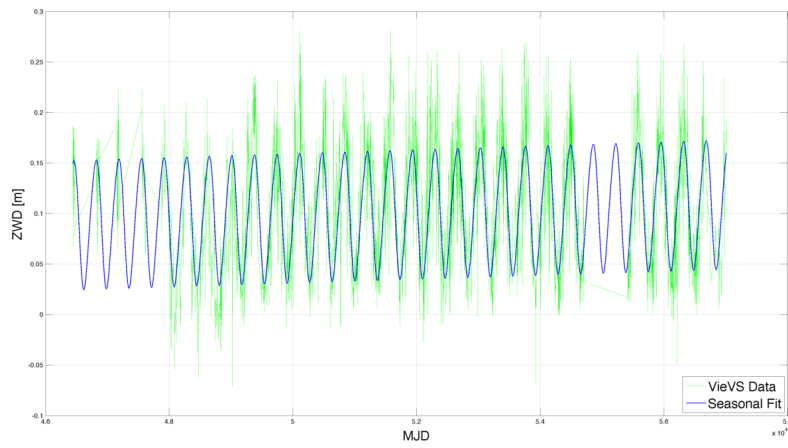
(a) Hartrao NGS, Trend = 0.7 mm/year
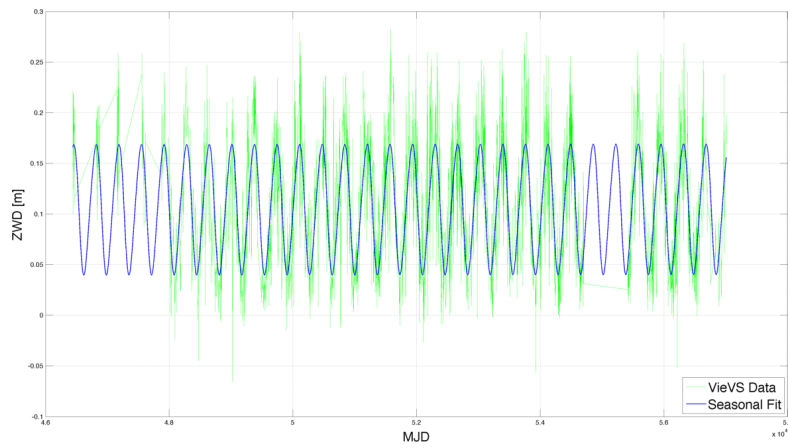
(b) Hartrao NWM, Trend = 0.02 mm/year
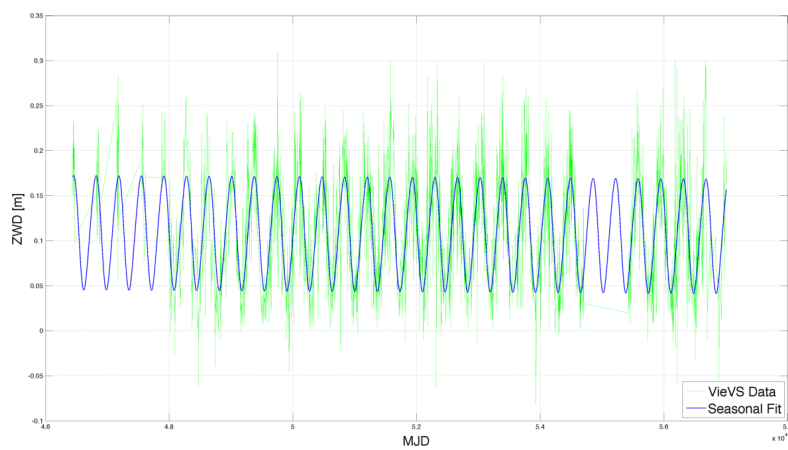
(c) Hartrao GPT2, Trend = -0.1 mm/year

Figure A.7: *Example of a data processing for VLBI data at the station Hartrao*
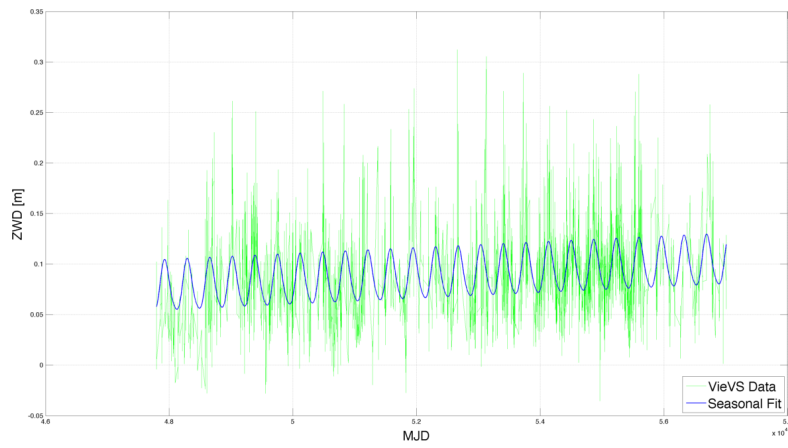
(a) Hobart26 NGS, Trend = 1.0 mm/year
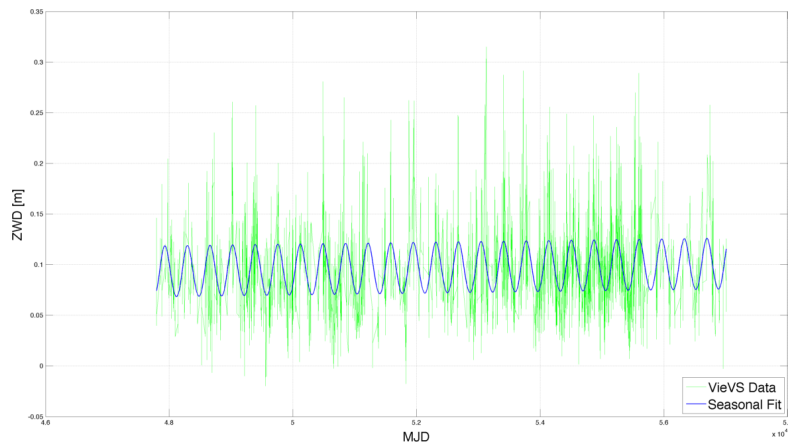
(b) Hobart26 NWM, Trend = 0.3 mm/year
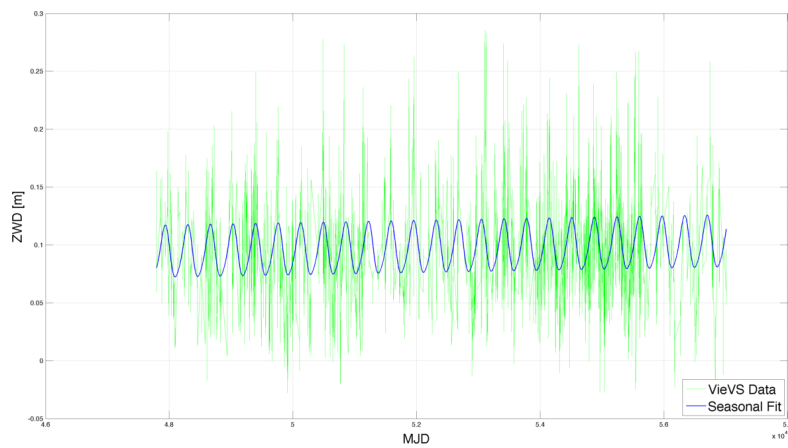
(c) Hobart26 GPT2, Trend = 0.4 mm/year

Figure A.8: *Example of a data processing for VLBI data at the station Hobart26*
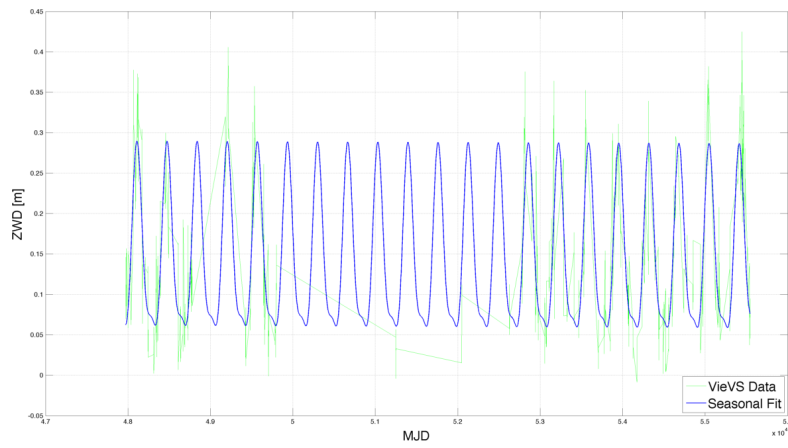
(a) Kashim34 NGS, Trend = -0.1 mm/year
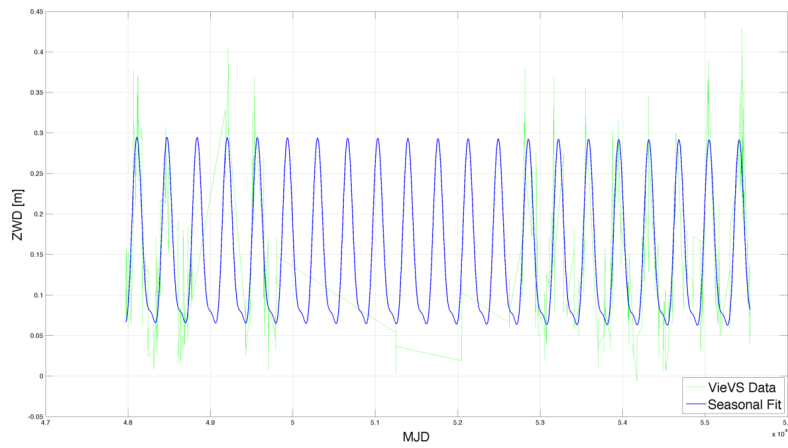
(b) Kashim34 NWM, Trend = -0.2 mm/year
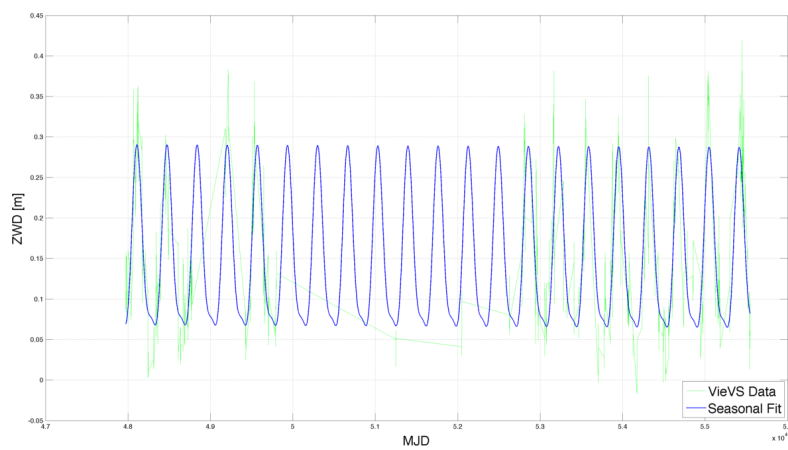
(c) Kashim34 GPT2, Trend = -0.2 mm/year

Figure A.9: *Example of a data processing for VLBI data at the station Kashim34*
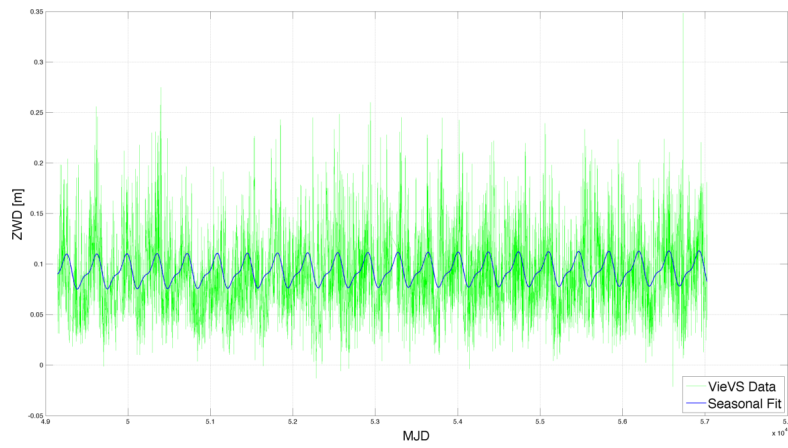
(a) *Kokee NGS, Trend = 0.1 mm/year*
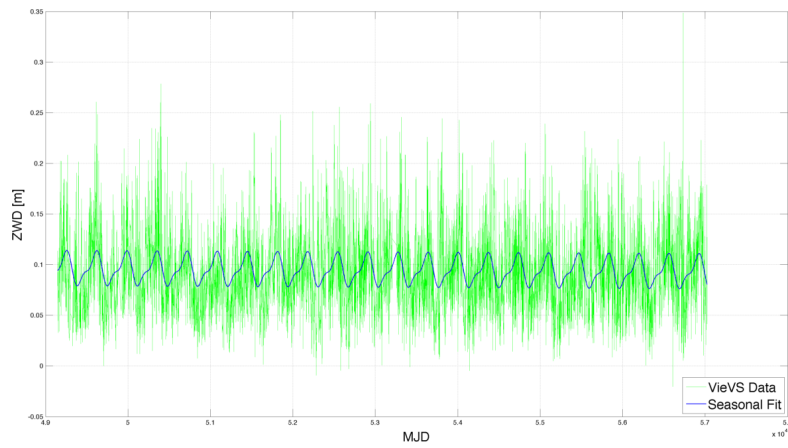
(b) *Kokee NWM, Trend = -0.1 mm/year*
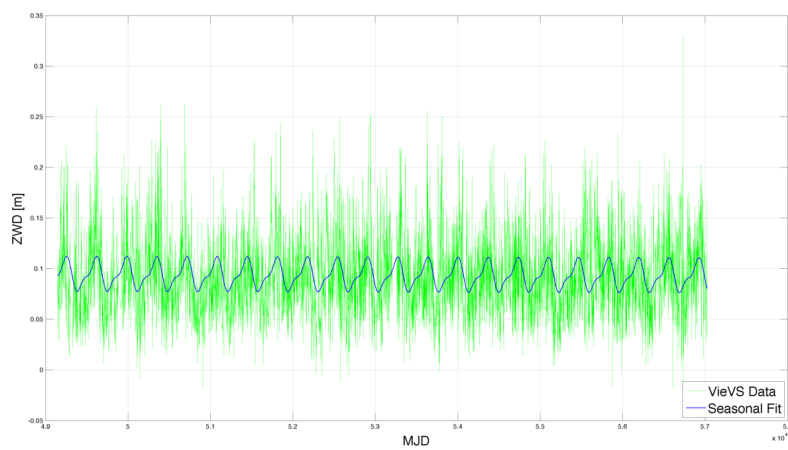
(c) *Kokee GPT2, Trend = -0.1 mm/year*

Figure A.10: *Example of a data processing for VLBI data at the station Kokee*
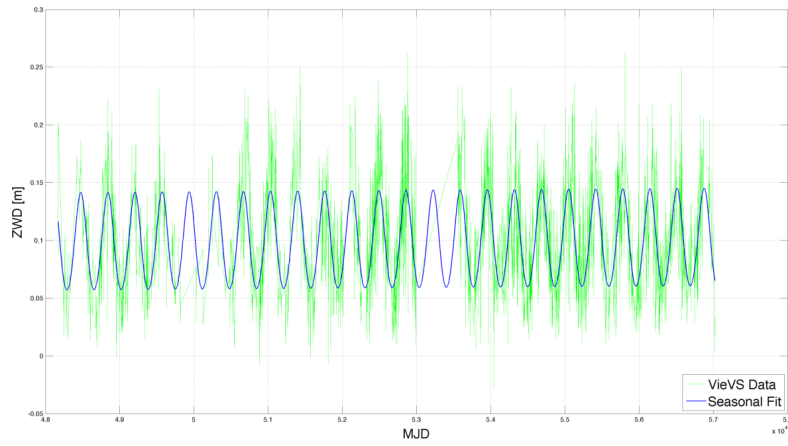
(a) Matera NGS, Trend = 0.2 mm/year
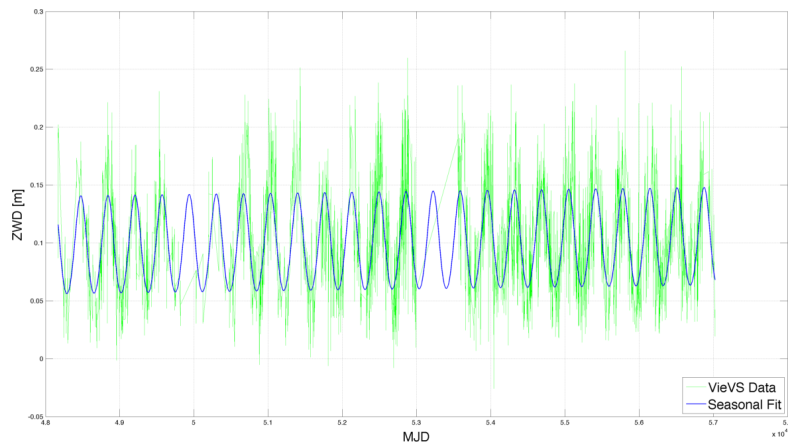
(b) Matera NWM, Trend = 0.3 mm/year
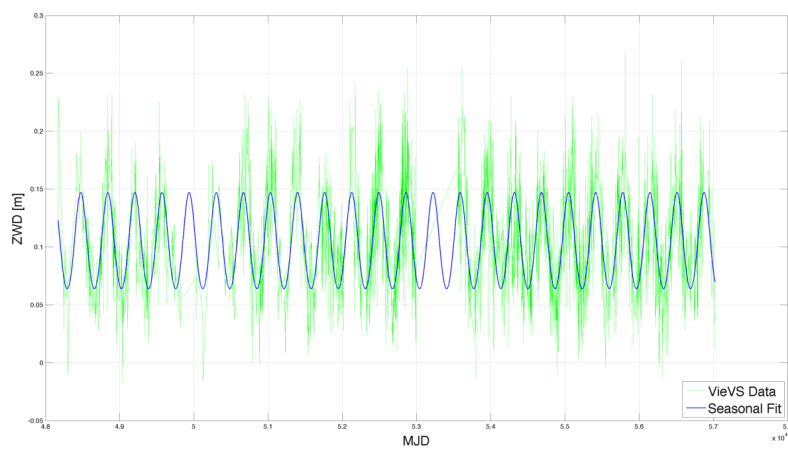
(c) Matera GPT2, Trend = 0.002 mm/year

Figure A.11: *Example of a data processing for VLBI data at the station Matera*
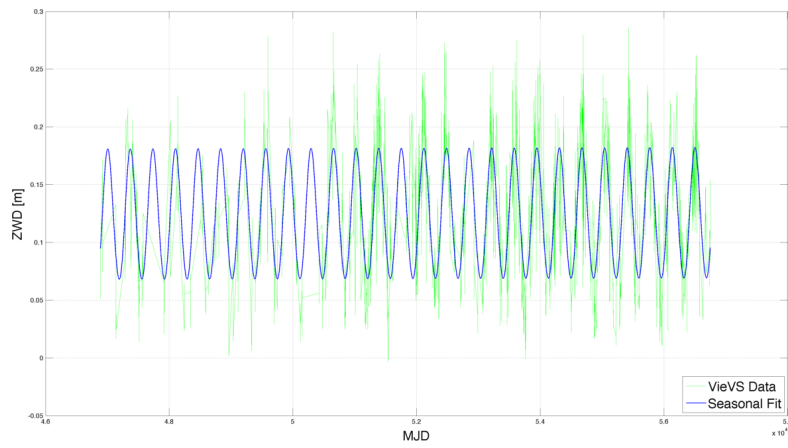
(a) Medicina NGS, Trend = 0.04 mm/year
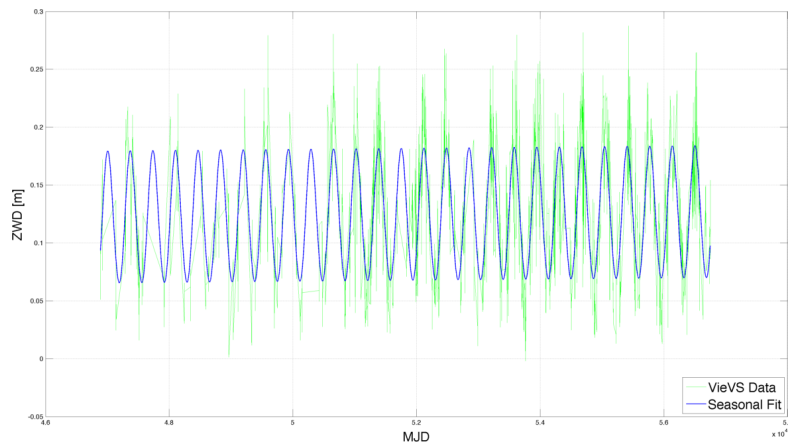
(b) Medicina NWM, Trend = 0.2 mm/year
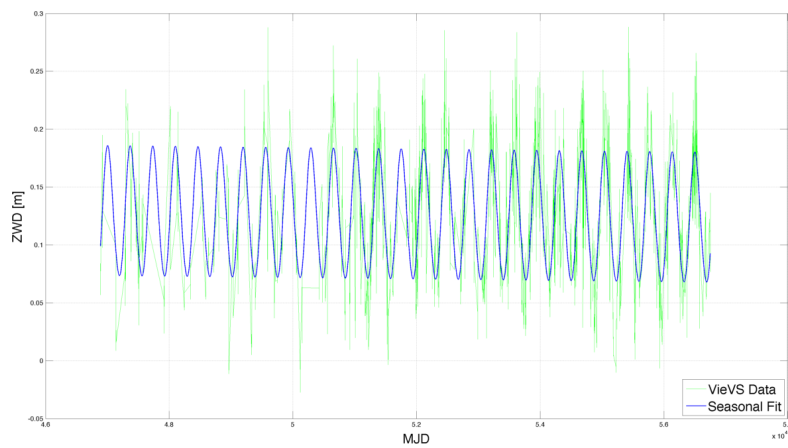
(c) Medicina GPT2, Trend = -0.2 mm/year

Figure A.12: *Example of a data processing for VLBI data at the station Medicina*
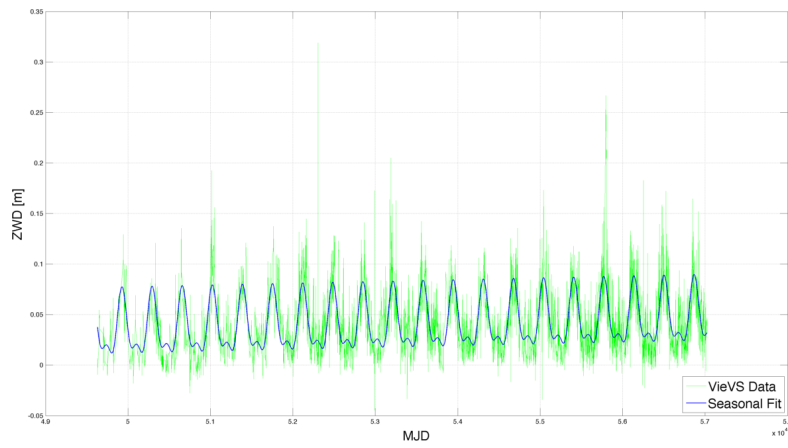
(a) Nyales20 NGS, Trend = 0.6 mm/year
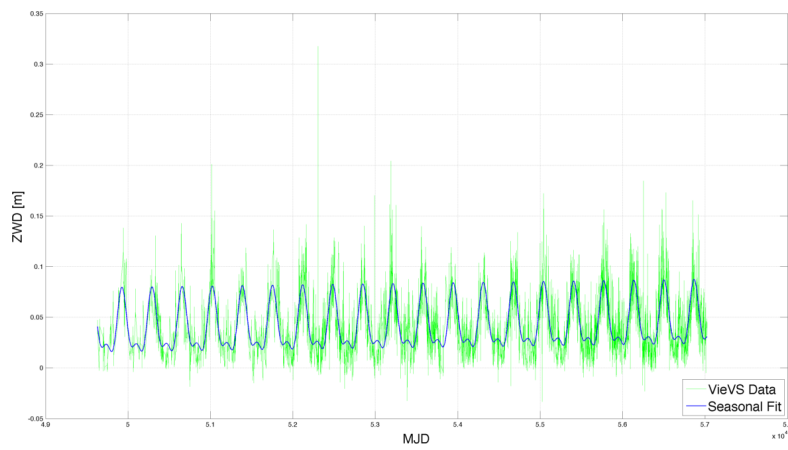
(b) Nyales20 NWM, Trend = 0.4 mm/year
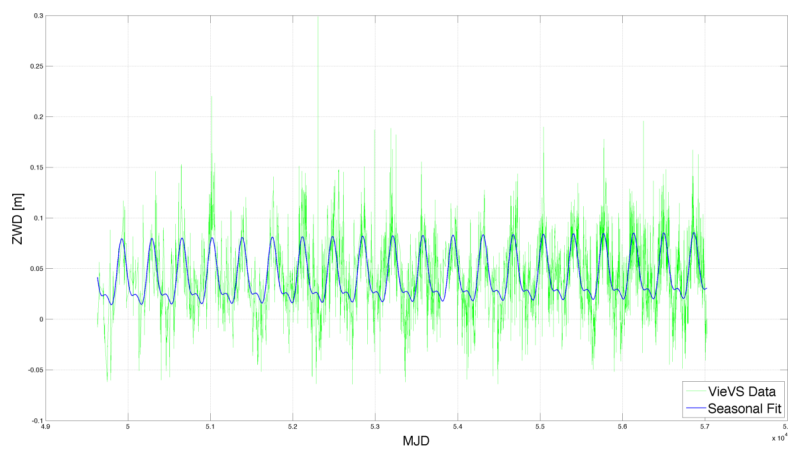
(c) Nyales20 GPT2, Trend = 0.3 mm/year

Figure A.13: *Example of a data processing for VLBI data at the station Nyales20*
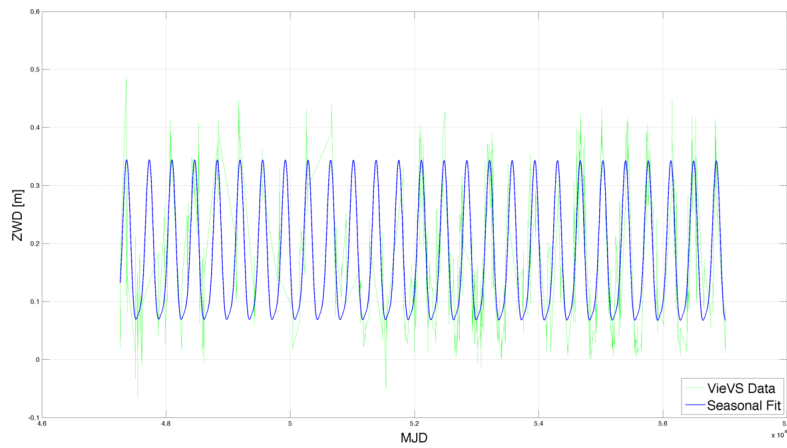
(a) Seshan25 NGS, Trend = -0.1 mm/year
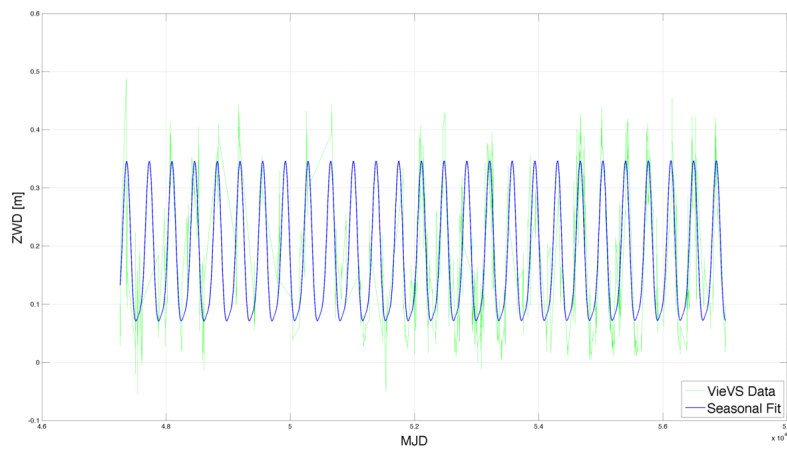
(b) Seshan25 NWM, Trend = 0.05 mm/year
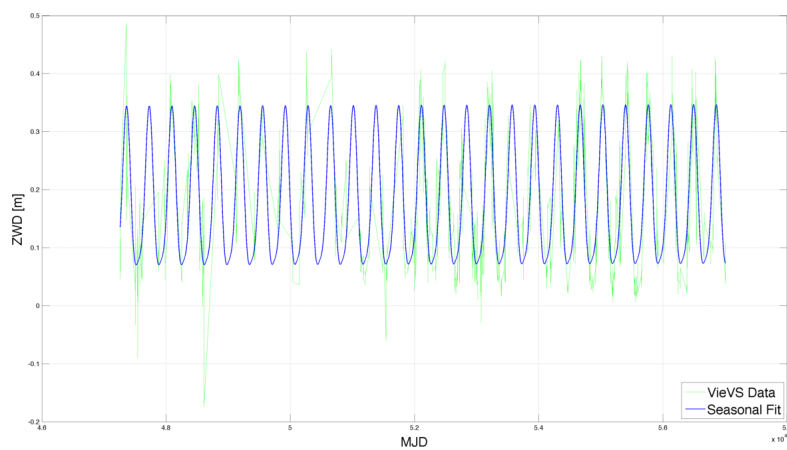
(c) Seshan25 GPT2, Trend = 0.1 mm/year

Figure A.14: *Example of a data processing for VLBI data at the station Seshan25*
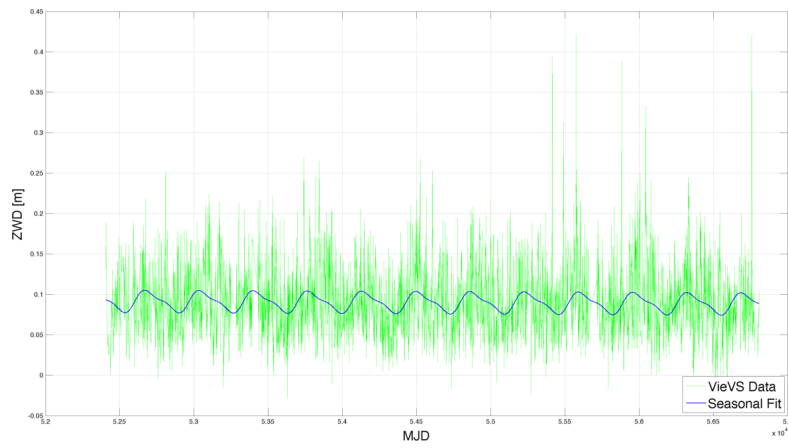
(a) *Tigoconc NGS, Trend = -0.3 mm/year*
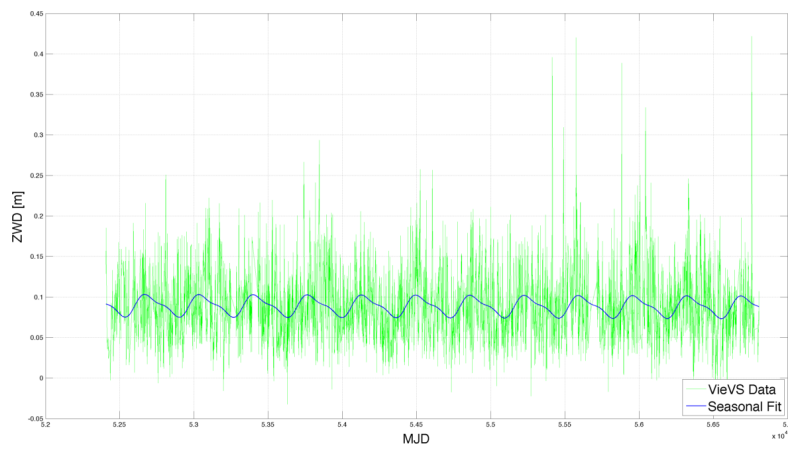
(b) *Tigoconc NWM, Trend = -0.2 mm/year*
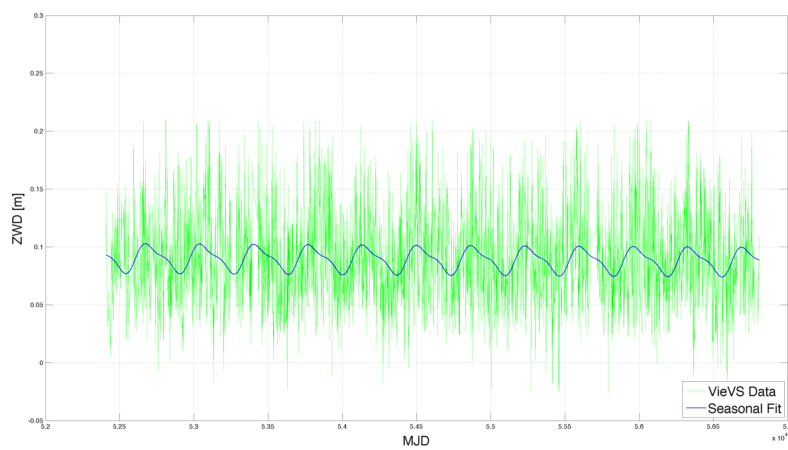
(c) *Tigoconc GPT2, Trend = -0.3 mm/year*

Figure A.15: *Example of a data processing for VLBI data at the station Tigoconc*
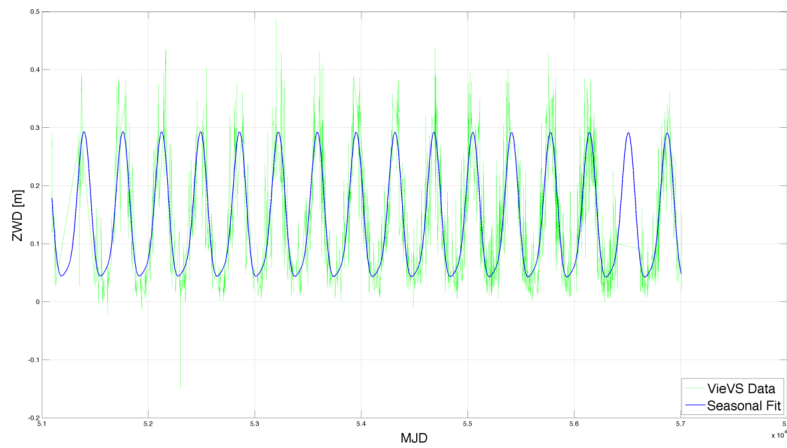
(a) *Tsukub32 NGS, Trend = -0.1 mm/year*
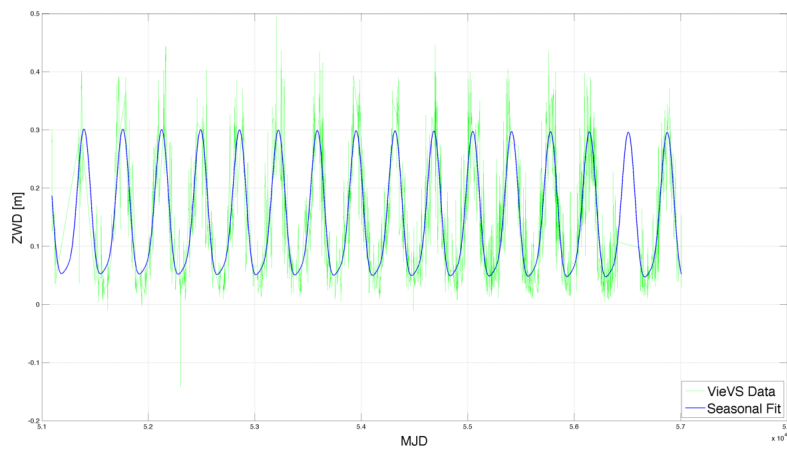
(b) *Tsukub32 NWM, Trend = -0.4 mm/year*
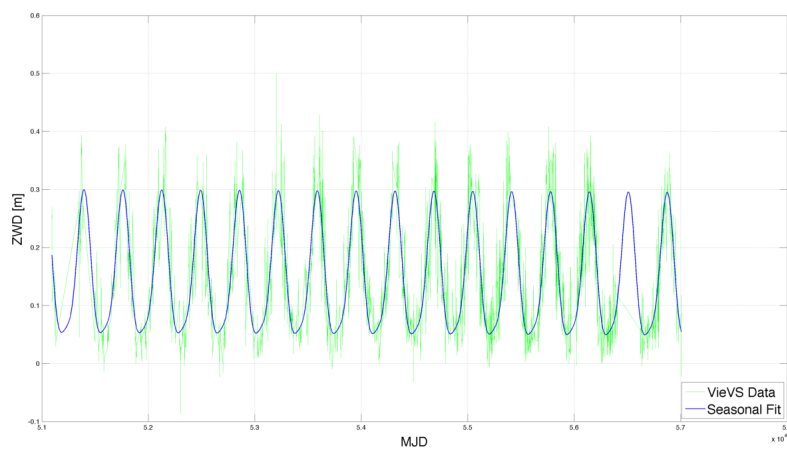
(c) *Tsukub32 GPT2, Trend = -0.3 mm/year*

Figure A.16: *Example of a data processing for VLBI data at the station Tsukub32*
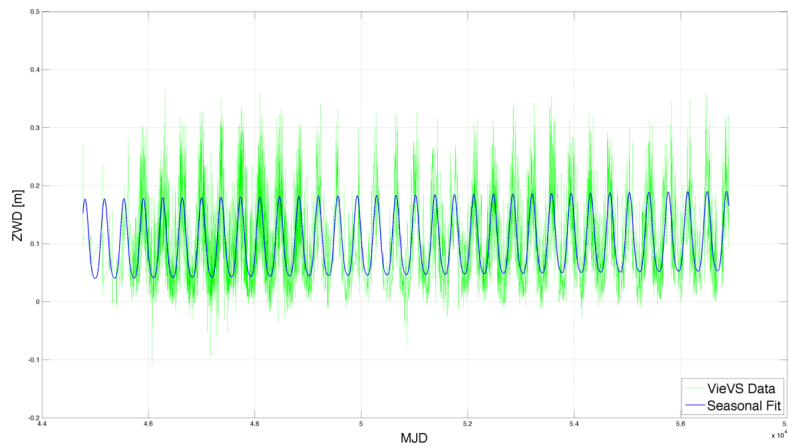
(a) *Westford NGS, Trend = 0.4 mm/year*
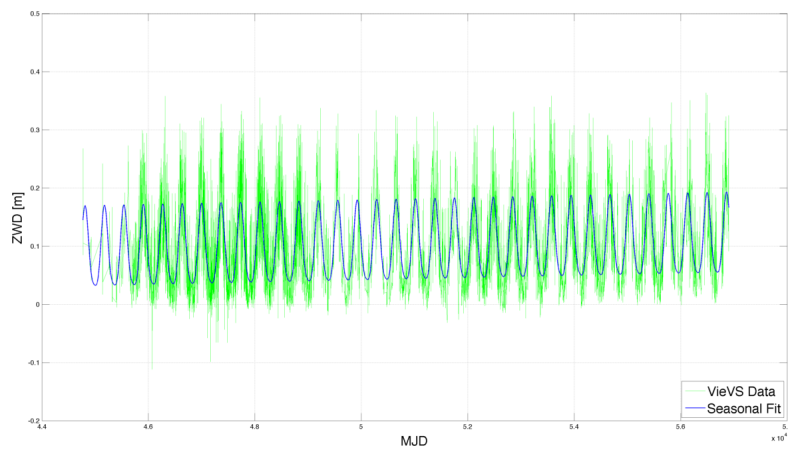
(b) *Westford NWM, Trend = 0.7 mm/year*
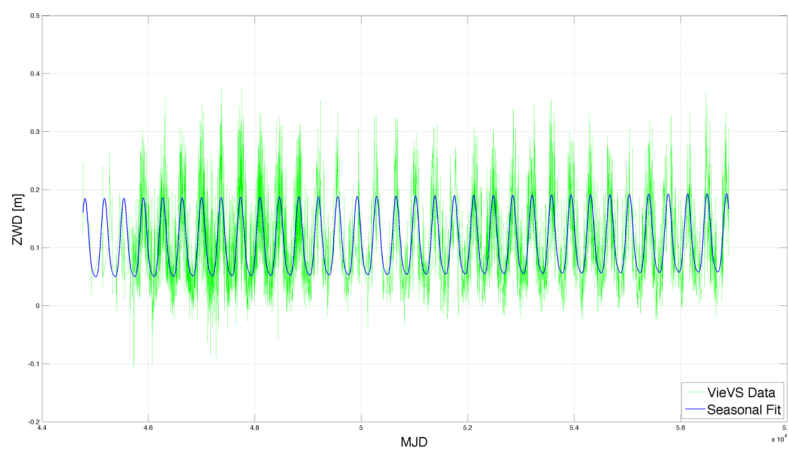
(c) *Westford GPT2, Trend = 0.3 mm/year*

Figure A.17: *Example of a data processing for VLBI data at the station Westford*
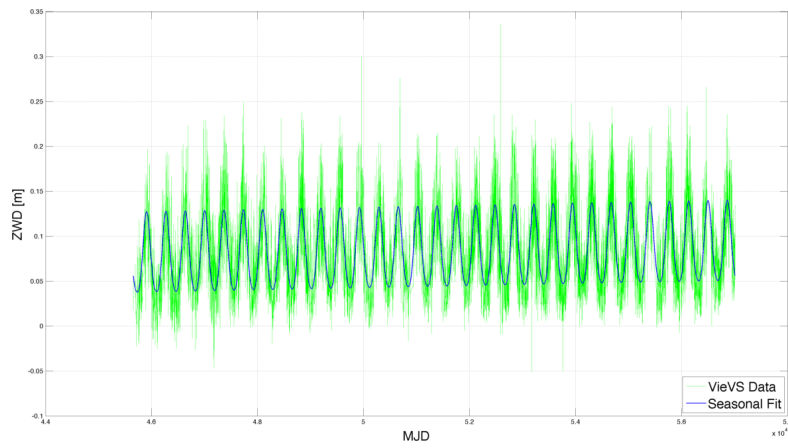
(a) Wettzell NGS, Trend = 0.4 mm/year
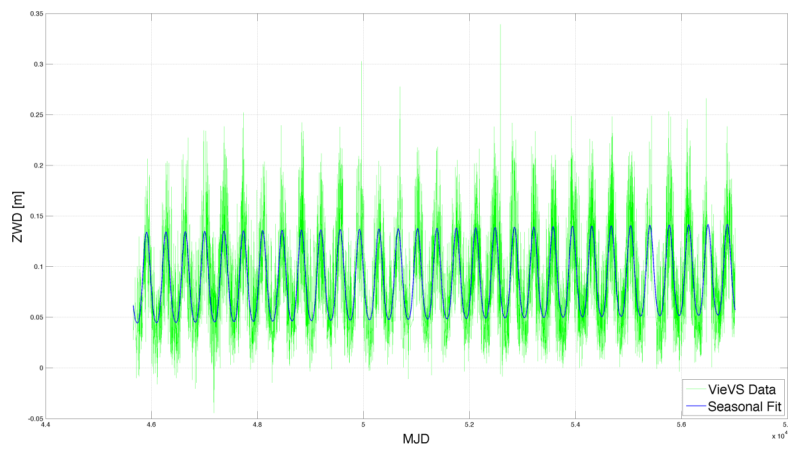
(b) Wettzell NWM, Trend = 0.3 mm/year
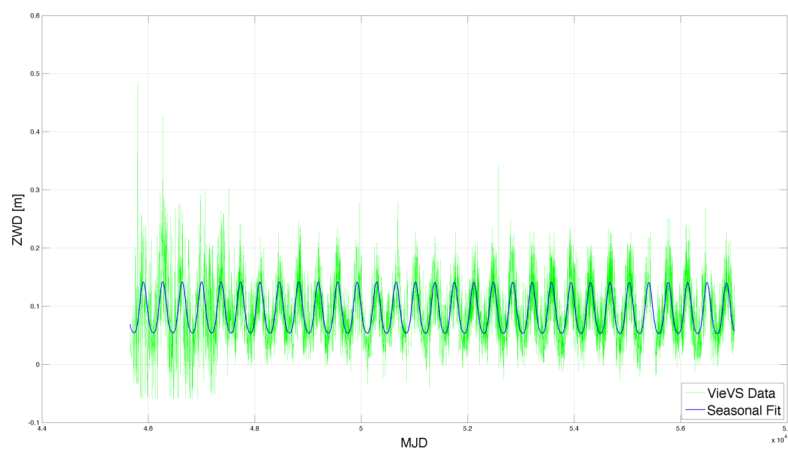
(c) Wettzell GPT2, Trend = -0.05 mm/year

Figure A.18: *Example of a data processing for VLBI data at the station Wettzell*
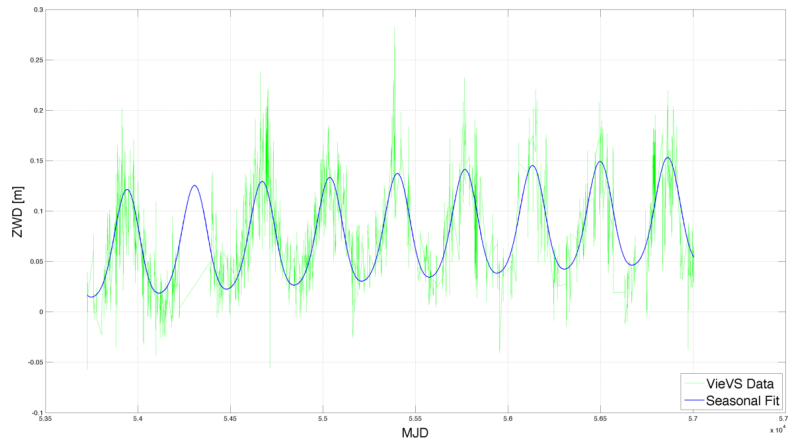
(a) Zelenchk NGS, Trend = 4.0 mm/year
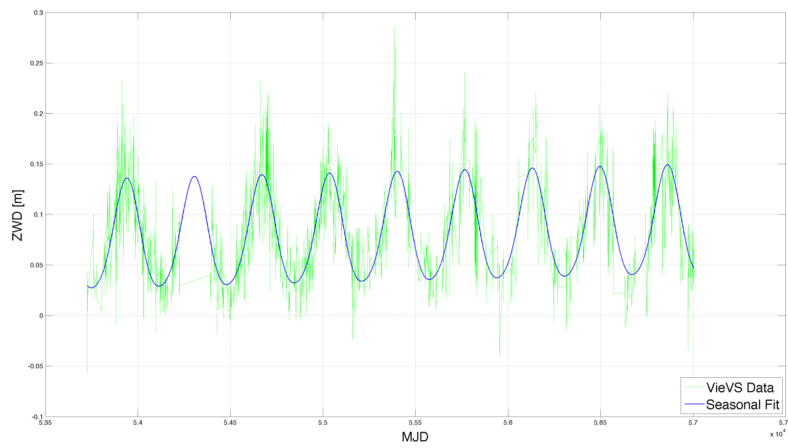
(b) Zelenchk NWM, Trend = 1.6 mm/year

(c) Zelenchk GPT2, Trend = 1.8 mm/year

Figure A.19: *Example of a data processing for VLBI data at the station Zelenchk*

A.3 Global Positioning System (GPS)
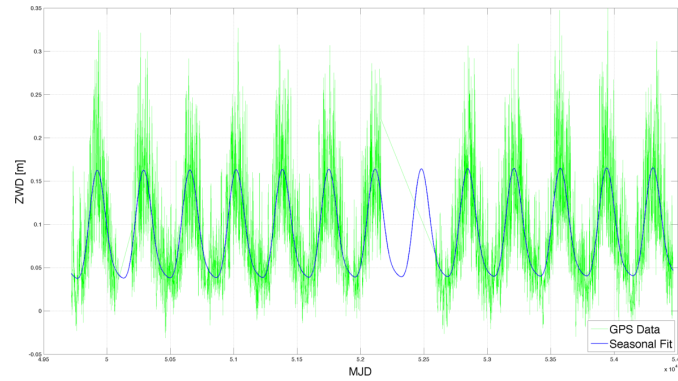
Figure A.20: *Algopark GPS, Trend = 0.3 mm/year*
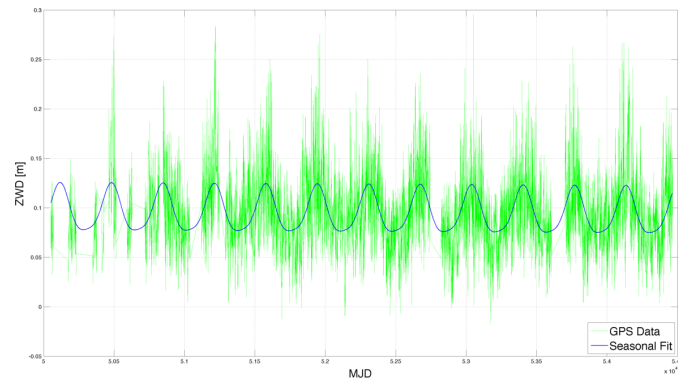
Figure A.21: *Hobart GPS, Trend = -0.3 mm/year*
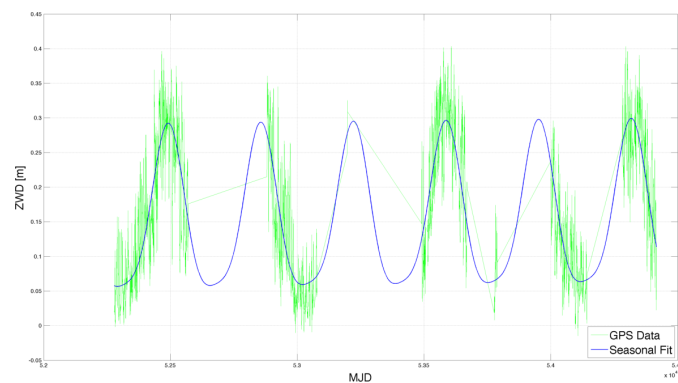
Figure A.22: *Kashima GPS, Trend = 1.4 mm/year*
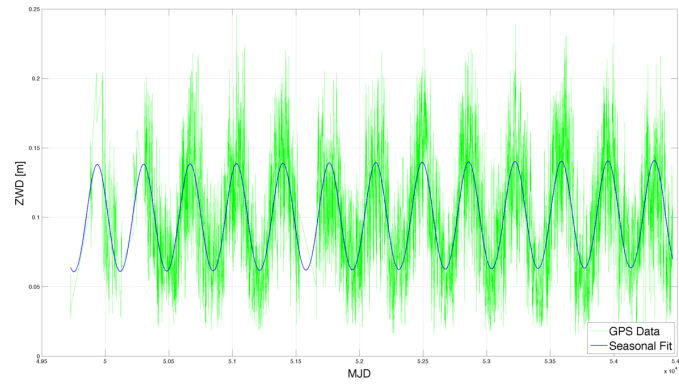
Figure A.23: *Matera GPS, Trend = 0.2 mm/year*
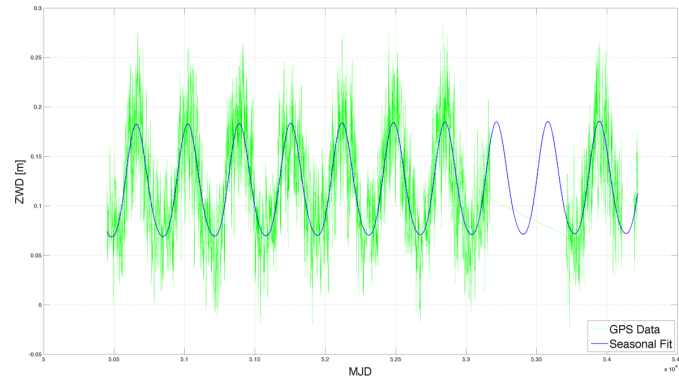
Figure A.24: *Medicina GPS, Trend = 0.3 mm/year*
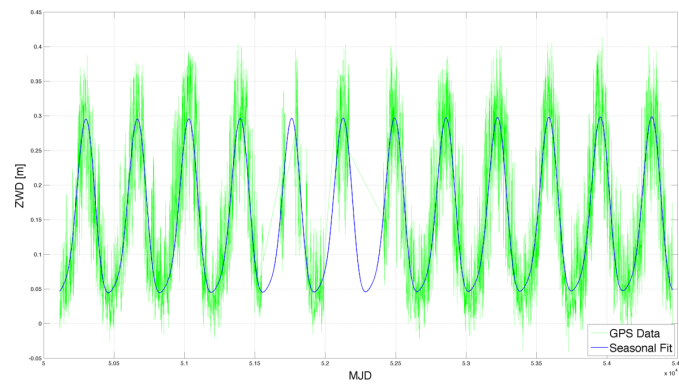
Figure A.25: *Tsukuba GPS, Trend = 0.3 mm/year*
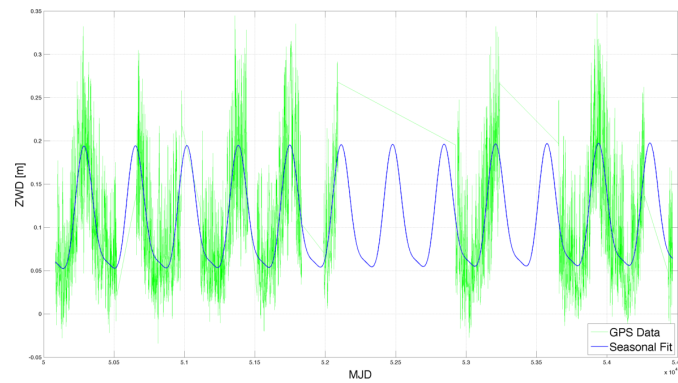
Figure A.26: *Westford GPS, Trend = 0.3 mm/year*

A.4 Vienna Mapping Function 1 (VMF1)
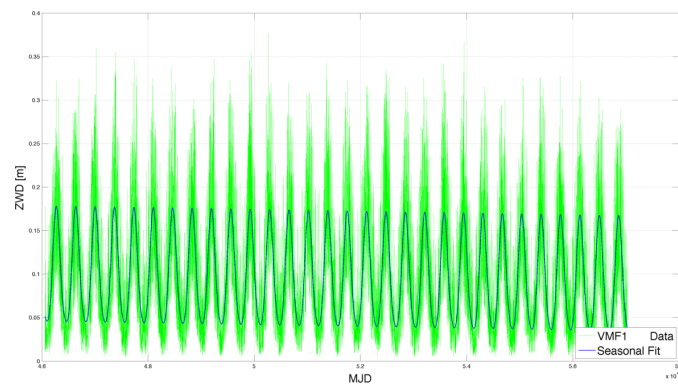
Figure A.27: *Algopark VMF1, Trend = -0.4 mm/year*
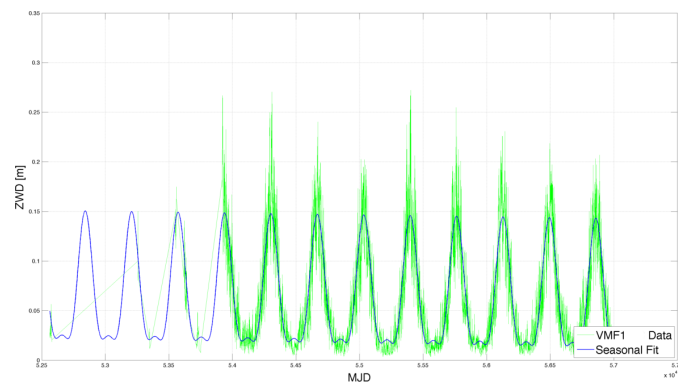
Figure A.28: *Badary VMF1, Trend = -0.7 mm/year*
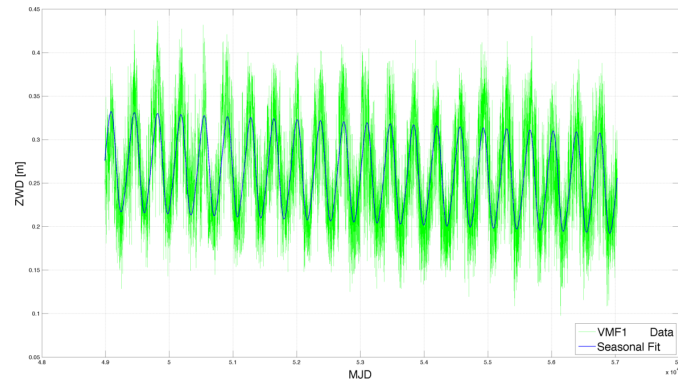
Figure A.29: Forlteza VMF1, Trend = -1.2 mm/year
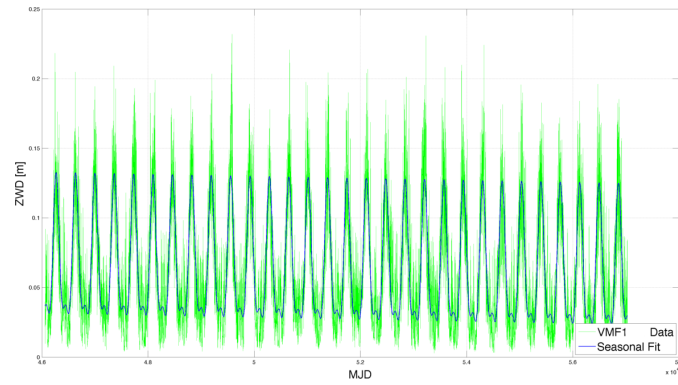
Figure A.30: Gilcreek VMF1, Trend = -0.3 mm/year
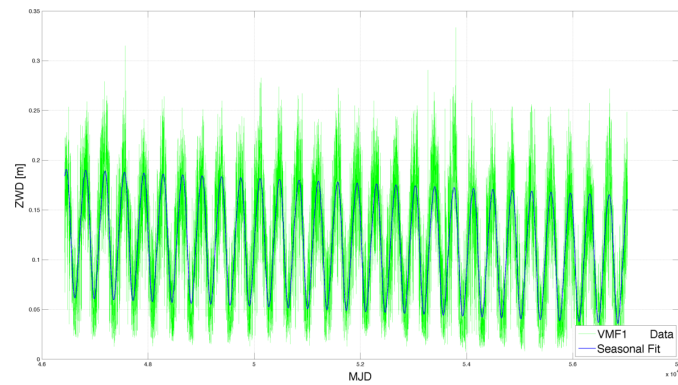
Figure A.31: Hartrao VMF1, Trend = -0.9 mm/year
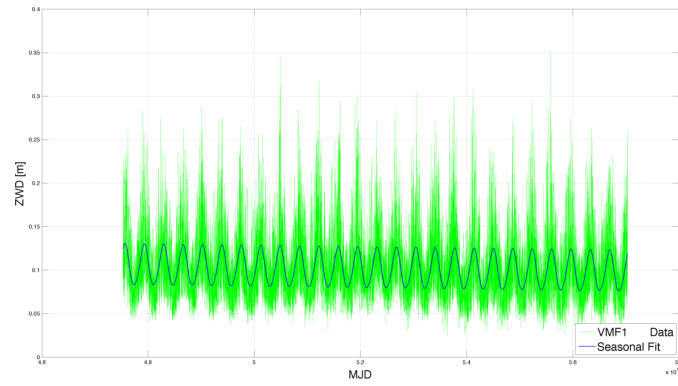
Figure A.32: *Hobart26 VMF1, Trend = -0.3 mm/year*
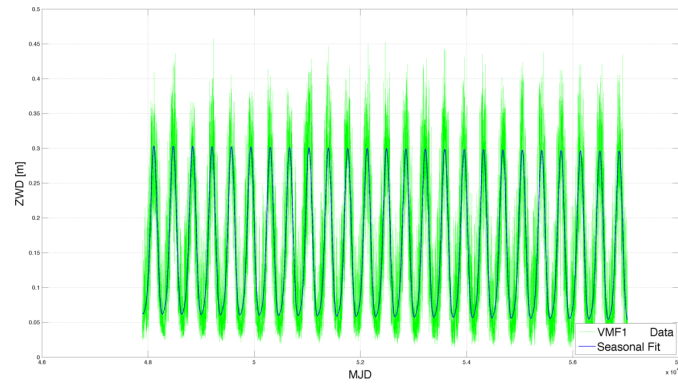
Figure A.33: *Kashim34 VMF1, Trend = -0.3 mm/year*
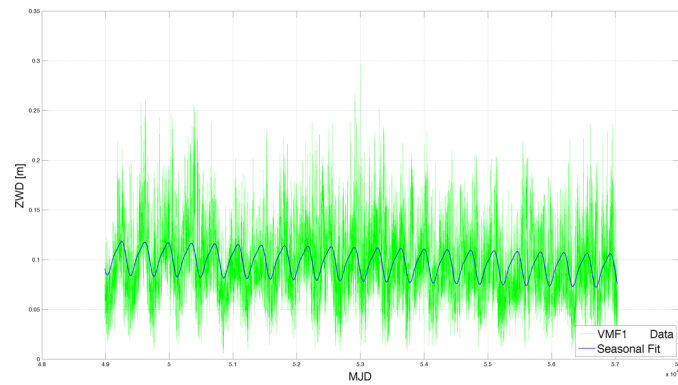
Figure A.34: *Kokee VMF1, Trend = -0.6 mm/year*
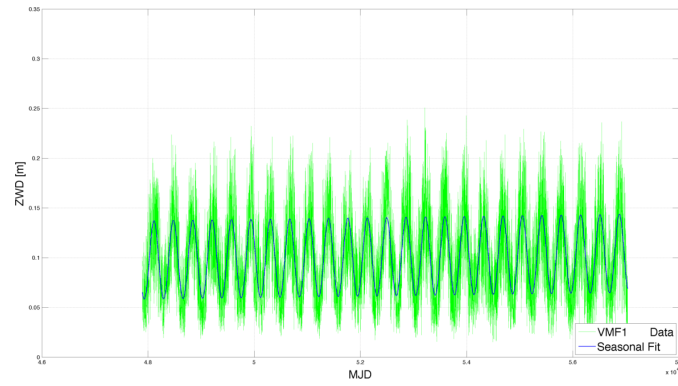
Figure A.35: Matera VMF1, Trend = 0.3 mm/year
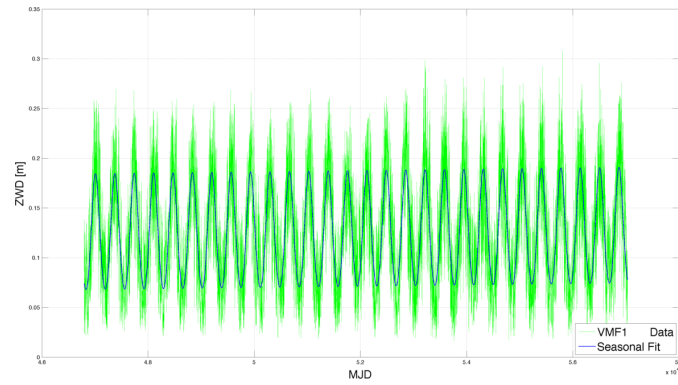
Figure A.36: Medicina VMF1, Trend = 0.2 mm/year
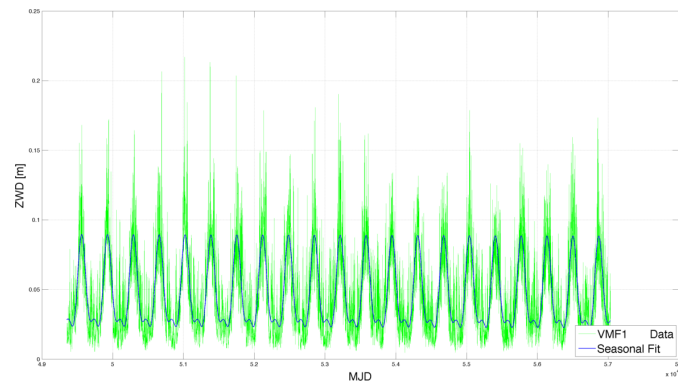
Figure A.37: Nyales20 VMF1, Trend = -0.1 mm/year
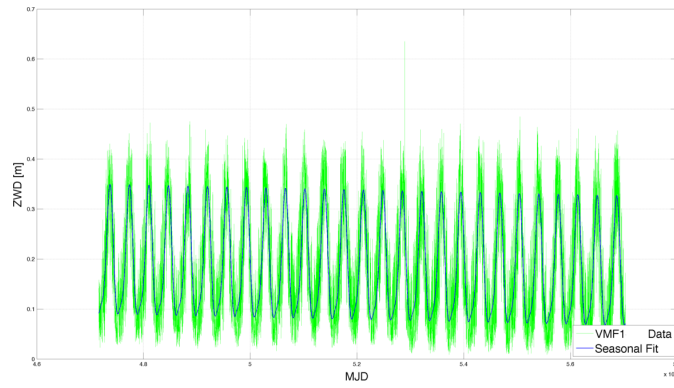
Figure A.38: *Seshan25 VMF1, Trend = -0.9 mm/year*
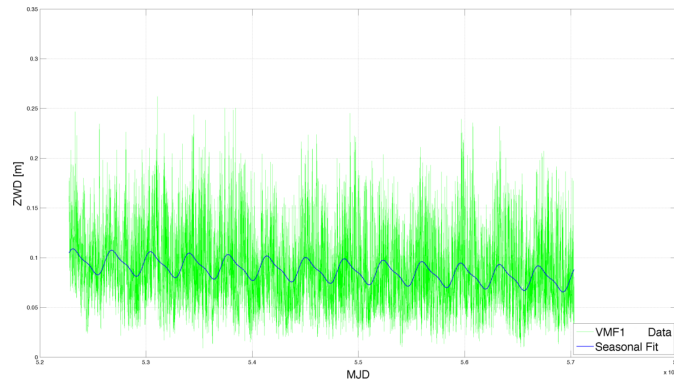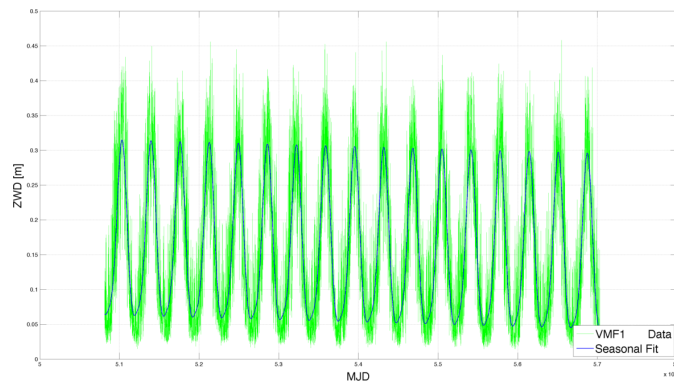

Figure A.39: *Tigoconc VMF1, Trend = -1.4 mm/year*
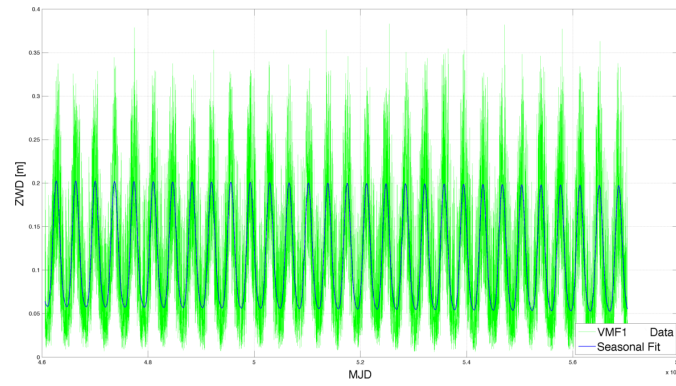

Figure A.40: *Tsukub32 VMF1, Trend = -1.2 mm/year*
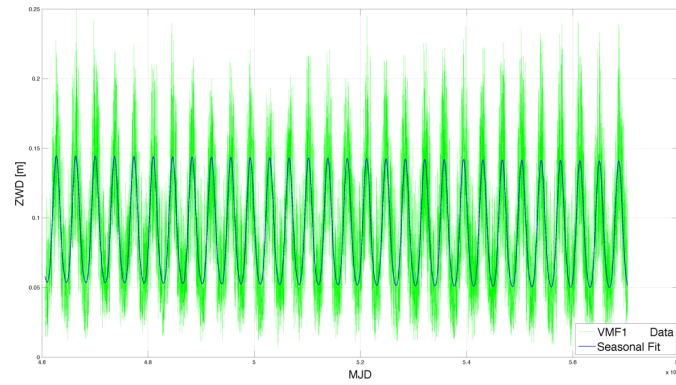
Figure A.41: *Westford VMF1, Trend = -0.2 mm/year*
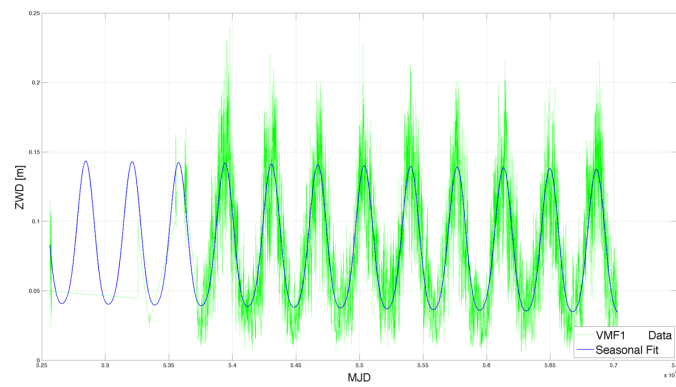

Figure A.42: *Wettzell VMF1, Trend = -0.1 mm/year*

Figure A.43: *Zelenchk VMF1, Trend = -0.5 mm/year*